Context dependent switching in the function of CD95

Dissertation

Jana Mallah

Fakultät
für Biologie
Universität Bielefeld

Vorlegt im März 2017
von Jana Mallah

Betreuung:
Prof. Dr. Philippe Bastiaens
Prof. Dr. Christian Kaltschmidt

Work presented in this dissertation was performed in the laboratory of Prof. Dr. Philippe Bastiaens at the Max-Planck-Institute of Molecular Physiology, Dortmund, Germany.

Eidesstattliche Versicherung

Ich versichere hiermit an Eidesstatt, dass die vorgelegte Dissertation von mir selbständig und unter Angabe aller verwendeten Quellen angefertigt wurde.

Dortmund, den …… .....……..

(Unterschrift)

Erklärung

Ich erkläre, dass meine Dissertation weder an der Universität Bielefeld noch an einer anderen Hochschule im Zusammenhang mit einer staatlichen oder akademischen Prüfung vorgelegt wurde. Ich habe mich an keiner anderen Hochschule einer Promotionsprüfung unterzogen.

Dortmund, den …… .....……..

(Unterschrift)

CONTENTS

LIST OF FIGURES

ABBREVIATIONS

°C	degree Celsius
a.u.	arbitrary units
aa	amino acids
Ab	antibody
Akt/PKB	protein kinase B
ALPS	autoimmune lympho-proliferative syndrome
ATP	adenosine triphosphate
Bis-Tris	bis-(2-hydroxyethyl) aminotris (hydroxymethyl) methane
bp	base pair
BSA	bovine serum albumin
c-FLIP	cellular FLICE-like inhibitory protein
C-termius	carboxyl terminus
CAP	cytotoxicity-dependent APO-1-associated proteins
Caspase	cysteine-aspartate protease
CD95	cluster of differentiation 95
CD95L	CD95 ligand
CIP	calf intestinal phosphatase
COS	CV-1 origin, SV-40
CRD	cysteine-rich domain
DD	death domain
ddH_2O	double distilled water
DED	death effector domain
DED	death effector domain
DISC	death-inducing signaling complex
DMEM	Dulbecco's minimal essential medium
DMSO	dimethyl sulfoxide
DNA	deoxyribonucleic acid
DR	death receptor
dsDNA	double stranded DNA
DTT	dithiothreitol
e.g.	*exempli gratis*
EB	elution buffer
EDTA	ethylenediaminetetraacetic acid
EGF	epidermal growth factor
EGFP	enhanced green fluorescence protein
EGFR	epidermal growth factor receptor
ER	endoplasmic reticulum
Erk	extracellular signal-regulated kinase
FADD	Fas-associated protein with a death domain
FAP1	Fas associated phosphatases 1
FasL	Fas ligand
FCS	fetal calf serum

Fig.	figure
FLICE	FADD-like interleukin-1 beta-converting enzyme
FLIM	fluorescence lifetime imaging microscopy
FLIP	FLICE-like inhibitory protein
FP	fluorescent protein
FRET	Förster resonance energy transfer
GFP	green fluorescent protein
hr(s)	hour(s)
i.e.	*id est*
ICCB	intensity correlation coefficient-based
ICQ	intensity correlation coefficient
IP	immunoprecipitation
IRF	instrument response function
IRFs	interferon-regulatory factors
JNK	c-jun-N-terminal kinase
kb	kilo base pair
kD	kilo dalton
kd	kinase dead
KD	kinase domain
l	liter
L-Glu	L-glutamine
LB	lysogeny broth
MAPK	mitogen-activated protein kinase
MeOH	methanol
min	minute
ml	milliliter
N-terminus	amino-terminus
n.s	not significant
NEAA	non-essential amino acids
NF-κB	nuclear factor- κB
nm	nanometer
ns	nanosecond(s)
o.n.	over night
PAGE	polyacrylamide gel electrophoresis
PBS	phosphate buffered saline
pH	*potentium hydrogenii*
PH domain	pleckstrin homology domain
PI3K	phosphoinositide-3-kinase
PLAD	pre ligand assembly domain
PM	plasma membrane
PMT	photomultiplier tube
PTB	phosphotyrosine binding
pTyr	phosphotyrosine
PVDF	polyvinylidene fluori
RE	recycling endosome
RIP	receptor interacting protein
ROI	region of interest

rpm	rounds per minute
RT	room temperature
RTK(s)	receptor tyrosine receptor(s)
s	second
SDS	sodium dodecyl sulphate
SEM	standard error of mean
SFM	serum free media
SH2	src homology 2
SHIP	SH2-containing inositol phosphatase
SHP1	SH2-containing tyrosine phosphatase 1
TAE	Tris-acetate-EDTA
TBS	Tris buffered saline
TCSPC	time correlated single photon counting
TE	Tris-EDTA
TIM	TRAF interacting motif
TKI	tyrosine kinase inhibitor
TM	transmembrane
TNF	tumor necrosis factor
TNF-α	tumor necrosis factor alpha
TNFR	tumor necrosis factor receptor
TRAF	TNFR-associated factor
TRAIL	TNF-related apoptosis inducing ligand
Tris	Tris[hydroxymethyl]aminomethane
U	units
UV	ultraviolet
V	volt
WT	wild type
µ	micro
τ	lifetime
τ_{av}	average lifetime
τ_{D}	donor-only lifetime
τ_{DA}	donor-acceptor lifetime

ABSTRACT

CD95 is considered as the classical death receptor and well studied for its role as apoptosis mediator. Consequently CD95 is often associated as a tumor suppressor. Recent data indicate that CD95 activation also transmits non-apoptotic signals and that CD95 has a growth-promoting role during tumorigenesis. The exact mechanisms that lead either to cell death or survival/proliferation mediated by CD95 seem to be highly context dependent and yet not completely understood.

In this work, we investigated whether the receptor tyrosine kinase receptor EGFR and CD95 share similarities in their spatial and temporal dynamics and whether EGFR activation can alter the response properties of CD95 in terms of its reactivity towards FasL. For that we used two cell lines, Huh7 liver carcinoma cells ectopically expressing CD95 and EGFR and HCC827, a non-small cell lung cancer line, expressing wild-type CD95 but harboring a constitutively active EGFR mutation. We were able to show that EGFR and CD95 interact with each other and that EGF treatment leads to CD95 phosphorylation. Moreover, we show that the pre-treatment with EGF is sufficient to protect cells from FasL-induced apoptosis, which is dependent on EGFR-mediated phosphorylation. Finally, we used the non-small cell lung cancer cell line HCC827 to verify our findings in a relevant cancer model. We were able to show that inhibition of the constitutive activity of EGFR by utilizing the tyrosine kinase inhibitor (TKI) Erlotinib re-sensitizes HCC827 cells towards FasL-induced apoptosis.

Considering EGF exposure and consequently a high EGFR activity as 'historical context' of a cell, we provide evidence that the responsiveness of CD95 to its own ligand is not following a simple 'binding-and-respond pattern' but rather that the intrinsic state of CD95 is influenced by the prior history of the cell and in turn determines the cellular response to subsequent FasL stimulation.

ZUSAMMENFASSUNG

CD95 wird als der klassische ‚Todesrezeptor' angesehen und seine Rolle als Apoptose-induzierendes Protein ist sehr gut beschrieben. Auf Grund dessen wird CD95 häufig als Tumorsuppressorprotein wahrgenommen. Neuere Veröffentlichungen deuten allerdings daraufhin, dass die Aktivierung von CD95 auch nicht-apoptotische Signale vermittelt und sogar eine wachstumsfördernde Rolle während der Tumorentstehung hat. Die genauen Mechanismen, die entweder zu CD95-induziertem Zelltod oder zu CD95-induziertem Überleben bzw. Wachstum führen, scheinen jedoch höchst kontextspezifisch zu sein und sind nur ungenügend beschrieben.

In dieser Arbeit wurde untersucht, ob die Rezeptortyrosinkinase EGFR und CD95 Gemeinsamkeiten in ihrer räumlichen und zeitlichen Dynamik zeigen und ob die Aktivität vom EGF Rezeptor die Reaktionseigenschaften von CD95 beeinflusst, indem beispielsweise die Aktivierung von CD95 durch FasL beeinflusst wird. Um dies zu untersuchen, wurden zum einen eine Leberkarzinomzelllinie verwendet, die sowohl CD95 als auch EGFR ektopisch exprimiert und eine ‚non-small cell lung cancer'-Zelllinie, die zwar wildtyp-CD95 exprimiert, allerdings eine mutierte EGFR-Variante mit konstitutiver Aktivität. Wir konnten zeigen, dass EGFR und CD95 miteinander interagieren und dass die Stimulation mit EGF zur Tyrosin-Phosphorylierung von CD95 führt. Weiterhin konnten wir zeigen, das die prä-Stimulation mit EGF ausreicht, um Zellen vor FasL-induziertem Zelltod zu schützen und dass dies von der EGFR-vermittelten Phosphorylierung abhängt. Schlussendlich, haben wir unsere Erkenntnisse in der Krebszelllinie HCC827 validieret. Dort konnten wir zeigen, dass die Inhibition der konstitutiven EGFR-Aktivität durch den Tyrosin-Kinase-Inhibitor Erlotinib zur Wiederherstellung der Sensibilität von FasL-vermittelter Apoptose führt.

Wenn EGF-Stimulation und die daraus resultierende erhöhte EGFR-Aktivität als ‚historischer Kontext' einer Zelle angesehen werden kann, deuten unsere Ergebnisse daraufhin, dass die Reaktionseigenschaften von CD95 gegenüber FasL nicht einem simplen ‚Bindungs-und-Reaktionsmuster' folgen, sondern stattdessen stark vom ‚historischen Kontext' der Zelle beeinflusst werden. Dieser prägt im

besonderen Maße den intrinsischen Zustand von CD95 und hat im weitern Verlauf maßgeblichen Einfluss ob und wie CD95 auf Stimulation mit FasL reagiert.

1. INTRODUCTION

1.1 A PROTEIN ON THE EDGE

A correct balance between apoptosis and proliferation is necessary in embryonic development and later for tissue maintenance. While during embryogenesis the internal structure of each organ and tissue is defined, later this complex internal structure must be preserved. For this essential task cells evolved complex intercellular communication mechanisms whereby signals from neighboring cells are interpreted and an appropriate response for the current tissue context can be engaged. This appears especially remarkable as under physiological conditions cells are exposed to a high amount of different and often opposing signals. Yet, cells can efficiently distinguish signals from noise and respond precisely. The main regulator that orchestrates the cellular response to incoming signals is the plasma membrane (PM). The composition of the plasma membrane, in relation to the concentration of a particular receptor, for example, can be modulated by the cellular context/surrounding. This raises the question of how the historical context of a cell, in terms of exposure to a certain stimuli, influences the cellular fate by determining e.g. the concentration of a particular receptor and thereby promoting a certain response.

Two well-known classes of membrane proteins that regulate cell fate are the receptor tyrosine kinase (RTK) family of receptors, like EGFR, and cytokine receptors, like CD95 (*1, 2*). While EGFR is well known for its growth-promoting role, CD95 is often referred to as the death receptor. So both receptors regulate opposing cellular responses, but still, if contemplated in a bigger scale, like for example a tissue, both pathways are tightly linked. In a recent review dealing with life-death signaling in single cells, Flusberg and Sorger give nice examples showing the tight bond between both pathways (*3*). Stress-response signaling is mentioned as an example as it often has a dual role; survival pathways are activated to buffer and repair damage, and death pathways are required to kill cells when the damage is beyond repair. But also under “normal”, healthy conditions, individual tissues and/or organs operate at a cellular homeostasis where cell proliferation is

required to counter continuous cell death. This equilibrium between cell production and cell death needs to be tightly maintained since already small differences would cause extensive effects. Despite that the essential players that determine cell fate are well known, other equally important aspects like different cellular states in a multicellular organism and a resulting cell-to-cell variability are less well understood. Accordingly, the question of what makes one cell die and what let the others survive, is dependent on a variety of environmental states. So, whether a cell survives or dies after a certain stimuli is dependent on both the extra- but also intracellular context, like the activity state of involved proteins, the microenvironment of certain proteins but also on the cell type and on specific adoptions.

It becomes even more complicated as some proteins are pleiotropic and exhibit several functions simultaneously and the surroundings of those proteins determine whether one over the other function dominates. This can be influenced by several means, e.g., inhibition/activation through interactors or positive and negative feedback loops. The death receptors of the tumor necrosis factor (TNF) family, like CD95, represent this phenotype exceptionally as some members activate opposing pathways in a strongly context-dependent manner. The particular case of CD95 and its duality will be in the following sections discussed in depth and moreover how the EGFR is linked to this duality despite its opposing function as a growth factor receptor.

1.1.1 THE TUMOR NECROSIS FACTOR SUPERFAMILY

The cytokines of the TNF super family have numerous cellular functions, ranging form apoptosis to proliferation and can be found in several tissues and cells. The allegory of the ‘double-edged sword’ is often used to describe TNFs and their cognate receptors due to the high duality and the often-opposing functional tendencies of individual TNFs. Until now the TNF superfamily encompass 19 ligands and 29 receptors (*2*).

Almost all TNF ligands are type II transmembrane proteins with an intracellular amino-terminal and an extracellular carboxy-terminal. Characteristic for all TNF ligands is the TNF homology domain at the extracellular C-terminus, which is responsible for receptor binding (Fig. 1.1). TNF ligands are mainly

expressed by cells of the immune system including B cells, T cells, NK cells, monocytes and dendritic cells. The transmembrane expression of TNFs is a feature indicating that TNFs are destined to rather act locally. This is exemplified by the interesting observation that some ligands, once present in their soluble form, act antagonistically, as for example shown for CD95 and its cognate ligand FasL (*2, 4-6*).

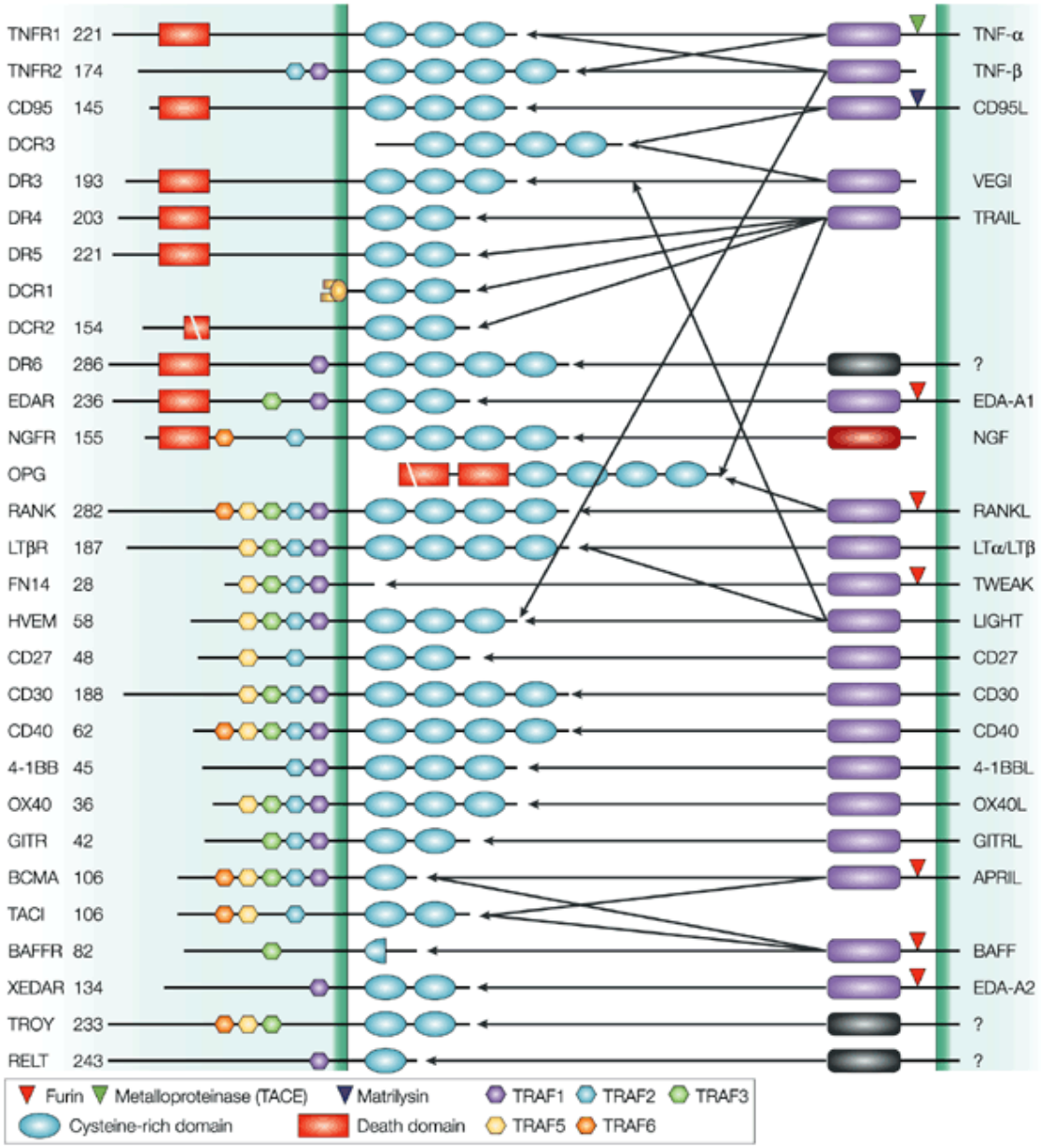

Figure 1.1: The ligands and receptors of the Tumor Necrosis Factor Superfamily.
Shown are the 19 ligands and 29 receptors of the TNF superfamily. On the left side the receptors are illustrated and on the right side the ligands. The arrows pointing from the ligands to the receptors indicate receptor-ligand-binding potential. The number next to the receptor name represents the number of amino acids in the cytoplasmic domain of the receptor. The composition of the different structural domains is color-coded and the key is presented in the box. TRAF= TNFR-associated factor (Figure adapted from (*2*))

Unlike the ligands, TNF receptors (TNFRs) are type I transmembrane proteins and are expressed in a broad diversity of cells. Common for all receptors is a cysteine-rich domain (CRD) in the extracellular fraction of the proteins (Fig. 1.1). Generally, TNFRs can be largely divided into two groups – the ones with the death domain (DD) and the ones without a death domain.

The death domain is an amino acid sequence of approximately 80 residues and localized in the intracellular domain of the receptors (Fig 1.1). Two different research groups first described the death domain as cytoplasmic region of CD95 and TNFR1 and showed independently that mutations in that region abolish ligand-induced apoptosis (*7, 8*). While receptors with the death domain are referred as 'death receptors', the ones without the death domain are called 'activating receptors'.

The activating receptors contain TNFR-associated factor (TRAF)-interacting motifs in their intracellular region and depending on the individual TRAFs that bind the receptor different signaling pathways are activated (*9, 10*). The main proteins activated by TNFRs are nuclear factor-κBs (NF-κBs), mitogen-activated protein kinases (MAPKs), or interferon-regulatory factors (IRFs) (*10, 11*). In four TNFRs, a functional cytosolic domain is lacking and they mainly act as decoy receptors by reducing ligand signaling (*2*).

1.1.2 CD95 – A SHORT JOURNEY THROUGH ITS HISTORY

CD95 (also known as Fas, APO-1 or TNFR6) is one of the most famous members of the TNF superfamily. Its function as a death receptor is well described and also its role apart from apoptosis induction has been intensively studied since the early nineties.

CD95s ability to induce apoptosis was firstly discovered in 1989 independently by two different groups, which performed monoclonal antibody screenings (*12, 13*). While one group characterized cell surface molecules by testing monoclonal antibodies on lymphocytes, the other group used primarily the rhabdomyosarcoma A673 cell line but tested also other, mostly cancer cell lines. Both discovered antibodies, once called anti-APO-1 (*12*) and one called anti-Fas (*13*), completely blocked proliferation and induced cell death. As Trauth and colleagues showed this effect on activated human lymphocytes, on malignant

human lymphocytes but also on some patient-derived leukemic cells, anti-APO-1 was immediately considered as a therapeutic drug in the treatment of malignancy (*12*). With those first studies a huge interest in CD95 grew and more and more details were published in the following decades about its structure, activation and overall function.

In 1991, for example, the polypeptide sequence for CD95 was first described and the classification into the TNF superfamily occurred (*14*). Two years later two different groups described a domain in the cytoplasmic region of CD95 and TNFR1, which is required for ligand-induced apoptosis and thus called the 'death domain' (*7, 8*). In the same year Suda *et al.* identified the ligand for CD95 (in the following denoted as FasL) and successfully cloned, expressed and described the amino acid sequence of the protein (*15*). The full structure of the human CD95 gene was published in 1994 and further details about the exact gene locus, the exon/intron distribution and the transcriptional starting sides were described (*16*). First insights into the protein structure were given two years later. NMR spectroscopy revealed the three-dimensional structure of the death domain in the C-terminal part of CD95 and one year later, in 1997, the structure of the extracellular part was predicted and modeled (*17, 18*).

Apart from the structural characterization of CD95 also more and more functional aspects, like interactors and posttranslational modifications were described. In this context one of the most important discoveries was the 'death-inducing signaling complex' (DISC), which was already introduced in 1995 by Kischkel *et al.* (*19*). The authors not only discovered the cytotoxicity-dependent APO-1-associated proteins (CAP) 1-4 but also that those proteins are only bound to aggregated CD95. They could also identify CAP1 and CAP2 as MORT1/FADD (*19*). The meaning of the interaction between CD95 and MORT1, which is better known as 'Fas-associated protein with death domain' (FADD) was described in the same year independently by two different groups (*20, 21*). Both groups showed that MORT1/FADD is mandatory for CD95-mediated induction of apoptosis and thus represents one of the most important interactors (*20-23*). Another essential protein of the DISC is Caspase-8. In 1996 it was first shown that Caspase-8, initially known as MACH or also as FLICE, is associated to FADD and important for CD95-mediated apoptosis (*24, 25*). Also in 1996, it was shown that FLICE/Caspase-8 is part of the DISC and finally CAP3/4 was identified as FLICE/Caspase-8 (*26-28*).

Since the discovery of CD95 the role of tyrosine kinase activity and protein phosphorylation upon CD95 activation has been controversial. Already in 1994 it was published that activation of lck and fyn, both src family kinases, provides an early and necessary signal for Fas-induced apoptosis in lymphocytes (*29*). One year later, a study was published showing that src kinase activity is not required for CD95 activation but that inhibition of kinases rather enhances CD95-driven apoptosis (*30*). In the following years further paradoxical reports were published, showing either that src family kinases are activated upon FasL ligation and required for apoptosis induction or that kinase activity has no effect on CD95-medaited apoptosis (*31-33*). The overall opinion derived from this controversy is that the requirement of tyrosine kinase activity for CD95 signaling is highly cell type specific and also strongly context dependent.

The context dependency and cell type specificity of CD95-driven effects became even more obvious in 1995 when the first report was published showing that CD95 is promoting proliferation (*34*). Aggarwal *et al.* showed that in human diploid fibroblasts CD95 activation leads to proliferation in a dose-dependent manner. Since then a whole new field of CD95-related science appeared. Shortly after Aggarwal's publication a similar study showed that CD95 either triggers proliferation or apoptosis in human fibroblasts, depending on the context (*35*). A dual role of CD95 was also shown in immune system, which was especially surprising, as CD95s role particularly in the immune response was strongly coupled to apoptosis (*36, 37*). In the following years, more reports accumulated showing that the role-played by CD95 is not restricted only to that of a death receptor but rather a multifunctional protein involved in several cellular tasks (for reviews see (*38-40*)). Until today the exact mechanisms of switching the function of CD95 are not completely understood and even those studies that describe the switch-like behavior of CD95 do not always provide a concrete mechanism explaining corresponding observations.

1.1.3 PROPERTIES OF CD95

The human gene encoding for CD95 is located on chromosome 10 and approximately 25 kb in length (*16*). It is composed of 9 exons separated by 8 introns. Exons 1-5 encode the extracellular region, exon 6 the transmembrane region and exons 7-9 encode the intracellular region. According to Ensembl, the gene has 18 splice variants and three of those encode for proteins (*41, 42*). While the longest protein version contains 335 amino acids, the shortest has 220 amino acids and in the third version the transmembrane domain is lacking resulting in a soluble form of the receptor (*42*).

CD95 is a type I transmembrane proteins and accordingly its N-terminus is located extracellular and the C-terminus intracellular. The distinctive feature of all TNF receptors is several CRDs in the extracellular part of the receptors. CD95 harbors three CRDs in the N-terminal domain, which are termed CRD1-3 and reach from aa 46 to aa 167 (Fig. 1.2; all aa numbering for CD95 always includes the signal peptide) (*43*). In the ligand-unbound state CD95 exists a pre-associated trimer. This is accomplished via the so-called pre-ligand binding assembly domain (PLAD), which is part of the CRD1 and reaches from aa 59 to aa 82 (Fig. 1.2) (*44-46*). CRD2 and the N-terminal part of CRD3 interact with FasL and are consequently required for ligand binding (Fig. 1.2)(*47*). The transmembrane domain reaches from aa 174 to aa 191 and makes a single pass to the PM.

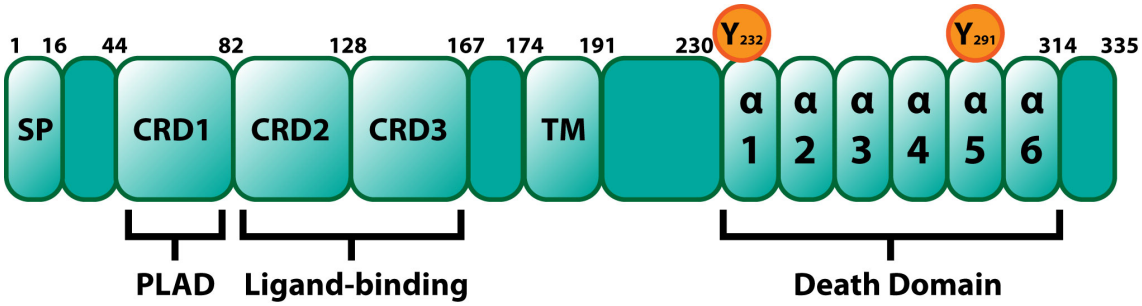

Figure 1.2: Schematic representation of a CD95 monomer.
As CD95 belongs to the type I transmembrane protein, the transmembrane (TM) domain makes a single pass through the PM. The extracellular part of CD95 contains the N-terminal domain including the signal peptide (SP) and the three cysteine-rich domains (CRD) 1-3. While CRD1 contains the pre-ligand binding assembly domain (PLAD), CRD2 and CRD3 are important for the CD95-FasL interaction. The C-terminal part of CD95 contains the death domain, which is composed of 6 alpha helices. Numbers represent the amino acid position, including the signal peptide (adapted from (*43, 48*)).

The intracellular part of CD95 contains the 84 aa long DD, which reaches from aa 230 to aa 314 (Fig. 1.3) (*17, 49*). The DD is composed of six-amphipathic α-helices, which are arranged anti-parallel to one another (*31*). Within the DD are two tyrosine residues at position Y232 and Y291, whose functions are not yet completely understood. However, already in 1996 it was shown that CD95 is phosphorylated *in vitro* and also *in vivo* (*50*). Moreover it was shown that CD95 harbors a conserved phosphotyrosine-containing motif within the death domain that under certain circumstances is recognized by SH2-containing tyrosine phosphatase 1 (SHP-1) and SH2-containing inositol phosphatase (SHIP), resulting in inhibitory functions (*51*). Apart from that, the apoptotic function of CD95 is inhibited by the interaction of Fas associated phosphatase 1 (FAP1), which binds the last 15 aa of CD95 (*52, 53*).

1.1.4 ACTIVATION MECHANISMS OF CD95

CD95 mediated apoptosis is generally initiated by binding of FasL. FasL is mainly expressed by T lymphocytes and natural killer cells but was also found in immune privileged tissues like eyes, brain and testis (*15, 54-56*). Both proteins exist as pre-associated homo-trimers on the cell surface (*45, 57*). The exact mechanism by which FasL activates pre-associated CD95 is not yet solved (*43*). The main question in this context that remains to be solved is whether all CD95 molecules are already pre-assembled into stable complexes or if also a pool of monomeric molecules exists. In case of a complete pre-assembly of CD95 molecules prior to ligand binding, the signaling induction is most likely due to structural reorganization (*58*). The other model of signaling induction is based on a dynamic equilibrium between a large fraction of monomeric CD95 molecules and a smaller fraction of pre-assembled CD95 complexes. While monomeric CD95 is supposed to have a low affinity for FasL, the pre-assembled complexes of CD95 are supposed to have a high affinity for FasL. Signaling activation in this model is driven by the dynamics of the equilibrium, which would eventually lead to an accumulation of ligand-bound, signal competent CD95 complexes (*43*).

Regardless of the exact mechanism that activates the pre-associated receptor, once CD95 binds FasL and gets eventually activated, CD95 undergoes conformational changes of its DD. It was shown that ligand binding leads to a shift

of helix 6 and fusion with helix 5, which leads to FADD recruitment and oligomerization of CD95-DD:DD-FADD complexes (*49, 59, 60*). Especially oligomerization and cluster formation of CD95-DD:DD-FADD complexes are mandatory for DISC formation and represent the initial step in this process (*60, 61*). The DISC is further composed of procaspases-8, procaspases-10 and cellular FLICE-like inhibitory proteins (c-FLIPs) (see Fig. 1.3).

The occurring interactions in the DISC are all based on homotypic contacts. While FADD binding is accomplished by the DD of both proteins, all other binding events are mediated via the so-called death effector domain (DED) (Fig. 1.3)(*62*). The actual apoptotic cascade is then induced by activation of the initiator caspases, which in turn activate the executor caspases, caspase-3 and -7. Only recently it was unraveled how exactly the initiator caspase-8 is activated in the DISC. It was shown that procaspase-8 is activated via the formation of DED chains at the DISC, which allow for the formation of homodimers that enable full activation of caspase-8 due to autoproteolytic processing and eventually the formation of fully active heterotetramers (Fig. 1.3) (*63, 64*). Another important protein group of the DISC are c-FLIPs, which also contains a DED, but unlike the other components, c-FLIPs mostly inhibit apoptosis induction. c-FLIPs hamper the apoptosis induction by interfering with procaspase-8 and -10 recruitment (*65, 66*).

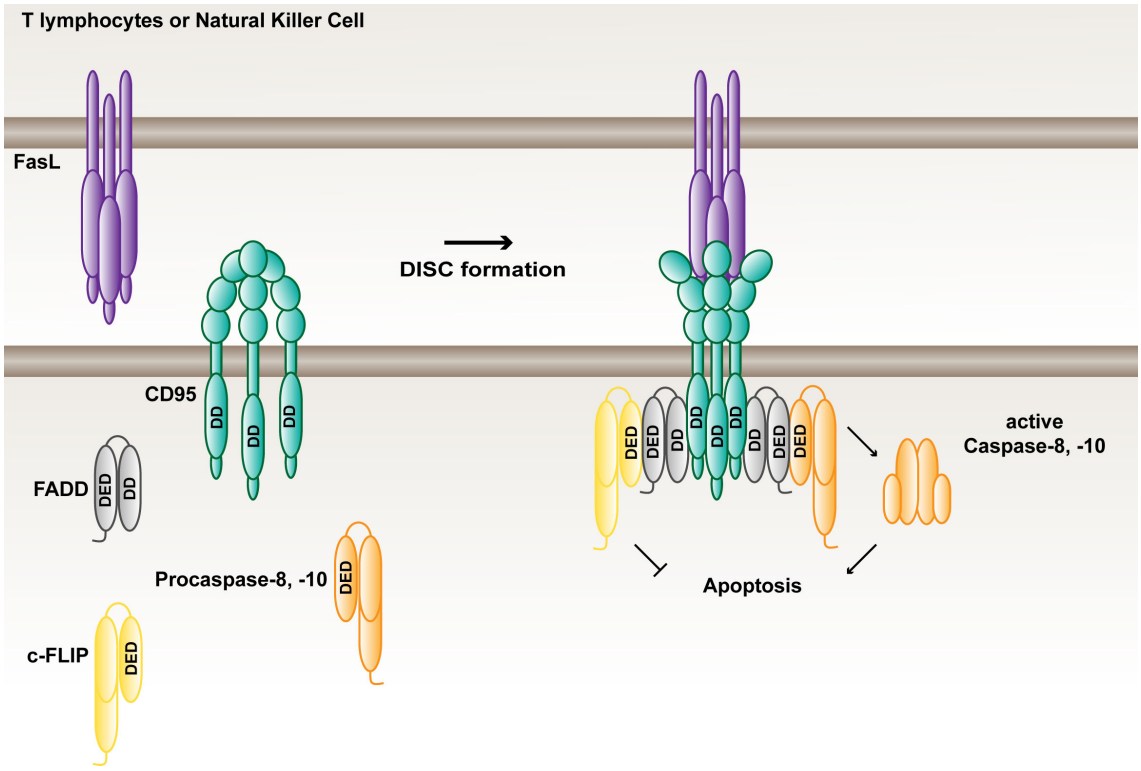

Figure 1.3: FasL-induced DISC formation
Scheme represents the classical model of FasL-induced apoptotic signaling. Both, the receptor and the ligand are expressed at the plasma membrane as pre-associated homotrimers. Binding of FasL leads to formation of the DISC. The DISC is composed of CD95/FADD/Procaspase-8, -10 and c-FLIPs. Recruitment of procaspase-8/-10 to the DISC leads to auto-processing of the caspases followed by the release of active caspases into the cytoplasm, which in turn, leads to apoptosis execution and eventually cell death. A higher concentration of c-FLIP binding at the DISC, however, inhibits apoptosis formation (based on (*43*)).

Beside the ligand-induced oligomerization of CD95 and the thereby enhanced DISC formation, an alternative apoptosis-signaling pathway mediated by CD95-FasL occurs *in vivo*. In fact, there are two prototypic apoptotic CD95 signaling pathways that operate in a cell type-specific manner and accordingly are classified in the type I/type II cell model (*67, 68*). While type I cells show a rapid DISC formation and a large amount of active caspase-8/10 that is released into the cytosol, in type II cells the released amount of active caspase-8/-10 is insufficient to activate caspases-3 and -7. Apoptosis induction in type II cells is activated via the so-called intrinsic apoptosis pathway, which involves the mitochondria and formation of a complex called apoptosome. Upon FasL binding only a small amount of procaspase-8/-10 is activated, which is just sufficient to cleave BID and thus initiate the intrinsic apoptosis cascade. BID is a BH3-only protein and after cleavage designated as truncated BID (tBID). Active tBID translocates to mitochondria and triggers the release of pro-apoptotic factors from the mitochondria and the formation of the apoptosome, which is composed of the

adapter protein 'apoptotic protease activating factor 1' (Apaf-1), cytochrome c and the initiator procaspase-9. Gathering of procaspase-9 in the apoptosome leads to autoproteolytic activation of caspase-9, which in turn activates caspase-3 and eventually leads to apoptosis execution (*67*). Apart from the different apoptosis execution mechanism, another substantial difference between type I and type II cells exists, which further elucidates especially the mitochondrial dependency. In type II cells members of the inhibitor of apoptosis (IAP) protein family are higher concentrated and prevent caspase activity (*69*). The proteins XIAP, c-IAP1 and c-IAP2 are, for example, able to directly bind caspases-3, -7 and procaspase-9 and degrade those, thus leading to apoptosis inhibition (*70-72*). This inhibition is eliminated by 'second mitochondria-derived activator of caspase' (SMAC; DIABLO 'direct IAP-binding protein with low PI'), which is released from the mitochondria by tBID and separates IAPs from caspases and thereby restores the apoptotic induction (*73*). Even thought type II cells show a reduced DISC formation they are not less sensitive to CD95-mediated apoptosis induction in comparison with type I cells (*67, 68*).

1.1.5 CD95 AS DEATH RECEPTOR

The importance of the CD95/FasL system became oblivious when both proteins were linked to three mutant mouse strains that showed lymphadenopathy and "systemic lupus erythematosus" (SLE)-like autoimmune diseases. It was shown that those mouse strains carry homozygous defects in the genes either encoding CD95 or FasL. For instance, the so-called lymphoproliferation mice ($Fas^{Lpr/Lpr}$) have an insertion of a retrotransposon in the CD95 gene, which leads to a down regulation of the receptor expression (*74, 75*). The lpr gene complementing gld mice ($Fas^{lprcg/lprcg}$) show an impaired DISC formation caused by a spontaneous mutation within the DD of CD95 (*76, 77*) and the generalized lymphoproliferative disease mice ($FasL^{gld/gld}$) show a reduced affinity of FasL for CD95, due to a mutation in the FasL gene (*78*). Even more important was the discovery that also patients of the "autoimmune lymphoproliferative syndrome" (ALPS) have heterozygous mutations in the FAS gene (*79, 80*). ALPS is an inherited genetic disorder and also known as Canale-

Smith syndrome (*81*). ALPS patients mostly suffer from chronic non-malignant lymphoproliferation, autoimmune diseases, and secondary cancers (*82*).

Taken together, the general consensus of both studies, with CD95- or FasL-deficient mice and ALPS patients, show that the CD95/FasL system has an important function in immune surveillance and is, for example, responsible for the elimination of obsolete and potentially dangerous lymphocytes, but also transformed and infected cells (reviewed in (*83*)). Moreover, both proteins are responsible for immune system homeostasis.

1.1.6 THE NON-APOPTOTIC ROLE OF CD95

Apart from the well-known function as death receptor, during the last twenty years the interest in CD95s non-apoptotic functions grew tremendously. Already in 1993 it was shown for the first time that under certain circumstances CD95 stimulation results in the activation and proliferation of normal T cells (*37*). Two years later Aggarwal and colleges showed that CD95 signals also in non-immune system related cells proliferation. In fact they showed that CD95 signals proliferation in fibroblasts (*34*). Other reports soon followed and more and more functions were described for CD95 and FasL of being different from inducing apoptosis. Even though initially most studies showed non-apoptotic functions of the CD95/FasL system primarily in the immune system, especially in the late nineties also other tissues and cell types came to the fore.

It was shown, for example, that CD95 engagement is able to activate the release of pro-inflammatory cytokines, like IL-1, IL-6 and IL-8, and thus induce inflammatory changes (*84-87*). Further, it was shown that CD95 stimulation leads to inflammatory angiogenesis in a murine model after application of the agonistic anti-Fas mAb. In comparison, CD95-mediated angiogenesis was absent in the Fas^{Lpr}-mice (*88*). CD95 is also able to induce the up-regulation of cell surface integrins leading to increased cell migration (*89*). One of the most striking early studies showed that CD95 is involved in liver regeneration upon partial hepatectomy (*90*). Desbarats and colleges showed that partial hepatectomy protected mice against the pro-apoptotic effects of CD95 *in vivo* and that CD95 engagement accelerated liver regeneration (*90*). The same group showed some years later that CD95 is even important for brain development and might have a

growth receptor-like function in some cells of the nervous system (*91, 92*). Likewise, several reports showed that CD95 is enhancing proliferation in tumor cells originating from many different tissues (reviewed in (*93-95*)). A tumor growth-promoting role of CD95 could also be shown in *vivo* (*96*). A remarkable connection between cancer and CD95 signaling was found by Hadji *et al*. in 2014. They showed that elimination of CD95 or FasL results in a 'new' form of cell death that preferentially affects cancer cells and resembles a necrotic form of mitotic catastrophe (*97*). This process was designated as 'death induced by CD95R/L elimination' (DICE) and might offer the possibility of a new cancer therapy (*98*).

Even though many details regarding the alternative functions of CD95 and FasL have been elucidated, so far neither a well-defined mechanism nor a global mechanism has been provided that explains the duality of CD95. However, at least for certain cell types and/or tissues some involved proteins and their participation in switching CD95's function is described.

A promising group of proteins being involved in switching the outcome of the activity of CD95 are the cFLIP proteins. They contain a DED and via a direct interaction with FADD they are components of the DISC. So far five c-FLIP proteins have been characterized, three c-FLIP isoforms and two cleavage products. Two of the three c-FLIP isoforms are considered as short c-FLIP isoforms, c-$FLIP_S$ and c-$FLIP_R$, and one as long isoform, c-$FLIP_L$ (*99*). The short isoforms exclusively block caspase-8 activation, whereas the long isoform can both block and accelerate caspase-8 activation, depending on the c-$FLIP_L$ concentration (*100*). The two cleavage products of c-FLIP are called p43-FLIP and p22-FLIP and are cleavage products of caspase-8. Both cleavage products are capable of inducing NF-kB activity by binding to the IKK complex (*101*). The contribution of the individual cFLIP proteins in blocking apoptosis after CD95 stimulation is mainly dependent on the ratio between procaspase-8 and c-FLIPL at the DISC (*102, 103*). However, as mention above cFLIP protein are also able to activate anti-apoptotic proteins, like NF-κB.

Various studies that describe the non-apoptotic functions of CD95 from a more mechanistic perspective are based on cancer cells lines from different origins (for review see (*40, 95, 104*)). There, it was shown that CD95 engagement leads to activation of, for example, NF-κB and all three major MAPK pathways: ERK1/2, p38, and JNK1/2.

However, depending on the exact cell type, activation of those pathways is resulting in different CD95-mediated cell responses including inflammation, proliferation and migration/invasion (Fig. 1.4). In this context, NF-κB represents a fitting example, as it is known for mediating different cellular outcomes after CD95-mediated activation, like inflammation and invasion. The first study describing a link between NF-κB and CD95 was already published in 1996 and showed that CD95 activation leads to NF-κB activation and that this activation is independent from CD95s cytotoxic function (*105*). This was in good agreement with the observation that an enhanced NF-κB activity was especially observable in apoptosis-resistant tumor cells (*106*). In those tumor cells an increased motility and invasiveness was observed after FasL engagement, which was dependent on NF-κB as well as Erk1/2 and caspase-8. In contrast, another study showed that the CD95-induced NF-κB activation is mediated via FADD, caspase-8 and the 'receptor interacting protein kinase' (RIPK), which also contains a death domain and is able to bind CD95 (*23, 107, 108*). There it was shown that NF-κB activation is switching CD95's function from a pro-apoptotic signal into an inflammatory mediating response. Later it was found that also in CD95-sensitive tumor cells, NF-κB activity was detectable (*109*). This finding lead to the hypothesis that activation of NF-κB is part of a default CD95 pathway in some cells and has different functions depending on its activity resulting in different cell fates.

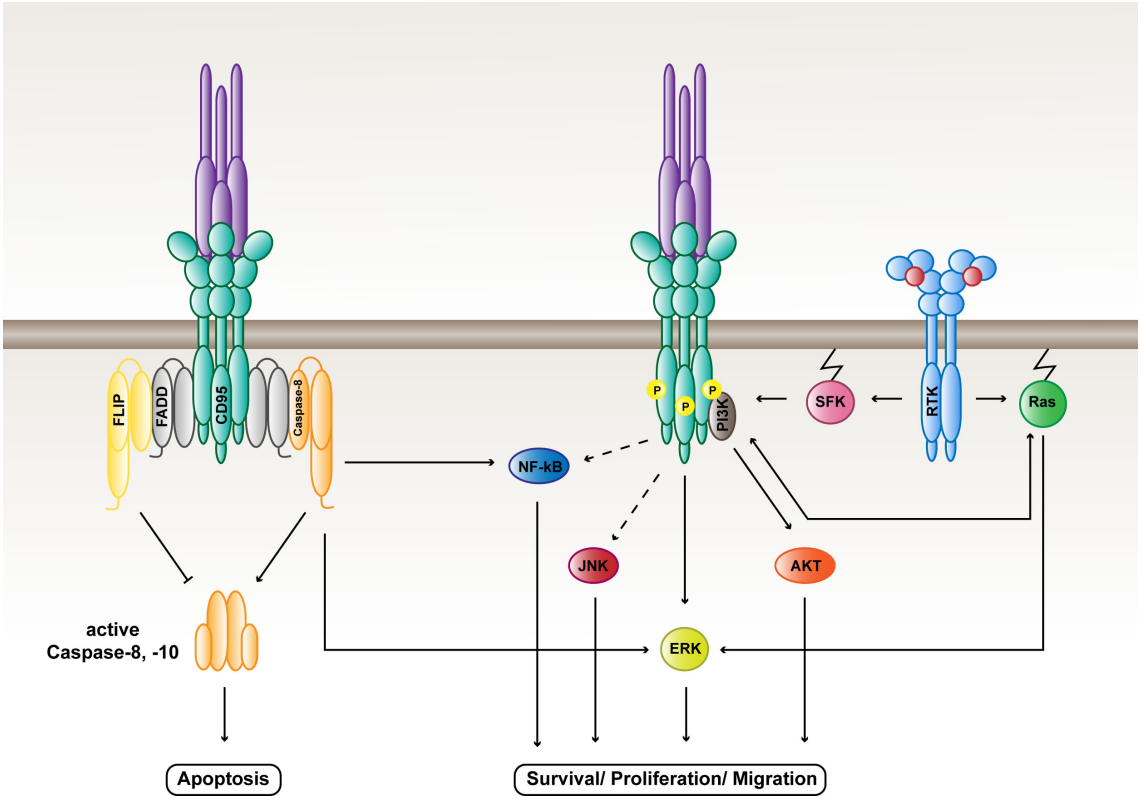

Figure 1.4: CD95 signaling outcomes
The scheme illustrates the different cellular outcomes after CD95 activation and the involved proteins. While the left side shows simplified CD95-mediated apoptosis, the right side gives an overview about the proteins involved in the non-apoptotic CD95 signaling (adapted from (*95*)).

One important route in the pro-survival signaling of CD95 leads towards Erk1/2 activation. CD95-mediated Erk activation plays an important role especially in the central nervous system. It was for example shown that CD95 ligation activates Erk and thus induces neurite outgrowth in sensory neurons (*91*). In addition, MAP kinase activation was also observed in fibroblast, neurons and neural progenitor cells but also in gliomas and epithelial tumor cells (*95, 110, 111*).

Another interesting candidate, who is mostly associated with non-apoptotic functions of CD95, is PI3K. Activity of PI3K is typically connected to proliferation and survival upon growth factor stimulation (for review see (*112*)). PI3K is composed of a regulatory subunit, generally referred as p85 and a catalytic subunit, which is called p110. The regulatory subunit p85 is recruited to receptor tyrosine kinases (RTK), which are activated by growth factor stimulation and binds phosphorylated tyrosine residues via a Src-homology domains 2 (SH2). In the canonical PI3K pathway activation of the catalytic subunit leads to phosphorylation of the membrane lipid 'phosphatydilinositol-4,5-bis-phosphate' (PIP2) resulting in 'phosphatydilinositol-3,4,5-tris-phosphate' (PIP3). PIP3 enables

the recruitment of the 'Pleckstrin Homology' (PH) domain containing proteins, PDK1 and AKT. PDK1 phosphorylates AKT, which in turn phosphorylates many different cellular substrates mostly involved in survival and cell cycle. Interestingly, the first study showing a connection between CD95 and PI3K observed a prevention of apoptosis if PI3K was inhibited in CD95 apoptosis-sensitive glioma cells (*33*). Moreover, Gulbins *et al.* connected the CD95-mediated PI3K phosphorylation to Lyn, a member of the 'Src family kinases' (SFK) and known to get activated by CD95 ligation (*32*). In 2008, Kleber *et al.* linked CD95-induced PI3K activation to basal invasion of glioblastoma in vivo (*113*). They observed recruitment of PI3K and Yes to CD95 upon receptor activation.

In this context, phosphorylation of CD95 as a conceivable interface participating in the paradoxical signaling of CD95 has been discussed since the mid-nineties. CD95 contains two tyrosine residues in its DD at position 232 and 291 (Fig 1.2). The function of these tyrosine residues and whether they get phosphorylated upon CD95 activation is still controversial. The first study, however, showing that both tyrosine residues in the DD can be phosphorylated has been published almost two decades ago (*50*). Since then both tyrosine residues are often mentioned as potential binding sites for proteins, which are mainly participating in apoptosis-independent functions of CD95 (*113-116*). In this context Chakrabandhu *et al*. recently showed that phosphorylation indeed functions as a dominant anti-apoptosis and a pro-survival mechanism in SW480 and SW620 cells (*117*). Yet, the idea that phosphorylation serves a switch mechanism, requires the activity of kinases. Several lines of evidence exist that especially SFK are activated upon CD95 activation and might phosphorylate CD95. This was also confirmed by Chakrabandhu and colleges, since they identified Src and Yes as regulators for the detected phosphorylation of CD95 in the two cell lines (*117*). Another promising group of proteins that may be involved in affecting CD95-mediated signaling by phosphorylating CD95 are RTKs, especially the EGFR, as evidence for an interaction between both proteins exists already (*118, 119*).

Apart from downstream proteins, the composition of the PM also participates in the signaling output of CD95. In this context, membrane raft domains and phosphatidylinositol phosphates were, for example, shown to play an important role in the outcome of CD95s signaling (*94, 120*). Membrane raft domains strongly participate in the regulation of cell fate, as they control the promotion of survival

and cell death by tethering respective proteins. Most reports describing the membrane raft domains in relation to CD95 signaling link these structures with enhanced apoptosis signaling. However, depending on the context, membrane raft domains can be depleted, apoptosis signaling prevented and thus the cell fate influenced (*120, 121*). Another membrane component that typically affects cell signaling are phosphatidylinositol phosphates. As the level of individual phosphatidylinositol phosphates is regulated via the PI3K/Akt pathway, it is, as mentioned above, directly influencing CD95 signaling (*38*). Moreover, internalization and vesicular trafficking were shown to influence the signaling of CD95. In fact, not much is known about CD95 trafficking, but one study from Lee and colleges demonstrate that internalization of CD95 is indeed important for the outcome of CD95 stimulation (*122*). They showed a general requirement of CD95 internalization for ligand-induced DISC formation and apoptosis induction in type I cells. Moreover, they showed that recruitment of the DISC components predominantly occurs in the endosomal compartment and that inhibition of CD95 internalization impairs apoptosis. On the other hand, CD95 stimulation of cells that are unable to internalize CD95 results in activation of Erk and NF-κB signaling pathways.

One of the most essential modulators of the CD95-mediated cell fate is probably FasL itself. Several studies show that FasL can exist in two configurations, membrane-bound or as soluble form (sFasL) and that depending on the configuration either apoptosis or survival is induced (*4, 6, 54, 94, 106, 123, 124*). The key regulators of sFasL are metalloproteinases (MMP) and over the last years several different MMPs were identified that cleave membrane-bound FasL, such as MMP3, MMP7, MMP9 and 'A disintegrin and metalloproteinase 10' (ADAM-10) (*125*). However, the exact mechanisms about how the soluble form of FasL is changing the receptor's output are not known.

Taken together, the non-apoptotic signaling of CD95 is highly tissue-, cell type- and especially context-dependent and the question whether a ubiquitous mechanism exists that switches CD95s function towards survival remains open.

1.2 EPIDERMAL GROWTH FACTOR RECEPTOR

EGFR (also refereed as ErbB1 or Her1) belongs to the ErbB receptor family, which is one of 20 subfamilies of receptor tyrosine kinases (RTKs) (*1*). In total the ErbB receptor family has four members, which are ErbB1 (EGFR or Her1; in the following referred to as EGFR), ErbB2 (Her2/Neu), ErbB3 (Her3), and ErbB4 (Her4). The main tasks of the four members of the ErbB receptor family include proliferation, differentiation and migration during embryogenesis but they are also responsible for carcinogenesis. EGFR is the most thoroughly investigated member of the ErbB receptor family, as it is abundantly expressed and often constitutively active in different types of cancers due to activating mutations.

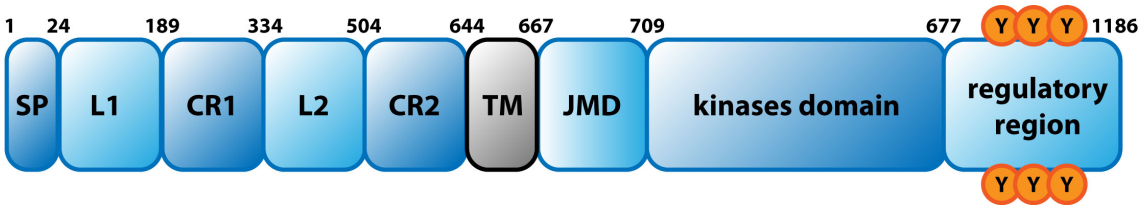

Figure 1.5: Schematic representation of an EGFR monomer.
As all four members of the ErbB receptor family, EGFR consists of an extracellular domain, which contains four subdomains including the ligand binding domain, followed by a single transmembrane helix and an intracellular domain, which contains the juxtamembrane domain, the kinase domain and a C-terminal tail, which functions as a regulatory region. The first and the third extracellular subdomain are important for ligand binding and often referred as L1 and L2; the second and fourth subdomain are cysteine-rich domains (*126*).

Like all RTKs, each ErbB receptor contains a large extracellular region, a single transmembrane helix, an intracellular juxtamembrane (JM) domain, a tyrosine kinase domain and a C-terminal regulatory region (Fig. 1.5) (*126*). The extracellular domain of the ErbB family members contains four subdomains (I-IV), where two domains (L1 and L2 or domains I and III) are homologous ligand binding domains and the other two (CR1 and CR2 or domains II and IV) are cysteine rich domains. The transmembrane domain makes a single pass through the membrane and is followed by the juxtamembrane domain, which is important for activation of the catalytic domain (*127*). The intracellular part contains the catalytic or kinase domain and the regulatory region. Activation of the receptor leads to autophosphorylation of tyrosine residues in the cytoplasmic tail and eventually to recruitment of effector proteins, which induce different signaling pathways.

1.2.1 FROM ACTIVATION TO DEGRADATION

In the ligand-unbound state EGFR exists in two conformations, the 'tethered conformation' and the 'extended conformation' (*126, 128*). In the tethered conformation, dimerization of the receptor is auto-inhibited by an interaction of the subdomains II and IV. In the extended conformation the so-called 'dimerization arm' of subdomain II is exposed, which increases the ligand binding affinity. The extended conformation is stabilized upon ligand binding (*128*). Ligand binding is accomplished by the subdomains I and III and leads to active dimer formation (*129, 130*). The main ligand for the EGFR is epidermal growth factor (EGF) but also other ligands are known to bind EGFR, such as transforming growth factor alpha (TGF-α), heparin-binding epidermal growth factor-like factor (HB-EGF), epiregulin, betacellulin and amphiregulin (*131*). An interesting feature of EGFR is that the process of dimerization is 'receptor-mediated' rather than 'ligand-mediated', which means that dimerization occurs also independently of ligand binding (*132, 133*). In fact, it is still a matter of discussion how the signaling dimer is formed. One theory suggests that dimer formation occurs between two EGF-bound receptor monomers, while another theory implies the existence of so-called pre-dimers or inactive dimers (*133, 134*). Independently from the way the dimer forms, upon ligand engagement the so-called 'signaling dimer' or 'asymmetric dimer' is formed, where the term 'asymmetric' refers to the intracellular kinase domains (*135*). In this active conformation the kinase domain of one receptor catalyzes the trans-phosphorylation of the other receptor or in other words one receptor is acting as an 'activator' and the other as a 'receiver' kinase (*135*). Phosphorylation of specific tyrosine residues in the regulatory region of EGFR leads to recruitment of several adaptor proteins, which directly interact with EGFR through either phosphotyrosine binding (PTB) domains or SH2 domains. Upon binding of the adaptor proteins different signaling pathways are activated including, for example, the Ras/Raf/MEK/ERK and the PI3K/Akt/mTOR pathway (Fig. 1.6).

One of the most important adaptor proteins binding the EGFR is growth-factor-receptor bound-2 (Grb2). Grb2 can form a complex with, for example, 'Son of Sevenless' (SOS), which leads to activation of Ras and eventually to initiation of the 'mitogen-activated protein kinase' (MAPK) cascade. This in turn leads to activation of a number of transcriptional regulators that provoke cell growth and

proliferation (*136-138*). Grb2 also activates the PI3K/Akt/mTOR signaling pathway via recruitment of Gab1 and PI3K (*112*). Activation of the PI3K/Akt/mTOR pathway is important for the regulation of the cell cycle and survival. Another essential protein that is bound by Grb2 is the ubiquitin ligase c-Cbl, which is responsible for signal termination. c-Cbl attaches ubiquitin monomers to EGFR and thus targeting the receptor for endocytosis and degradation.

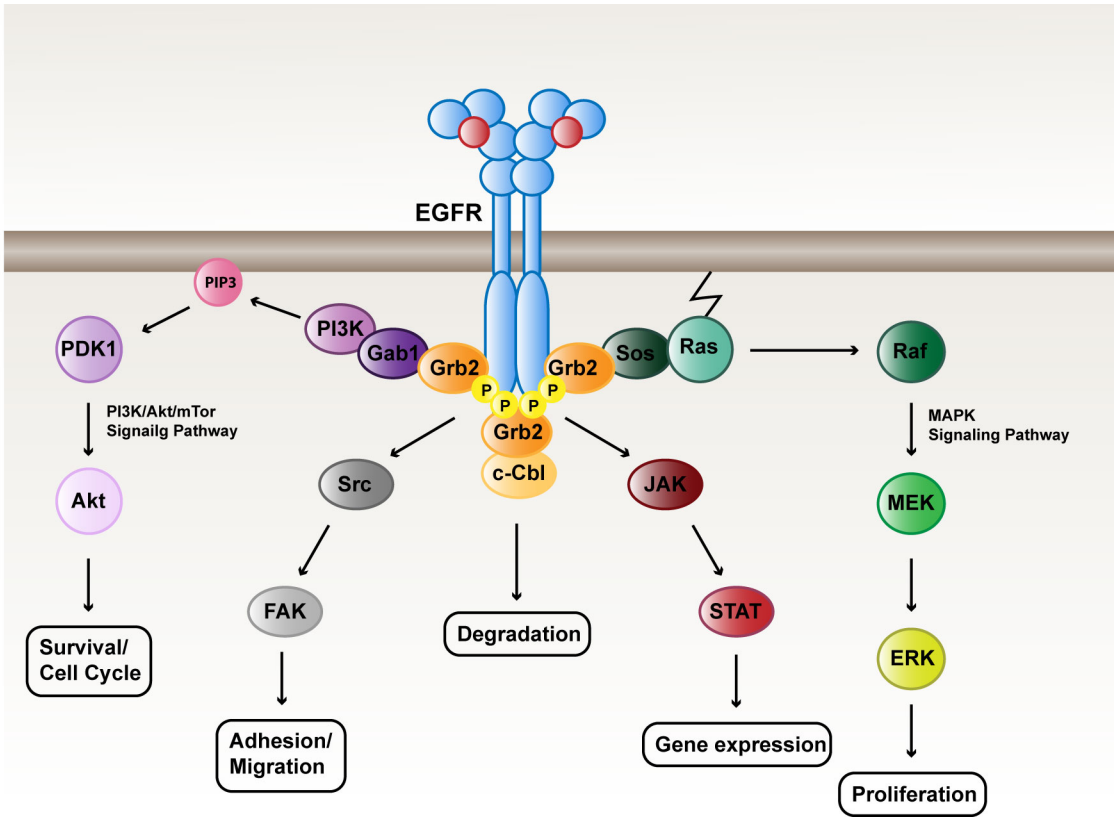

Figure 1.6: EGFR signaling network.
The schematic illustration shows some of the EGFR-activated signaling pathways, such as the PI3K/Akt/mTor signaling pathway or the MAPK signaling pathway. Upon EGFR phosphorylation specific adaptor proteins are binding to phosphorylated tyrosine or serine residues, leading to recruitment of further proteins. To the EGFR-mediated cell responses belong among other, survival, cell cycle regulation, migration and proliferation.

The process of endocytic trafficking is a crucial regulatory mechanism that ensures a robust EGFR activity in space and in time (*139-141*). Endocytic trafficking can either culminate in receptor recycling or degradation, depending on the activity state of receptor. Generally, internalization of EGFR helps to avoid an excessive receptor expression level at the PM, which would possibly elevate the basal phosphorylation and thus the activation state of EGFR. In this regard, un-ligated receptors are constitutively internalized from the PM to endosomes and

simultaneously recycled from endosomes to the PM. Therefore, the recycling rate to the PM is more or less equal to the internalization rate, which still guarantees a high level of receptors at the PM (*142*). Another important aspect about vesicular recycling is the regulation of spontaneous phosphorylation. Recently it was shown that receptor endocytosis into the perinuclear area suppresses autocatalytic phosphorylation of un-ligated EGFR monomers, as the perinuclear areas contains a high phosphatase activity (*143*). Upon ligand binding, Grb2 and c-Cbl are recruited to phosphorylated receptors, where c-Cbl polyubiquitinates EGFR and guides it into clathrin-coated pits (*144, 145*). Clathrin-coated vesicles then release their cargo after fusing with early endosomes (*141*). Early endosomes are highly dynamic and from there receptors get either rapidly recycled via the recycling endosome or early endosomes mature into late endosomes and eventually fuse to lysosomes where receptors are degraded.

Besides internalization, several other mechanisms exist that regulate the activity of EGFR. Protein tyrosine phosphatases (PTPs) play, for example, an essential role in safeguarding the EGFR activity but are also involved in positive and negative feedback loops. How crucial a tight regulation of the EGFR signaling network is can often be seen in cancer, as overexpression and hyper-activation of EGFR leads to oncogenic transformation.

1.2.2 EGFR IN CANCER

The expression of EGFR and other ErbB receptors has been described to appear in the majority of human carcinomas. On average, 50% to 70% of lung, colon and breast carcinomas have been found to express members of the ErbB family and particularly EGFR (reviewed in (*146, 147*)). The most common genetic transformation that is found in tumors with EGFR contribution is an amplification of the EGFR gene and consequently a protein over-expression. Other mechanisms of enhanced EGFR activation include overexpression of receptor ligands, loss of negative regulation pathways and activating mutations of the EGFR tyrosine kinase domain (*147*).

In non-small-cell lung cancer (NSCLC), for example, which comprises up to 80% of all primary pulmonary tumors, EGFR is expressed in up to 93% of patients. While about 45% of NSCLC patients show EGFR gene amplifications, in 17% of the

cases mutations in the EGFR tyrosine kinase are found (*148*). Although a variety of different mutations are found in the TK domain of EGFR, 89% occur in exons 19 and 21. In fact, two mutations are of particular significance; first, the deletion of amino acids 746–750 in exon 19 and a leucine to arginine substitution at 858 in exon 21 (L858R). Both mutations account for approximately 66% of all alterations found in the EGFR gene (*149*). Both mutations affect the activation loop of the kinase domain and lead to a constitutive EGFR activity even without EGF stimulation. Some NSCLCs with those mutations are reported to respond to two competitive tyrosine kinase inhibitors (TKI), namely Gefitinib and Erlotinib (*150-152*). Both TKIs are small molecules that bind to the ATP binding site of the kinase and the binding affinity of Gefitinib, for example, is about 20-fold stronger than to the wild type EGFR (*153*). However, still the majority of patients with NSCLCs show no response to both TKIs and only the combination of different therapies increases the median survival (*149, 154*).

1.3 CD95 AND EGFR – EVIDENCE FOR A LINK BETWEEN GROWTH AND DEATH

One promising candidate that may be involved in affecting the signaling of CD95 towards survival is the epidermal growth factor receptor (EGFR). The first article describing a connection between EGFR signaling and CD95 was published in 1999 by Gibson *et al*., who showed that EGF stimulation protects epithelial cells against Fas-induced apoptosis (*155*). They used two breast adenocarcinoma cell lines, T47D and MCF7 cells, as well as an embryonic kidney epithelial cell line (HEK293 cells) and successfully established a correlation between EGF-mediated RTK activation, subsequent Akt activation and apoptosis blockade in these cells. In the same year a different group published an article showing exactly the opposite effect of EGFR activation on Fas- mediated apoptosis (*156*). They showed that Fas-mediated apoptosis is enhanced by EGFR activation in human endometrial epithelial cells, since increased Fas-mediated DNA fragmentation could be detected upon EGF pretreatment. In fact, the literature connecting EGFR/EGF signaling and CD95 is ambiguous, and at points contradictory.

In this regard, one of the most puzzling examples is by far the liver. An early report shows that mouse hepatocytes were protected from FasL-induced apoptosis by EGF treatment (*157*). This protection was partially decreased when

cells were treated with two specific inhibitors that abolish the TK activity of EGFR. In rat hepatocytes it was shown that EGFR catalyzes phosphorylation of CD95 upon FasL stimulation and that both receptors interact and translocate to the PM (*119*). Further it was presented that CD95 phosphorylation and translocation is necessary for apoptosis induction and that inhibition of the EGFR association with CD95 abolished cell death. Similar observations were also described in the liver carcinoma cell line, Huh7, where Fluorescence Resonance Energy Transfer (FRET) experiments revealed a direct interaction of CD95 and EGFR upon FasL. Mutagenesis experiments identified the two tyrosine residues, Y232 and Y291, as essential for CD95–EGFR interaction and trafficking to the PM (*118*). In quiescent hepatic stellate cells (HSCs), however, FasL stimulation triggers anti-apoptotic signaling, which is dependent on a ligand-dependent EGFR phosphorylation (*123*). Unlike Musallam *et al.,* the latter publications could not detect effects on CD95 after EGF stimulation. The exact role played by EGFR in the liver seems to be highly cell type, species and context dependent.

Another interesting example, which points to a protective role of EGFR in relation to CD95, was found in human glioma cells (*158*). Steinbach and colleagues reported that FasL-induced apoptosis is enhanced after EGFR inhibition. They showed that the anti-apoptotic effect of EGFR is mediated through a caspase 8-dependent pathway. Indeed, a few years later it was shown that the tyrosine kinase Src phosphorylates procaspase-8 upon EGFR activation (*159*). Phosphorylation of procaspase-8 blocks the catalytic activity of caspase-8 and protects cells from FasL-induced apoptosis. Moreover it was shown that phosphorylated procaspase-8 supports the recruitment of the p85 subunit of PI3K and thus actively promotes the non-apoptotic signals induced by CD95 (*160*). Recently a link between EGFR, CD95 and PI3K was described also in a caspase 8-independent manner (*161*). In this study soluble FasL enhanced the motility of triple-negative breast cancers cells (TNBC), which lack estrogen and progesterone receptors and HER2. In these cells, mobility was stimulated by production of nicotinamide adenine dinucleotide phosphate-oxidase oxidase-3 (Nox3)-driven reactive oxygen species (ROS), which activates the Src kinase c-yes and eventually leads to PI3K signaling through activation of the EGFR in an EGF-independent manner. Noteworthy is a recent study showing that knockdown of CD95 and NF-κB enhanced cell death induced by the EGFR tyrosine kinase inhibitor (TKI)

Erlotinib in lung cancer cells. The authors used human lung adenocarcinoma cell lines that harbor constitutively active EGFR. They showed that even Erlotinib-resistant EGFR-mutant lung cancer models were sensitized for Erlotinib-induced apoptosis after inhibition of CD95 and NF-κB.

Taken together, the existing literature that connects CD95 and EGFR contains meaningful evidence that EGFR can affect CD95 signaling, and vice versa, which may function in regulating the balance between cell life and death.

1.4 RATIONALE

In dynamic multicellular systems, life and death signals orchestrate the surveillance of tissue homeostasis and thus help to maintain the intrinsic structure of tissues and organs. There, the response to such opposing signals is on one hand regulated by the individual cellular composition within the tissue, as one cell type, for example, expresses a certain protein that reacts to a particular stimuli and another does not and, on the other hand, by a high cell-to-cell variability among the same cell type. Especially the latter form of regulation is important for cell fate determination but yet not well understood. An essential question in this regard is for example, from where this cell-to-cell variability originates and how exactly it participates in the process of cell fate determination? It becomes particularly difficult as some proteins by themselves have a dual character. Such a protein is CD95, which is known as the classical death receptor but at the same time has several non-apoptotic functions.

The mechanisms that control the duality of CD95 are not yet completely understood and seem to be highly context dependent. In this regard, posttranslational modifications represent likely interfaces in modulating CD95's function. One promising candidate for adjusting the function of CD95 via phosphorylation is EGFR. In literature several reports describe a relation between both receptors, but so far, a clear defined function is missing.

The global objective of this work is to elucidate how the historical context of a cell influences the response properties of CD95 towards its ligand and whether this provokes CD95's duality. In this regard, activation of EGFR will be used to simulate a 'defined' cellular context, in which the responsiveness of CD95 will be

investigated towards its cognate ligand and how cell fate is influenced in such a framework. To accomplish this, the following sub-questions were addressed:

1. Do EGFR and CD95 share similarities in their spatial and temporal dynamics? How does the activity state of either protein influence the other?
2. Is there a direct interaction between both proteins? Is a potential interaction between both proteins influenced by the activity state of either protein?
3. Is CD95 phosphorylated and is this phosphorylation EGFR-mediated? How does phosphorylation affect CD95's response properties?

2. MATERIALS AND METHODS

2.1 MATERIALS

2.1.1 CHEMICALS

2-Mercapto-ethanol	SERVA Electrophoresis GmbH
Acetic acid	Sigma-Aldrich®
Ammonium persulfate (APS)	SERVA Electrophoresis GmbH
Ampicillin sodium salt	SERVA Electrophoresis GmbH
Bromophenolblue	Sigma-Aldrich®
Dimethyl sulfoxide (DMSO)	SERVA Electrophoresis GmbH
Dithiothreitol (DTT)	Fluka® Analytical
Ethanol	J.T.Baker
Ethylenediaminetetracetic acid (EDTA)	Fluka® Analytical
Fluorescein isothiocyanate	EGA-Chemie
Glycerol	GERBU Biotechnik GmbH
Isopropanol	J.T.Baker
Kanamycin sulfate	GERBU Biotechnik GmbH
Magnesium chloride (MgCl2)	Merck KG/J.T.Baker
Methanol	AppliChem GmbH
Monopotassium phosphate (KH2PO4)	J.T.Baker
N,N,N',N'-Tetramethylene-diamine (TEMED)	Sigma-Aldrich®
Para-formaldehyde (PFA)	SERVA Electrophoresis GmbH
Sodium chloride (NaCl)	Fluka® Analytical
Sodium dodecyl sulfate (SDS)	SERVA Electrophoresis GmbH
Tris-base	Carl Roth GmbH
Tris-HCl	J.T.Baker
Tritox X-100	SERVA Electrophoresis GmbH
Tween 20	SERVA Electrophoresis GmbH
UltraPure™ Agarose	Invitrogen™ Life Technologies

2.1.2 ENZYMES

AgeI-HF (10,000 U/ml)	New England Biolabs Inc.
Calf Intestinal Phosphatase (10,000 U/ml)	New England Biolabs Inc.
HindIII-HF (20,000 U/ml)	New England Biolabs Inc.
NheI-HF (20,000 U/ml)	New England Biolabs Inc.
T4-DNA ligase	Invitrogen™ Life Technologies
XhoI (20,000 U/ml)	New England Biolabs Inc.

2.1.3 ANTIBODIES

2.1.3.1 PRIMARY ANTIBODIES

Antibody	Dilution (WB)	Dilution (ICC)	Supplier
goat anti-CD95	1:500		AF326, R&D Systems, Minneapolis
goat anti-EGFR	1:1000	1:100	AF231, R&D Systems
Living colors® mouse anti-GFP	1:1000		632681, Clontech
Living colors® rabbit anti-GFP	1:1000		632593, Clontech
mouse anti-Akt	1:1000		2920, Cell Signaling Technology
mouse anti-CD95	1:500		LifeSpan BioSciences, Inc.
mouse anti-Erk	1:1000		ab36991, Abcam
mouse anti-GAPDH	1:5000		CALBIOCHEM
mouse anti-phosphotyrosine (PY72)	1:730		P172.1, InVivo Biotech Services GMBH
mouse anti-α-tubulin	1:7500		Sigma-Aldrich®
rabbit anti-Caspase-3	1:100		H-277, Santa Cruz Biotechnologies
rabbit anti-CD95	1:500		Cell Signaling Technology
rabbit anti-CD95		1:25	Santa Cruz Biotechnologies
rabbit anti-EGFR	1:1000	1:50	4267, Cell Signaling Technology
rabbit anti-GAPDH	1:2000		14C10, Cell Signaling Technology
rabbit anti-Parp	1:500		Cell Signaling Technology
rabbit anti-phoshpo Akt	1:500		9271, Cell Signaling Technology
rabbit anti-phoshpo Erk	1:500		Cell Signaling Technology

2.1.3.2 SECONDARY ANTIBODIES

Antibody	Dilution (WB)	Dilution (ICC)	Supplier
Alexa Fluor® 488 donkey anti-rabbit IgG		1:200	Invitrogen™ Life Technologies
Alexa Fluor® 546 goat anti-mouse IgG		1:200	Invitrogen™ Life Technologies
Alexa Fluor® 555 donkey anti-goat IgG		1:200	Invitrogen™ Life Technologies
IRdye® 680 donkey anti-goat IGg	1:10000		LI-COR® Biosciences
IRdye® 680 donkey anti-mouse IGg	1:10000		LI-COR® Biosciences
IRdye® 680 donkey anti-rabbit Igg	1:10000		LI-COR® Biosciences
IRdye® 800 donkey anti-goat IGg	1:10000		LI-COR® Biosciences

IRdye® 800 donkey anti-mouse IGg	1:10000	LI-COR® Biosciences
IRdye® 800 donkey anti-rabbit IGg	1:10000	LI-COR® Biosciences

2.1.4 KITS AND COMMERCIAL SOLUTIONS

2.1.4.1 MOLECULAR BIOLOGY

BigDye® Terminator v3.1 cycle sequencing kit	Applied Biosystems
100x BSA	New England Biolabs Inc.
2-log DNA ladder	New England Biolabs Inc.
DyeEx® 2.0 Spin kit	QIAGEN
NucleoBond® Xtra Maxi EF kit	Macherey-Nagel GmbH & Co. KG.
NucleoSEQ	Macherey-Nagel GmbH & Co. KG.
QIAprep® Spin Miniprep kit	QIAGEN
QIAquick® Gel Extraction kit	QIAGEN
RedSafe nucleic acid staining solution	iNtRON
10x Restriction Enzyme Buffer 1-4	New England Biolabs Inc.
Roti®-Prep Plasmid MINI	Carl Roth GmbH
T4 DNA Ligase	Invitrogen™ Life Technologies
5x T4 DNA Ligation Buffer	Invitrogen™ Life Technologies

2.1.4.2 CELL CULTURE

Dulbecco's Modified Eagle's Medium (DMEM)	PAN™ Biotech
Dulbecco's Phosphate Buffered Saline (DPBS)	PAN™ Biotech
Fetal calf serum (FCS)	PAN™ Biotech
FuGENE® HD Transfection Reagent	Promega
L-Glutamine	PAN™ Biotech
Lipofectamine® Transfection Reagent	Invitrogen™ Life Technologies
Non-essential amino acids 100x	PAN™ Biotech
OptiMEM	Gibco® by Invitrogen™ Life Technologies
Roswell Park Memorial Institute (RPMI) medium 1640	PAN™ Biotech
Trypsin/EDTA	Macherey-Nagel GmbH & Co. KG.

2.1.4.3 PROTEINBIOCHEMISTRY

30 % Acrylamide/Bis solution	Bio-Rad Laboratories, Inc.
Bradford reagent	Sigma-Aldrich®
Cell lysis buffer 10x	Cell Signaling Technology
Chameleon Duo Pre-Stained Protein Ladder	Li-Cor® Biosciences GmbH
Complete Mini EDTA-free protease inhibitor tablets	Roche Applied Science
Dynabeads® Protein G	Novex™
MES buffer	
Novex NuPAGE LDS-Sample Buffer 4x	Invitrogen™ Life Technologies
Odyssey Infrared Imaging System blocking buffer	LI-COR Biosciences GmbH
Phosphatase Inhibitor Cocktail 2	Sigma-Aldrich®
Phosphatase Inhibitor Cocktail 3	Sigma-Aldrich®
Precision Plus ProteinTM Dual Color Prestained standards	Bio-Rad Laboratories, Inc.
XT Reducing Agent 20x	Bio-Rad Laboratories, Inc.
XT Sample Buffer 4x	Bio-Rad Laboratories, Inc.

2.1.5 BUFFERS, MEDIA AND SOLUTIONS

2.1.5.1 MOLECULAR BIOLOGY

2-log DNA ladder	1 mg/ml 2-log DNA ladder (NEB) diluted in 1x DNA loading buffer (50 µg/ml)
DNA loading buffer	50% glycerol, 0.1% Orange G, 0.1 M EDTA
LB medium	10 g/l Bacto-Trypton, 5 g/l yeast extract, 10 g/l NaCl, pH7.4
LB agar	15 g/l agar in LB medium (ZE Biotechnologie, MPI Dortmund)
SOC medium	20 g/l Bacto-Trypton, 5 g/l Bacto yeast extract, 0.5 g/l NaCl, 2.5 mM KCl, 10 mM $MgCl_2$, 20 mM glucose (ZE Biotechnologie, MPI Dortmund)
1x TAE	40 mM Tris/Acetate (pH 7.5), 20 mM NaOAc, 1 mM EDTA

2.1.5.2 CELL CULTURE

4% PFA	4 % (w/v) Paraformaldehyde, 10 mM NaOH, 1x PBS (pH 7.4)
CGM-DMEM	10 % FCS, 1 % NEAA and 2 mM L-Glutamine in DMEM
CGM-RPMI 1640	10 % FCS in RPMI 1640
1x PBS	137 mM NaCl, 10 nM Na2HPO4, 2.6 mM KCl, 1.8 mM KH2PO4 (pH 7.4)
Starvation Medium (DMEM)	0.5 % FCS, 1 % NEAA and 2 mM L-Glutamine in DMEM
Starvation Medium (RPMI 1640)	0.5 % FCS in RPMI 1640

2.1.5.3 PROTEINBIOCHEMISTRY

RIPA lysis buffer	50mM Tris (pH 7.5), 150 mM NaCl, 1 mM EGTA, 1 mM EDTA, 1% IGEPAL, 0.25% Na deoxycholate, 2.5 mM Na pyrophosphate, 1 mM β-glycerophosphate, 0.1 mM PMSF
SDS running buffer	25 mM Tris-base, 192mM glycine, 0,1% SDS
SDS sample buffer 5x	60 mM Tris-HCl (pH 6.8), 25 % glycerol, 2 % SDS, 14.4 mM 2-mercapto-ethanol, 0.1 % bromo-phenolblue
1x TBS	100 mM Tris-HCl, 150 mM NaCl
1x TBS-T	100 mM Tris-HCl, 150 mM NaCl, 0.1 % Tween®-20
Transfer buffer	25 mM Tris-base, 192mM glycine, 20% methanol

2.1.6 CELL LINES

Cell line	Origin	Supplier
Cos-7	Grivet kidney fibroblast	ATCC
HCC827	Human epithelial adenocarcinoma	German Collection of Microorganisms and Cell Cultures
Huh7	Human hepato carcinoma	Kindly provided by our collaborators of University Düsseldorf

2.1.7 OLIGONUCLEOTIDES

All oligonucleotides were purchased from MWG Eurofins as unmodified DNA Oligos.

pECFP-C1-1548R	GTAACCATTATAAGCTGCAATAAAC
FAS_822-F	GTTCAACTGCTTCGTAATTGGC
Human_CD95_481	AGCAACACCAAGTGCAAAGAGGAAGGATCC
CMV-F	CGCAAATGGGCGGTAGGCGTG

2.1.8 PLASMIDS

Plasmid name	Description	Origin
CD95-mCitrine	Encoding CD95 with C-terminally fused mCitrine	Georgia Xouri @ MPI Dortmund
CD95-mTagBPB	Encoding CD95 with C-terminally fused mTagBFP	this study
CD95-mTFP	Encoding CD95 with C-terminally fused mTFP	this study
CD95-Y232,291F-mCitrine	Encoding CD95-mCitrine with point mutations Y232F and Y291F	Georgia Xouri @ MPI Dortmund

EGFR-mCherry	Encoding ErbB1 with C-terminally fused mCherry	Jenny Ibach @ MPI Dortmund
EGFR-mCitrine	Encoding ErbB1 with C-terminally fused mCitrine	Jenny Ibach @ MPI Dortmund
EGFR-mTFP	Encoding ErbB1 with C-terminally fused mTFP	Doro Vogt @ MPI Dortmund
mTagBFP-N1	mTagBFP-N1 encoding plasmid	Clontech Laboratories Inc.
mTagBFP-Rab11	encoding human Rab11 into mTagBFP-C1 vector	Jutta Luig, Lisawata Roßmannek
mTFP-N1	mTFP-N1 encoding plasmid	Evrogen Laboratories Inc.
PTB-mCherry	Encoding PTB domain from Shc with C-terminal mCherry	Jenny Ibach @ MPI Dortmund
SNAP-ErbB1 K721A	Encoding SNAP-ErbB1 with point mutation K721A	Jenny Ibach @ MPI Dortmund

2.1.9 LIGANDS AND INHIBITORS

EGF, human	Sigma-Aldrich®
Erlotinib	Cayman Chemical
***Super*FasLigand™**	Enzo Life Sciences, Inc.

2.1.10 EQUIPMENT

1.5 mm 10-well combs	Invitrogen™ Life Technologies
1.5 mm cassettes for western blots	Invitrogen™ Life Technologies
35-mm MatTek petri dishes	MatTek Corporation
4-well LabTek chambers	Nunc by Thermo Fischer
8-well LabTek chambers	Nunc by Thermo Fischer
BD LSM II Flow Cytometer	BD Bioscience
BioRad ChemiDoc™ XRS	Bio-Rad Laboratories, Inc.
BioRad Power Pac HC	Bio-Rad Laboratories, Inc.
Cell scraper 16cm 2-Pos.-blade	Sarstedt AG and Co.
Centrifuge 5415R	Eppendorf
Centrifuge 5810R	Eppendorf
Centrifuge RC 26 Plus	Sorvall®
Cuvettes (1 ml) Ref. 67.742	Sarstedt Aktiengesellschaft & Co.
ddH_2O	Millipore
Dual Plate xCELLigence	Roche Applied Science
Eppendorf safe lock tubes (0.5/1.5/2 ml	Eppendorf
Falcon tubes (15/50 ml)	BD Falcon™
Heatable magnetic stirrer 'IKMAG®RCT'	IKA®Labortechnik
Incubation box for western blots	LI-COR Biosciences
Mini and Midi agarose gel chamber	Carl Roth GmbH
Molecular Imager Gel Doc XR	Bio-Rad Laboratories
NALGENE® Cryo 1 °C freezing container	Nunc by Thermo Fischer

Nanodrop® ND-1000 spectrophotometer	Peqlab Biotechnologie GmbH
Nuaire™ Cellgard Class II Biological Safety Cabinet Integra Biosciences	Integra Biosciences
NuPage 4-12% Bis-Tris Gel	Novex by Life Technologies
Odyssey Infrared Imager	Licor® Biosciences
Parafilm®	Pechiney Plastic Packaging
Pipetboy acu	Integra Biosciences
PVDF membrane	Bio-Rad Laboratories, Inc.
Sarstedt serological pipettes (5/10/25 ml)	Sarstedt AG & Co.
T25 tissue culture flask	Sarstedt AG and Co.
T75 tissue culture flask	Sarstedt AG and Co.
Test tube rotator 34528	Snijders
Tissue culture plates (24-well)	Sarstedt AG and Co.
Tissue culture plates (6-well)	Sarstedt AG and Co.
Vacuum centrifuge	Eppendorf
Vi-CellTM XR cell viability analyzer	Beckman Coulter, Inc.
XCell II™ Blot Module	Invitrogen™ Life Technologies
XCell SureLock™ Mini-Cell Electrophoresis System	Invitrogen™ Life Technologies

2.1.11 MICROSCOPES

Cell^R	Olympus
Fiber coupling unit	PicoQuant GmbH
Fluo View FV1000	Olympus
HCX PL APO 40x/1.25- 0.75	Leica MICROSYSTEMS
HCX PL APO (λ blue) 63x/1.4	Leica MICROSYSTEMS
HCX PL APO CS2 63x/1.4	Leica MICROSYSTEMS
IU-LH75XEAPO: 75W xenon APO lamp	Olympus
IX 81: inverse microscope	Olympus
IX2-UCB controlling unit	Olympus
Leica TCS SP5	Leica MICROSYSTEMS
Leica TCS SP8	Leica MICROSYSTEMS
LUCPlanFL N 40x/0.6	Olympus
Orca/ER CCD camera	Hamamatsu
PR-IX2 motorised stage	Olympus
Scan Stage	Olympus
Sepia II	PicoQuant GmbH
U-HSTR2: hand switch	Olympus
U-RFL-T	Olympus
UPlanSApo 60x/1.35 NA	Olympus
UPLSApo 20x/0.75 NA	Olympus
UPLSApo 40x/0.9 NA	Olympus
UPLSApo 60x/1.2 NA	Olympus

2.1.12 SOFTWARE

Adobe Illustrator CS4	Adobe Systems Inc.
ApE	http://biologylabs.utah.edu/jorgensen/wayned/ape/
BD FACSDiva v6.1.2	
Fiji	Schindelin et al. Nat. Meth. (2012)
FlowJo v10.1r5	FlowJo
FV10-ASW Fluoview Software	Olympus
Igor Pro v6.35A5	Wavemetrics
ImageJ64 v1.48i	http://imagej.nih.gov/
Leica Application Suite	Leica
Microsoft Office 2011	Microsoft Corporation
Prism 6	GraphPad Software, Inc.
RTCA Software v2.0	ACEA Bioscience, Inc.
SymPhoTime v5.12	Picoquant GmbH
VirtualBox v5.0.8	Oracle Corporation

2.2 METHODS

2.2.1 MOLECULAR BIOLOGY

2.2.1.1 SUBCLONING

Subcloning is a technique in molecular biology to move a certain gene of interest from one vector to another. Therefor the gene of interest is in a first step released from the parent vector by restriction digestion, purified by agarose gel electrophoresis and eventually inserted into the destination vector, which also is cut via restriction enzymes. In the following all required steps are explained in detail.

2.2.1.2 RESTRICTION DIGESTION

Restriction digestions are accomplished by the use of restriction endonucleases, which are enzymes that cut dsDNA at particular recognition sites within the DNA molecule, the so-called restriction sites. Each enzyme has a specific restriction site and usually inserts double strand breaks. The most commonly used group of restriction enzymes are the restriction endonucleases type II, which recognize mainly palindromic dsDNA sequences and either leave sticky ends or blunt ends. For subcloning it was targeted to find common restriction sites in the parent and the destination vector.

For each digestion reaction mix an appropriate amount of dsDNA, generally between 1-5 µg dsDNA was used and mixed with the enzyme specific 10x restriction buffer, 100x BSA if indicated, abundant restriction enzyme (usually 2-5 U/µ of DNA) and ddH_2O ad 30 µl or 50 µl, depending on the amount of dsDNA.

2.2.1.3 DEPHOSPHORYLATION OF 5'-PHOSPHORYLATED DNA FRAGMENTS

To inhibit self-ligation of the destination vector DNA, the 5'-end of the cut vector can be dephosphorylated by alkaline phosphatase. For dephosphorylation, 1 U/µg DNA CIP was added to the restriction digest reaction mix and incubated for an 1 h at 37 °C.

2.2.1.4 AGAROSE GEL ELECTROPHORESIS

Agarose gel electrophoresis is used to separate DNA fragments according to their size. Due to negatively charged phosphates on the backbone of DNA molecules, the net-charge of DNA is negative. By creating an electric field negatively charged DNA molecules migrate to the positively charged anode. Depending on the size of the DNA fragments, the distance of migration in the electric field is dependent on the pore size of the agarose matrix, as the mass to charge ratio per DNA fragment is the same. The pore size of the agarose matrix is dependent on the agarose concentration used per gel and chosen according to the size of the DNA fragments to be separated.

For all gels 1-2% agarose (1 % for DNA fragments of 0.5-7.0 kb, 1.5% for 0.3-3.0 kb and 2 % for 0.1-1.0 kb) was melted in 1x TEA buffer and supplemented with RedSafe nucleic acid staining solution (1:20000). RedSafe is a chemical dye that intercalates into dsDNA molecules and allows for DNA visualization if exited with UV light. RedSafe has two excitation maxima one at 309 nm and the other one at 419 nm and its fluorescence emission is at 537 nm. After cooling down the gel to RT and polymerization, gels were placed into electrophoresis chambers and filled with 1x TEA buffer. Samples containing the DNA fragments to be separated were mixed with DNA loading buffer (6x) and loaded into the gel. Electrophoresis was performed at constant voltage of 100-120V, depending on the size of the gel, for

about 20-30 min. For proper size to distance correlation of the separated DNA fragments 2-log DNA ladder was used.

2.2.1.5 ISOLATION OF DNA FRAGMENTS FROM AGAROSE GELS

To isolate DNA fragments (70 bp to 10 kb, up to 10 µg) from agarose gels the QIAquick® Gel Extraction Kit was used according to the manufacturer's protocol. First, the DNA fragments of interest were excised from the agarose gel and dissolved in the provided buffer at 50 °C for approximately 10 min while shaking. For DNA purification specific columns are provided, which bind DNA to a silica-membrane under high salt conditions. Contaminating proteins, agarose but also small DNA fragments (<50 bp) were washed out and in a final step the DNA of interest was eluted in 30-50 µl EB. The quality and concentration of the DNA was measured with a Nanodrop® spectrophotometer at a wavelength of 260 nm. The DNA quality was determined by measuring the 260/280 nm and the 260/230 nm ratios.

2.2.1.6 LIGATION OF DNA FRAGMENTS

To catalyze the insertion of the gene of interest into the destination vector T4-DNA ligase was used, which links the 3'-hydroxy and 5'-phosphate ends of double-stranded DNA. For each ligation mix 50 ng destination vector was used and different amounts of insert, usually a three-fold and a five-fold molar excess of the insert DNA. The actual amount of insert DNA was calculated according to the following formula:

$$Amount\ insert\ [in\ ng] = \frac{amount\ vector\ [in\ ng] \times insert\ size\ [in\ bp]}{vector\ size\ [in\ bp]}$$

The destination vector and the appropriate amounts of insert DNA were mixed with 5 x T4 DNA ligase buffer, 1 U T4 ligase and ddH_2O ad 20 µl. Ligation reaction was incubated overnight at 16 °C.

2.2.1.7 TRANSFORMATION OF CHEMICALLY COMPETENT E.COLI

For chemical transformations the competent bacterial cells *E. Coli XL 10 Gold* were used. First, 100 µl of cells were mixed with 3.25 µl of 2.25 mM DTT and divided into 50 µl aliquots. For each transformation 50 µl of cells were inoculated with 5 µl ligation mix, incubated on ice for 30 min and head shocked for 45 sec at 42 °C. After cooling down the tubes on ice for about 2-5 min, 250 µl SOC medium was added to the transformation mix and tubes were incubated for at least one hour at 37 °C, 225 rpm shaking. Finally the transformed bacteria cells were plated on agar plates containing the appropriate antibiotics and incubated at 37 °C overnight.

2.2.1.8 DNA PREPARATION USING QIAprep® Spin Miniprep Kit

To isolate plasmid DNA from transformed bacteria, the *QIAprep*® Spin Miniprep Kit was used by following the manufacturer's protocol. Generally, 5 ml LB medium supplemented with appropriate antibiotic was inoculated with bacterial cells transformed with the desired plasmid DNA and incubated overnight at 37 °C. On the next day cell suspension was centrifuged at 5000 x g at 4 °C to harvest the cells and processed as described in the manufacturer's protocol with cell lysis and DNA isolation. In a final step the purified plasmid DNA was eluted in 30 µl EB or ddH_2O.

2.2.2 CELL CULTURE

2.2.2.1 CULTIVATION OF IMMORTALIZED MAMMALIAN CELLS

The human hepatocyte derived carcinoma cell line Huh7 and the money kidney derived cell line Cos-7 were maintained in DMEM supplemented with 10% FBS, 1% L-glutamine and 1% NEAA. The non-small-cell lung carcinoma cell line HCC827 was cultured in RPMI 1640 medium supplemented with 10% FBS. All cell lines were grown at 37 °C in a humidified incubator with 5% CO_2. In order to avoid overgrowth of the cells, cells were split once cell density reached 80-90% confluency. Therefor, the medium was aspirated, the flask washed with DPBS and the cells detached from the dish with trypsin/EDTA solution (0.05% / 1 mM). After

5 min incubation at 37 °C, the enzymatic reaction was stopped by adding 10 ml CGM containing 10% FBS. Detached cells were transferred into a falcon tube and gently triturated with the 1ml pipet. To determine the cell number 500 µl of the cell suspension was used and counted with the Vi-Cell™ XR cell viability analyzer. Finally, the volume containing the desired cell number was calculated and seeded into fresh flasks or other cell culture dishes if required.

2.2.2.2 CRYO-PRESERVATION OF MAMMALIAN CELLS

For long-term storage of cell lines cryo-stocks were prepared and stored at temperatures below -80 °C. To avoid intracellular ice formation and thus increase cell viability after thawing, cryo-stocks were supplemented with the cryo-preservative DMSO.

For cryo-stock preparation T75 flasks were split as described above and cells were diluted in cryo-media (for HCC827: 60% RPMI 1640, 30% FBS and 10% DMSO; for all other cell lines: 90% CGM and 10% DMSO) at a concentration of 1.5 x 10^6 cells/ml. Cell suspension was applied into pre-cooled cryo vials and transferred to a NALGENE® Cryo 1 °C freezing box filled with isopropanol, which allows for a controlled freezing rate of 1 °C/min. Freezing boxes were kept at -80 °C overnight and on the next day the cryo-stocks transferred to a -150 °C freezer for long term storage.

Thawing of cells was done as quickly as possible in a 37 °C water bath. The cell suspension was after complete thawing transferred to pre-warmed culture flasks containing 10 ml CGM. On the next day medium was exchanged to remove DMSO and death cells.

2.2.2.3 TRANSIENT TRANSFECTION WITH PLASMID DNA

Cells were transiently transfected with FuGENE® HD Transfection Reagent or Lipofectamine® Transfection Reagent according to the manufacturer's guidelines. Both transfection reagents are based on lipofection, where liposomes are formed, which contain the plasmid DNA and are able to fuse with the cell membrane to release the genetic material into the cells.

Depending on the planned experiments cells were seeded in the appropriate culture dish one or maximum two days before transfection. The seeded cell density was chosen accordingly to the culture dish, the used transfection reagent and the seeding time point but always targeted to reach 50-80% confluency for transfections with the FuGENE® HD Transfection Reagent or 90% confluency for Lipofectamine® Transfection Reagent. The amount of DNA was dependent on the culture dish and the amount of transfection reagent was used in the following DNA to transfection reagent ratios: FuGENE® HD Transfection Reagent to DNA 3:1 and Lipofectamine® Transfection Reagent to DNA 2.5:1.

On the day of transfection the recommended end volume of serum free media (SFM) was divided into two tubes and into one tube the respective volume of transfection reagent was added and into the second tube the DNA. Both tubes were left aside for 5 min at RT and then mixed together. Next, the whole mix was incubated for 15-20 min at RT to allow complex formation. Finally the transfection reagent – DNA complexes were added drop wise to the cells and dishes were carefully swung. Cells were incubated at 37 °C in a humidified incubator with 5% CO_2 until next day.

2.2.2.4 REAL TIME CELL ANALYSIS (RTCA)

Real time cell analysis is a method, where the development of the cell number is measured over time by determining the impedance-based cell index (CI), which is a dimensionless parameter. RTCA assays are performed in specific 16-well E-plates with gold electrodes at the dish bottom to evaluate the ionic environment at the electrode/solution interface. The Dual Plate xCELLigence instrument correlates then this information to the cell number over time.

RTCA assays were performed with HCC827 cells and for each assay about 7.5 x 10^3 cells were seeded per well. Before the cells were added to the dishes 100 µl CGM-RPMI was used to measure a blank value to subtract the background. Afterwards the cells were added in another 100 µl CGM-RPMI so that the final volume was 200 µl per well. The dishes were then placed into the RTCA machine, which is stored in a humidified incubator at 37 °C and 5% CO_2. The CI was monitored every 15 min for up to 120 hours. After 24 hours in which the cells reached a steady growth, the desired treatment was applied. Each condition in

each assay was performed in duplicates. For better comparison of the individual stimuli the cell index was normalized to 1 at the time point of FasL administration. To finally summarize the individual experiments, each data set was normalized to the untreated condition and displayed as percentage from the untreated condition.

2.2.3 PROTEIN BIOCHEMISTRY

2.2.3.1 PREPARATION OF WHOLE CELL LYSATES

Whole cell lysates were prepared from cells cultured either in 6-well cell culture plates or in 6 cm cell culture dishes. Cells were places on ice, cell culture medium was removed and cells were washed once with ice-cold PBS. Shortly before use cell lysis buffer was supplemented with Complete Mini EDTA-free protease inhibitor cocktail and the phosphatase inhibitor cocktail 2 and 3. If cultured in 6-well cell culture plates 50 µl ice-cold cell lysis buffer was added to the cells and incubated for 5 min. For cells cultured in 6 cm cell culture dishes 400 µl ice-cold cell lysis buffer was used. After the 5 min incubation on ice cells were scraped and suspension transferred to pre-cooled 1.5 ml reaction tubes. Cell debits were removed from lysates by using a conventional tabletop centrifuge for 15 min at 13000 rpm and 4 °C. Supernatants were carefully transferred into fresh pre-cooled 1.5 ml reaction tubes and protein concentration was determined. If experiment was continued on a different day samples were flash-frozen in liquid nitrogen and stored at -80 °C.

2.2.3.2 PROTEIN CONCENTRATION DETERMINATION WITH BRADFORD REAGENT

Bradford-Assay is a photometrical method in which the Bradford-reagent, Coomassie brilliant blue G-250, is binding to hydrophobic amino acid residues in the solution of interest, leading to a change of its absorbance maximum. Is the dye in a complex with proteins the blue form of the dye is stabilized and its absorbance maximum is shifted from 465 to 595 nm. In combination with a calibration measurement the absorbance at 595 nm can be correlated to the protein concentration within the solution of interest.

The protein concentration of all cell lysates was determined by using the Bradford assay according to the manufacturers protocol. Briefly, protein standards

were prepared by a serial dilution of a 1 mg/ml BSA stock solution in ddH_2O to obtain concentrations ranging from 1-16 µg/µl in a total volume of 500 µl. Each standard was prepared in a separate plastic cuvette and 500 µl Bradford reagent was added to receive a total volume of 1 ml. Also for all samples of interest a total volume of 1 ml was prepared in a separate plastic cuvette, composed of 500 µl ddH_2O, 500 µl Bradford reagent and 1 µl cell lysate. The absorption values were measured at 595 nm in a spectrophotometer. To calibrate the spectrophotometer a blank sample was used composed of 500 µl ddH_2O, 500 µl Bradford reagent and 1 µl lysis buffer. The measured absorption values were plotted against the standard protein concentrations and the resulting standard curve was then used to calculate the protein concentration of the samples of interest.

2.2.3.3 SAMPLE PREPARATION FOR SDS-PAGE

After determination of the protein concentration samples were prepared for SDS-PAGE. 25-50 µg of total protein were mixed with 4x sample buffer supplemented with 50 mM DTT as reducing reagent and an appropriate volume of lysis puffer to receive a total volume of max 40 µl for 10 well gels and max 20 µl for 15 well gels with a thickness of 1.5 mm. After short centrifugation, samples were heated for 10 min at 70 °C to denature the protein structure and after cooling down on ice again briefly centrifuged. If experiment was continued on a different day samples were stored at -20 °C.

2.2.3.4 DENATURING SDS-POLYACRYLAMIDE GEL ELECTROPHORESIS (SDS-PAGE)

SDS-PAGE (Sodium-dodecylsulfate-polyacrylamid-gelelectrophoresis) is used to separate proteins in solution according to their size. SDS is an anionic detergent, which binds proteins, linearizes them and eventually creates a negative net-charge of the SDS-protein complex. By creating an electric field the linearized, negatively charged proteins migrate to the positively charged anode. Depending on the size of the protein the distance of migration in the electric field is proportional to the pore size of the polymerized acrylamide. The pore size is dependent on the amount of polyacrylamide and this was chosen accordingly to the molecular weight of the protein of interest.

For all SDS-PAGEs the Invitrogen-gel-system was used, which provides gel cassettes of 1.5 mm thickness. Each cassette was first filled with the separating gel and subsequently after polymerization of the separating gel the stacking gel was poured on top. Depending on the amount of samples either 10- or 15-well combs were inserted into the stacking gel and stayed inside the gels until samples were loaded. All gels were prepared using the following compositions:

	Compounds	8% Gel	10 % Gel	12 % Gel
Separation Gel	ddH_2O	9.3 ml	7.9 ml	6.6 ml
	Acrylamide 30%	5.3 ml	6.7 ml	8.0 ml
	1.5 M Tris (pH 8.8)	5 ml	5 ml	5 ml
	10% SDS	200 µl	200 µl	200 µl
	10 %APS (w/v)	200 µl	200 µl	200 µl
	TEMED	12 µl	8 µl	8 µl
	TOTAL	20 ml		
Stacking Gel	ddH_2O	6.8 ml		
	Acrylamide 30%	1.7 ml		
	1 M Tris (pH 6.8)	1.25 ml		
	10% SDS	100 µl		
	10 %APS (w/v)	100 µl		
	TEMED	10 µl		
	TOTAL	10ml		

After gel polymerization combs were carefully removed, pockets washed with ddH_2O and gels placed into a gel electrophoresis chamber (Invitrogen) filled with 1x running buffer. Protein samples were filled into individual pockets, while the first pocket was regularly used for the protein standard to determine size differences of the separated protein. If some individual pockets remained empty they were filled with sample buffer. Gel electrophoresis was performed first at 80 V until samples entered the separation gel and then voltage was increased to 130 V for approximately 1.5h.

For some assays commercial 4-12 % Bis-Tris precast gels (Novex) were used to separate proteins in a range of 3.5-200 kD according to the manufacturers instructions. The main differences to the above described procedure are the following: For gel electrophoresis with precast gels MES buffer supplemented with an antioxidant instead of the 1x running buffer was used and electrophoresis was performed at 200 V for approximately 40 min.

2.2.3.5 WESTERN BLOT

Western blotting is one form of immuno-blotting, in which electrophoretically separated proteins are transferred to a nitrocellulose or PVDF membrane, where the proteins of interest can get detected with antibodies.

All Western blots were performed with the XCell™ II wet tank blot modules according to manufacturer's instructions. After SDS-PAGE the stacking gel was removed and the separation gel was placed into ice-cold transfer buffer. After activation of PVDF membrane in methanol for 2-5 min also the membrane, two pieces of Whatman filter paper and the sponges for the blotting sandwich were placed into ice-cold transfer buffer to equilibrate. The blotting sandwich was then build as follows: two layers of blotting sponges, the first Whatman filter paper, gel, PVDF membrane, the second Whatman filter paper and finally three more sponges. The blotting module was placed in a running chamber, filled with transfer buffer and transfer was carried out for 1 h and 15 min at 40 V.

After the transfer membranes were moved into a Li-Cor® incubation box filled with Li-Cor® Odysseys blocking buffer and incubated for 1 h at room temperature on a shaker. For visualization of the proteins of interest, the blots were incubated with appropriate primary antibodies diluted in blocking buffer overnight at 4 °C on a shaker. On the next day, the membranes were washed three times for 10 min with TBS/T and incubated with appropriated secondary antibodies diluted in blocking buffer for 1 h at RT, shaking. The membranes were washed three times again with TBS/T and finally scanned with the Odyssey Imaging System.

2.2.3.6 IMMUNOPRECIPATION

Cell lysis and protein quantification were accomplished as described in 2.2.3.1 and 2.2.3.2. All Immunoprecipitations were done with magnetic Protein-G Dynabeads®. Before Dynabeads® were used the desired amount of beads was washed twice with 0.02% Tween®-20 in PBS to remove the preservative sodium azide. After sample preparation and concentration determination, the required volume of total cell lysate, to receive about 200-400 µg protein was mixed with lysis buffer to obtain a total volume of 200 µl per sample. To each sample the appropriate primary antibody was added and incubated overnight at 4 °C on a wheel-over-wheel-shaker. On the next day, about 15 µl Dynabeads® were added to each sample and again rotated for 2h at 4°C. Next, samples were washed 5 times with 300 µl lysis buffer and with the last wash step samples were transferred into new tubes. Proteins were re-suspended by adding 8 µl 4X NuPAGE® sample buffer and 16 µl lysis buffer. Finally, the samples were vortexed, briefly centrifuged (800 x g) and boiled for 10 minutes at 75°C. Western Blotting was performed as described in section 2.2.3.5. If SDS-PAGE was not immediately done samples were stored at - 20°C.

2.2.3.7 IMMUNOFLUORESCENCE

Transfected cells were first treated as desired and then fixed with 4% paraformaldehyde in PBS for 10 min at RT. Afterwards, the fixed cells were washed once with 50 mM NH4Cl/PBS for 5 minutes and then twice with TBS for 5 min at RT. Next, the cells were permeabilized with 0.1% TritonX-100 in TBS for 5 min at RT, followed by three wash steps with TBS for 5 min at RT. After washing, cells were blocked with Li-Cor® Odysseys blocking buffer for 30 min at RT and then incubated with the primary antibodies for 60 min at RT. Cells were washed three times with TBS and secondary antibodies were applied for 30 min at RT. After three further washing steps with TBS, the cells were incubated with Hoechst-reagent diluted in TBS (1:10000) for 15 min at RT and then washed once with water. Finally, cells were imaged in PBS with the appropriate microscope. If not imaged directly, cells were stored in 1% azide in TBS at 4 °C.

2.2.4 FLOW CYTOMETRY

Transfected cells were first treated as required and then stained with the PE Annexin V Apoptosis Detection Kit I according to the manufacturer's instructions. Briefly, medium was removed and transferred into pre-cooled Falcon™ round-bottom tubes. Cells were washed with cold PBS and the supernatant also collected in the tubes. To detach cells trypsin/EDTA solution (0.05% / 1 mM) was added and cells were incubated for 5 min at 37 °C. Detached cells were transferred into the Falcon™ tubes and culture dishes were rinsed with PBS to collect all the cells. Cell suspension was centrifuged at 1000 rpm for 5 min. Meanwhile, the staining mix was prepared, composed of 1X Binding Buffer supplemented with PE Annexin V and 7-AAD (5 µl per sample). After centrifugation the supernatant was discarded, cells were re-suspended in 100 µl staining mix and gently vortexed. Samples were incubated for 15 min at RT in the dark and measured with the BD LSR II Cytometer.

PE Annexin V and 7-AAD were excited with the 488 nm laser line (Coherent Sapphire™). For PE Annexin V the 530/30 nm longpass dichroic excitation-filter was used and fluorescence was detected using the 515/45 nm filter. The PMT was set to 330V. For 7-AAD the 695/40 nm longpass dichroic excitation-filter was used and fluorescence was detected using the 675-715 nm filter. The PMT was set to 450V. The forward (FSC) and side scatter (SSC) signals were also generated with the 488 nm laser. For instrument control and data acquiring the BD FACSDiva Software 8.0.1 was used. All data sets were analyzed with FlowJo v10.1r5.

2.2.5 MICROSCOPY

2.2.5.1 WIDEFIELD MICROSCOPY

Fluorescence images were obtained with an Olympus Cell^R IX81 inverted microscope. Excitation of fluorophores was done with a MT-20 150 W mercury arc burner. The following table lists the excitation and emission filters:

Plasmid name	Excitation filter	Dichroic mirror	Emission filter
TagBFP	BP425-445	U-M3DAFITR	BA460-510
mCitrine	BP490-500HQ	DM505	BA515-560HQ
mCherry	BP545-580	DM600	BA610IF

Images were sequentially acquired using a 40x air objective and an Orca CCD camera. For instrumental control and data acquisition the Cell^R software was used.

2.2.5.2 LASER SCANNING MICROSCOPE (LSM)

2.2.5.2.1 OLYMPUS FLUOVIEW FV1000

Confocal image were recorded with an Olympus FluoView FV1000 confocal laser-scanning microscope. The excitation source, wavelength and the respective emission filter bandwidth are presented in the table:

Plasmid name	Laser	Wavelength (nm)	Emission bandwidth (nm)
TagBFP	UV	405	425-478
mTFP	Multiline Argon	458	468-500
Alexa Fluor® 488	Multiline Argon	488	498-550
mCitrine	Multiline Argon	488	525-550
mCherry, Alexa Fluor® 546, Alexa Fluor® 555	DPSS	561	571-671

For sequential image recording the laser beam was separated using a SDM510 beam splitter to spectrally separate blue and yellow fluorescence and a SDM560 beam splitter to separate yellow and red fluorescence. For TagBFP or UV dyes a SDM490 emission beam splitter was used. Excitation light was focus towards the sample either by a 60x/1.35 NA oil objective or a 40x/0.9 NA air objective. Depending on the used fluorophore combinations either the DM405/488/561/633 or the DM458/515 dichroic mirror was used. Fluorescence was detected with a photomultiplier tube (PMT). Live cell imaging was done in an incubation chamber adjusted to 37 °C and if cells were fixed images were recorded at RT.

2.2.5.2.2 LEICA

Time-lapse microscopy was performed either with the Leica TCS SP5 confocal laser-scanning microscope or the Leica TCS SP8. The excitation source, wavelength and the respective emission filter bandwidth are listed in the table:

Plasmid name	Laser	Wavelength (nm)	Emission bandwidth
TagBFP	UV	405	425-478
mTFP	Argon or WLL	458	468-500
Alexa Fluor® 488	Argon or WLL	488	498-550
mCitrine	Argon or WLL	488	525-550
mCherry, Alexa Fluor® 546, Alexa Fluor® 555	DPSS or WLL	561	571-671

On the Leica Sp5 Acousto-optical tunable filters (AOTF) were used to select excitation wavelengths and the following excitation and emission filter cubes are used:

Filter cube	Excitation filter	Dichronic Mirror	Emission filter
CFP/TFP	BP 436/20 nm	455 nm	BP 480/40 nm
YFP	BP 500/20 nm	515 nm	BP 535/30nm
N2, 1	BP 515/560 nm	580 nm	LP 590 nm

The excitation light on the SP5 was focus into the sample by a HCX PL APO lambda blue 63.0x/1.40 oil objective. Fluorescence was detected with PMTs. On the Leica Sp8 excitation modulation is also achieved by AOTFs, with the following excitation and emission filter cubes:

Filter cube	Excitation filter	Dichroic Mirror	Emission filter
DAPI	BP 350/50 nm	435 nm	BP 460/50 nm
CFP/TFP	BP 436/20 nm	455 nm	BP 480/40 nm
GFP	BP 470/40 nm	500 nm	BP 525/50 nm
RHOD LP	BP 540/45 nm	580 nm	LP 590 nm

On the Leica SP8 the excitation light was focus into the sample by a HC PL APO CS2 63x/1.40 NA oil objective and fluorescence was either detected with PMTs or HyD

detectors. Live cell imaging was done in an incubation chamber adjusted to 37 °C and humidified with 5% CO_2.

2.2.5.3 FLUORESCENT LIFETIME MICROSCOPY (FLIM)

Fluorescence lifetime imaging microscopy (FLIM) is one of the most advanced fluorescence-based quantitative method and especially suitable to spatially resolve protein interactions. In particular, FLIM is basically a specialized method to analyze Förster resonance energy transfer (FRET) in a biochemical context (*162*). FRET is the non-radiative transfer of energy, resulting from dipole-dipole coupling between two fluorophores that are within a few nanometers of each other. The efficiency of FRET depends on the condition that the emission spectrum of the donor fluorophore sufficiently overlaps the excitation spectrum of the acceptor and the relative orientation of the fluorophores (*163*).

FRET reduces the fluorescence lifetime (τ) of the donor fluorophore, as it provides an additional channel through which the excited donor fluorophore can decay. The advantage of FRET-FLIM over other FRET monitoring techniques is predominantly that the lifetime reduction of the donor fluorophore is independent of the fluorescence intensity (both of donor and acceptor) and therefore also of bleaching (*162*).

The donor lifetime can be determined either in the time-domain or in the frequency-domain. For time-domain FLIM measurements the donor of the FRET pair is excited with a short laser pulse and its fluorescence emission, which decreases exponentially over time, is monitored. Thereby the laser pulse should be preferably shorter than the lifetime of the fluorophore (*164*). To obtain the fluorescence lifetime from experimental time-domain data, the fluorescence decay is fitted to a function describing the exponential decay (*164*). If the sample contains a single fluorescent species, the fluorescence decay is ideally fitted to a mono-exponential decay model:

$$\mathbf{I(t) = I_0 e^{-t/\tau}}$$

I(t) = fluorescence intensity at time t; I_0 = fluorescence intensity at t = 0; τ = fluorescence lifetime.

If the sample contains both, donor fluorophores and donor-acceptor pairs undergoing FRET, the lifetime of the donor fluorophore population has two components, τ_1 and τ_2, and the fluorescence decay model is bi-exponential:

$$\mathbf{I(t) = A_1 e^{-t/\tau_1} + A_2 e^{-t/\tau_2} + B}$$

A_1 and A_2 = amplitudes; B = background

To determine the donor fluorescence lifetime in the frequency-domain, the donor is excited with an intensity-modulated light source. Due to the inherent fluorescence lifetime of the fluorophore the emitted donor fluorescence is demodulated and phase-shifted relatively to the excitation light source. Both properties can be used to determine the lifetimes [REF]:

$$\boldsymbol{\tau_\phi = \omega^{-1} tan\, \phi} \quad \text{and} \quad \boldsymbol{\tau_m = \frac{1}{\omega}\left[\frac{1}{m^2} - 1\right]^{\frac{1}{2}}}$$

τ_ϕ = phase lifetime; τ_m = modulation lifetime

All functions are dependent on the fluorescence lifetime of the donor molecules, which is an intrinsic property of the specific fluorophore and independent of the fluorophore concentration, excitation intensity and light path length (*164*). In addition, the fraction of FRETing molecules can be calculated.

2.2.5.3.1 DATA ACQUISITION

FLIM measurements were acquired on the Olympus FluoView FV1000 laser scanning confocal microscope equipped with an external PicoQuant's time correlated single photon counting (TCSPC) system, PicoHarp 300. The pulsed lasers (repetition rate of 40 MHz) used for time-domain FLIM are coupled to the FV1000 through an independent port and are controlled by a Sepia II unit. Emitted photons were detected via a Single Photon Avalanche Photodiode (SPAD). For mCitrine excitation, the 507 nm pulsed laser and the DM458/515 dichroic mirror were used. Fluorescence emission was detected using a 537/26 bandpass filter. To

collect enough photons to reliably determine the fluorescence lifetimes, the image integration time was about 3 min. All FLIM measurements were obtained with the SymPhoTime software v5.12.

2.2.5.3.2 FLIM ANALYSIS

FLIM data was analyzed by global analysis (*165*) implemented into an in-house-developed software (jediFLIM), which is based on frequency domain analysis of TCSPC data (*166*). Briefly, TCSPC histograms were in a first step Fourier transformed. The complex Fourier coefficients are thereby calculated from the first Harmonic of the TCSPC histogram, which describes the change in phase and modulation. This calculation is performed for each pixel of the acquired images. In a second step the Fourier coefficients are corrected with an instrument response function (IRF). For this the "autoglobal" method was used, which utilizes higher harmonic content of the data to fit the IRF (*166*). The corrected Fourier coefficients are then plotted into a phasor plot, so that the Fourier coefficients from each pixel of the image are represented by one point in the phasor plot. By fitting a straight line through all points in the phasor plot, the "global lifetimes" τ_D and τ_{DA} are determined at the intersections with the half-circle. τ_{DA} is the donor fluorescence lifetime in presence of the acceptor and τ_D the donor-only lifetime. Finally, the projection of each point in the phasor plot into the fitted segment between τ_D and τ_{DA} can be used to calculate the relative fraction of donor-only and donor-acceptor pairs (α) in each pixel.

2.2.5.4 FLUORESCENCE ANISOTROPY MICROSCOPY

Fluorescence anisotropy microscopy is based on the fact that if a fluorescence molecule is excited using a polarized light source also the emitted light will be polarized. Thereby photoselection takes places, which means that molecules whose absorption moment is perpendicularly aligned to the polarization of the excitation light will not be excited. The rest of the molecules will be excited and will emit photons with a polarization dependent on the particular orientation of each molecule. The degree of polarization can be described by the anisotropy (r), a dimensionless parameter defined as, where $I_{\parallel}$ and $I_{\perp}$ are the parallel and

perpendicular intensities emitted by the excited molecules with respect to the polarization direction of the excitation light. The anisotropy value (ranging from 0 to 0.4) will decrease if there is an increase in depolarization.

$$\mathbf{r} = \frac{\mathbf{I}_{\parallel} - \mathbf{I}_{\perp}}{\mathbf{I}_{\parallel} - \mathbf{2I}_{\perp}}$$

$I_{\parallel}$ = Intensity (parallel polarized emission); $I_{\perp}$= Intensity (prependicular polarized emission)

Several processes can influence the fluorescence anisotropy and lead to depolarization of the emitted light. Some of those processes can be used as tools as they provide information about the local environment of the fluorescent species. One of such processes is homo-FRET, which is FRET between identical fluorophores. If the emission dipoles of the donor and acceptor fluorophore are not parallel, the measured fluorescence will be depolarized. This effect can, for example, be used to determine protein structure, protein oligomerization or protein clustering and protein interactions (*167*).

2.2.5.4.1 DATA ACQUISITION

Fluorescence anisotropy microscopy measurements were acquired on the Olympus IX81 inverted microscope equipped with an Olympus MT-20 150W mercury arc burner. For the anisotropy measurements three high extinction linear polarizers were used. One polarizer was used for the polarization of the excitation light, hence placed in the illumination path of the microscope. The other two polarizers are used for the detection and are placed in the motorized filter wheel in front of the camera. These two polarizers are oriented parallel and perpendicular, respectively, in relation to the excitation light. The microscope was equipped with a BP460-480 HQ filter for excitation light as well as a 485 dichroic and a 495-540 HQ filter for emission light. Fluorescence was collected using a 20x/0.7 NA air objective. All images were acquired sequentially with an Orca CCD camera. For data acquisition and instrumental control the Olympus Cell^R software was used.

2.2.5.4.2 ANISOTROPY MICROCOPY ANALYSIS

Anisotropy data was analyzed with an in-house-developed software. Briefly, the product of each anisotropy measurement is two images per field of view. Thereby, one image was acquired with the emission polarizer oriented parallel to the excitation polarizer ($I_{\parallel}$) and the other image with the emission polarizer oriented perpendicular to the excitation polarizer ($I_{\perp}$). From those two images the anisotropy was calculated in each pixel i by:

$$r^i = \frac{G^i I_{\parallel}^i - I_{\perp}^i}{G^i I_{\parallel}^i + 2I_{\perp}^i}$$

Before calculating the anisotropy, the corresponding parallel and perpendicular images were aligned. Cells were analyzed individually by selecting a region of interest (ROI). For each ROI, the background intensity was subtracted. The G-factor (G^i), that accounts for differences between the parallel and perpendicular detection channels, was determined by calculating the ratio of the fluorescence intensities at perpendicular and parallel orientations for mCitrine in solution, which steady-state anisotropy value is close to zero due to its fast rotation. For each cell, the obtained anisotropy values per pixel were binned by intensity.

2.2.5.5 IMAGE PROCESSING

All images were processed with Fiji ImageJ software. First, images were converted into 32-bit and then corrected by the subtraction of the mean intensity of the background. If specific ROIs were quantified for mean intensity values or integrated intensity values, the minimum intensity was set to 0 before the ROI was measured (e.g. for Western Blot quantifications). If images were used for calculations to, for example, divide it by itself to generate a mask, a threshold was set and background pixels were set to “Not a Number” (NaN). For representation, contrast and brightness of the particular images may have been adjusted and images may have been cropped to only show a ROI with the important information.

2.2.6 STATISTICAL ANALYSIS

Results are expressed as the mean ± SEM, unless otherwise stated. Statistical significance of ungrouped data was estimated either by one-way ANOVA or Student's t-test. Statistical significance of grouped data (e.g. wt vs. mut data sets) was estimated by two-way ANOVA. For one- and two-way ANOVA a Bonferroni correction was done and adjusted p-values were calculated and indicated in the figures. Significance level of $p=0.05$ was used, $p<0.05$ (*), $p<0.01$ (**) and $p<0.001$ (***).

3. RESULTS

3.1 THE EGF-MEDIATED CD95 RESPONSE

3.1.1 INTERACTION OF EGFR AND CD95

Stimulation with FasL often results in the initiation of the apoptotic cascade. If the stimulated cells are sensitive towards FasL-mediated apoptosis the classical indications of cell death, like membrane bubbling and cell shrinkage are observable after a certain amount of time. To validate that Huh7 cells, which are CD95 negative and consequently insensitive towards stimulation with FasL (*168*), serve as a proper model system and that the CD95-mCitrine construct is functional, we first determined how Huh7 cells transfected with CD95-mCitrine and EGFR-mCherry behave after FasL stimulation. Huh7 cells were transfected with both receptors and stimulated with 100 ng/ml FasL for a total of 120 minutes. The spatial distribution of both receptors showed a high degree of similarity within the cell prior to stimulation, with a strong accumulation in the perinuclear area (Fig 3.1). As exemplified in Fig 3.1 approximately 90 minutes after stimulation with FasL the first cells became apoptotic and after 120 min most cells underwent apoptosis. The localization of both receptors however did not change during the entire time of stimulation.

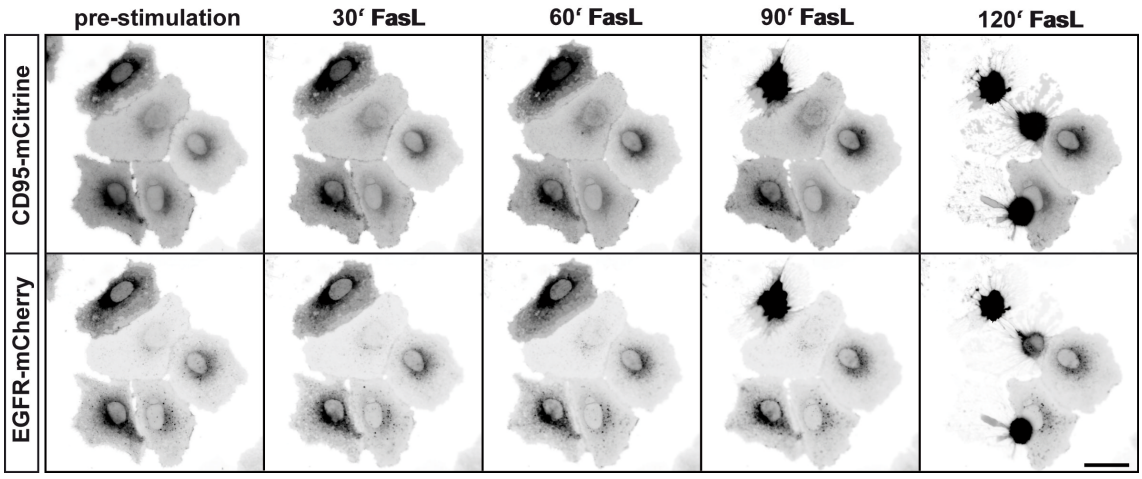

Figure 3.1: FasL induced cell death.
Huh7 cells co-expressing CD95-mCitrine and EGFR-mCherry were stimulated with 100 µg/ml FasL for 120 min and imaged with a fluorescence microscope. Approximately 90 minutes after FasL stimulation the first cells became apoptotic and after 120 min most cells underwent cell death. Scale bar represents 40 µm.

After validation that Huh7 cells recovered sensitivity towards FasL after transfection, that the CD95-mCitrine construct is functional and that co-expression of EGFR-mCherry is not affecting the apoptotic response in Huh7 cells, we now wanted to investigate whether EGF stimulation has an effect on CD95. As both receptors co-localize in unstimulated Huh7 cells (Fig 3.1), we first asked if EGF stimulation regulates this co-localization, as EGF stimulation usually leads to changes in the spatiotemporal distribution of EGFR. Huh7 cells ectopically expressing CD95-mCitrine and EGFR-mCherry were stimulated with 100 ng/ml EGF and co-localization was determined using Li's approach, which is a global statistic approach performing a intensity correlation coefficient-based (ICCB) analysis (*169, 170*). After EGF addition a clear translocation of both receptors towards the plasma membrane was observable. Both receptors co-localized especially at the PM but also in the perinuclear area (Fig. 3.2 (A)). For quantification the intensity correlation quotient (ICQ) was measured and plotted as mean ± SEM (Fig 3.2 (A)). The receptors showed a high fraction of co-localization with no significant difference before and after stimulation with EGF (ICQ value before= 0.452±0.017 vs. ICQ value after= 0.458±0.014; n= 62 cells of four independent experiments).

To investigate whether the observed co-localisation is due to an interaction between EGFR and CD95, co-immunoprecipitation experiments were performed. Huh7 cells were transfected with CD95-mCitrine and EGFR-mTFP and stimulated with EGF (100 ng/ml) or FasL (100 ng/ml), respectively. After cell lysis an antibody specific for CD95 was used to precipitate the receptor and its associated proteins in the total cell lysate. Subsequent Western Blots with antibodies specific for EGFR revealed a constitutive binding of EGFR to CD95 (Fig. 3.2 (B)). Moreover, it could be shown that following EGF treatment, the EGFR fraction associated to CD95 is phosphorylated (Fig. 3.2 (B)).

The co-localization between EGFR and CD95 was further investigated on endogenous protein level in Cos-7 cells by an immunocytochemical staining. Cos-7 cells were stimulated with 100 ng/ml EGF for 10 min, fixed and probed with antibodies specific for EGFR and CD95. Similar as in Huh7 cells, before stimulation both receptors co-localize in the perinuclear area and the PM (Fig. 3.3 (A)). After 10 min of stimulation, EGFR internalization could be observed, visible by vesicles

inside the cell and less receptor was visible at the periphery of the cells. CD95 in comparison remained at the PM and was not present in the EGFR-positive vesicles (Fig. 3.3 (A), see arrow).

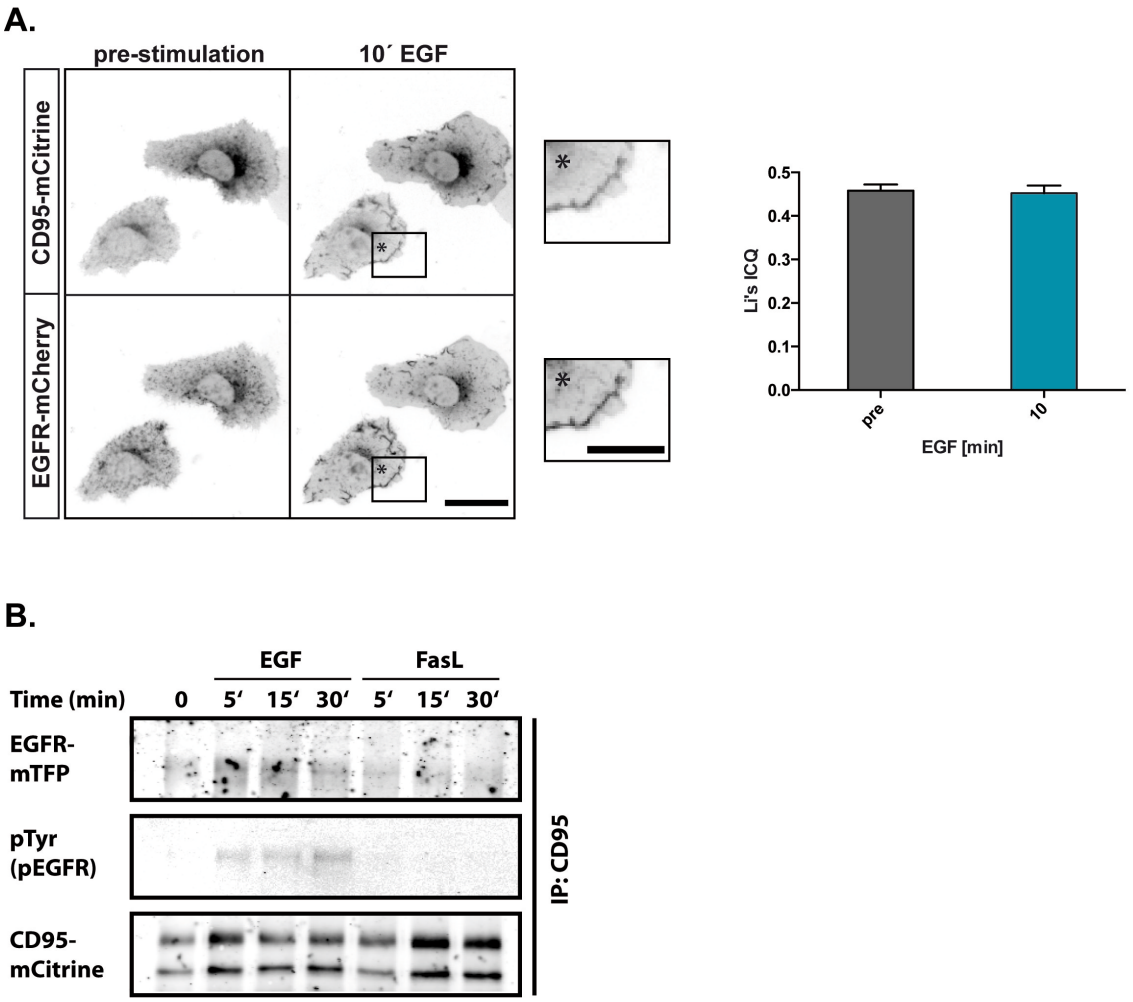

Figure 3.2: EGFR and CD95 interact before and after EGF stimulation.
(A) Huh7 cells ectopically expressing CD95-mCitrine and EGFR-mCherry were stimulated with 100 µg/ml EGF for 10 min and imaged with a fluorescence microscope. Both receptors co-localize before stimulation with EGF and remain associated 10 min after EGF addition. The blow-up shows that both receptors highly co-localize in the PM. The intensity correlation quotient (ICQ) shows a high fraction of association before (ICQ value= 0.458±0.014) and after (ICQ value= 0.452±0.017) stimulation with EGF. Data represent mean ICQ values ± SEM of n=62 cells of four individual experiments. **(B)** Co-Immunoprecipitation of CD95-mCitrine in Huh7 cells after stimulation with EGF (100ng/ml) or FasL (100ng/ml) for the indicated times. Co-IP was probed with an anti-CD95 antibody and Western Blot with anti-EGFR (EGFR-mTFP), anti-CD95 (CD95-mCitrine) and anti-pY72 (pEGFR) antibodies. Scale bar represents 40 µm and in the blow up 20 µm.

So far, in the experiments involving overexpression, after 10 min of EGF stimulation still a high fraction of receptors were co-localizing and the level of receptor internalization was low. To see if in transfected cells the association of both proteins remains for a longer time period or if also in Huh7 cells EGFR internalization can be observed but delayed compared to immunofluorescence,

Huh7 cells co-expressing both proteins were imaged over in total 60 min after the addition of EGF. Before stimulation with EGF the distribution of both proteins was again mainly restricted to the perinuclear area (Fig. 3.3 (B)). Upon EGF (100 ng/ml) addition both receptors clearly translocated towards the PM. At later time points EGFR was internalized by vesicular transport, while CD95 remained on PM (Fig. 3.3 (B), see arrows). The amount of vesicles however was not as high as in the immunofluorescence.

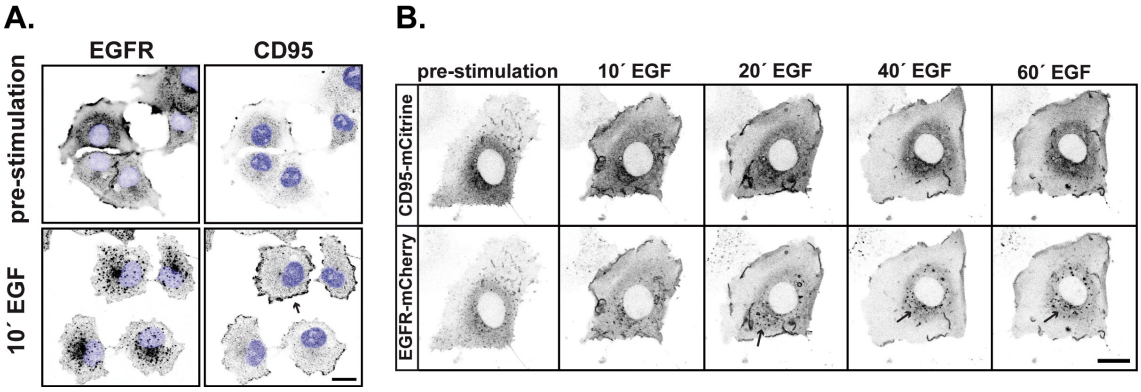

Figure 3.3: CD95 translocates to the PM upon EGF stimulation
(A) Cos-7 cells were stimulated with 100 ng/ml EGF for 10 min, fixed and immunocytochemically stained with antibodies specific for EGFR and CD95, respectively. Confocal images show that the EGFR receptor is internalized after 10 min EGF stimulation, while CD95 is accumulating at the PM. **(B)** Huh7 cells transfected with CD95-mCitrine and EGFR-mCherry were stimulated with 100 µg/ml EGF for 60 min and imaged over time with a confocal microscope. Both receptors co-localize before stimulation with EGF and remain associated in the beginning. At later time points the EGFR receptor is internalized and CD95 remains at the PM. All scale bars represent 20 µm.

To investigate whether the EGF-mediated internalization of EGFR leads to a loss of the interaction between CD95 and EGFR, 'Fluorescence Lifetime Imaging Microscopy' (FLIM) measurements were performed in Huh7 cells. For FLIM measurements we choose mCitrine and mCherry as FRET pair, with EGFR-mCherry as an acceptor for CD95-mCitrine. In the absence of EGF, an interaction between both receptors was observable, evident by a reduced fluorescence lifetime (τ) compared to the donor only lifetime (Fig 3.4 (B)). EGF stimulation (100 ng/ml) caused an increase of the fluorescence lifetime (τ) over time, indicating a loss of interaction (Fig 3.4 (A) & (B)). This increasing fluorescence lifetime was observable in various cells, showing a consistent trend of an EGF-mediated loss of interaction between both receptors (Fig 3.4 (C)).

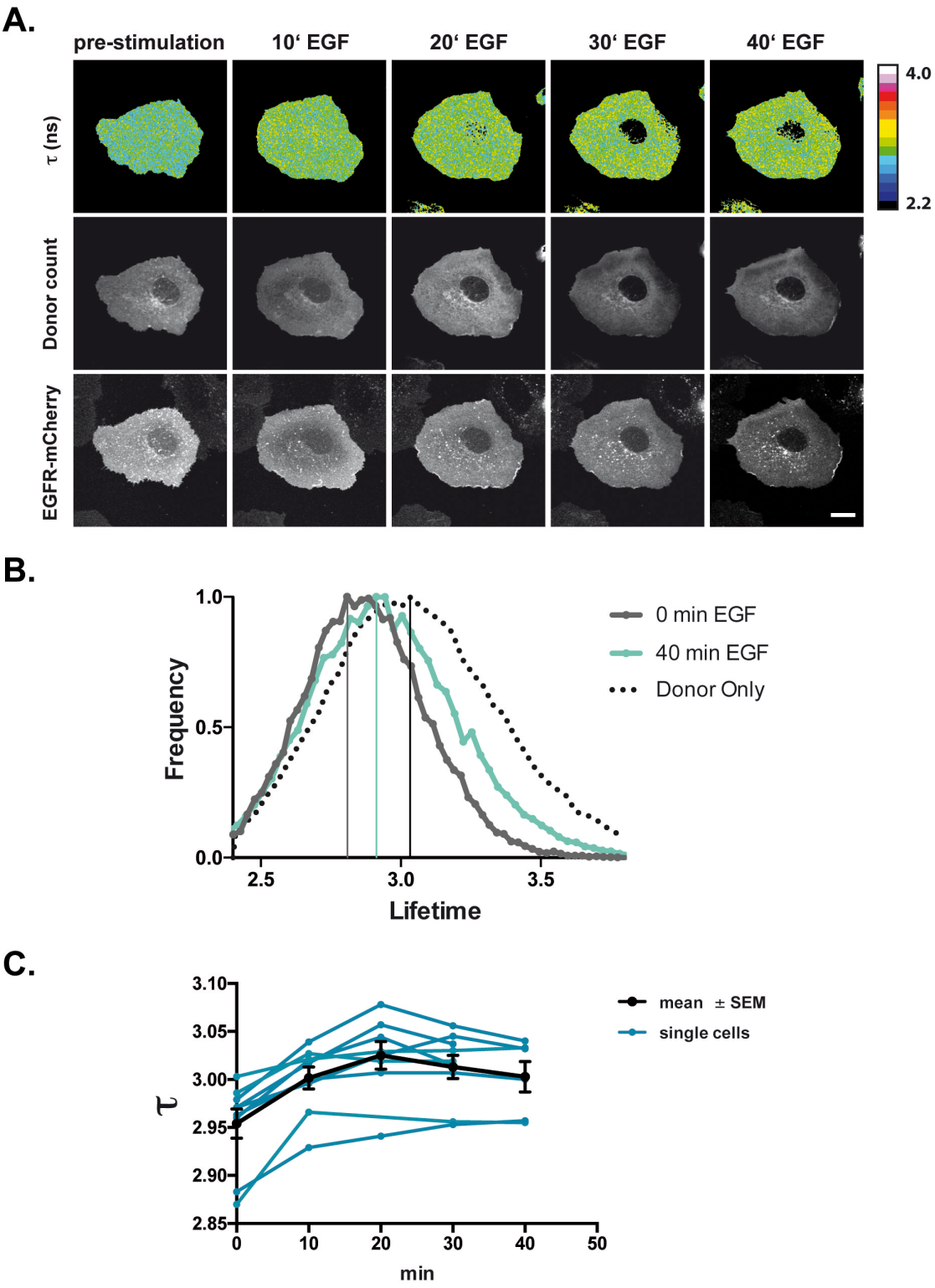

Figure 3.4: Loss of interaction between EGFR and CD95 measured by FLIM
(A) Huh7 cells ectopically expressing CD95-mCitrine and EGFR-mCherry were stimulated with 100 µg/ml EGF for 40 min and imaged over time. The FL (τ) of mCitrine was measured at various time points. In the upper row the average lifetime (τ) maps are shown (color coding is shown on the right); the middle row shows the corresponding images of the donor counts and the bottom row shows the EGFR-mCherry images, which were recorded with a confocal microscope. **(B)** Histogram shows the distribution of the measured average FL (τ) before stimulation and after 40 min EGF of the cell shown in (A). Dotted line represents the average FL (τ) of a donor only sample. The average FL (τ) distributions show that before stimulation the lifetime (τ) is reduced compared to the donor only sample (grey line) and that after 40 min EGF stimulation the average FL (τ) increases (green line). **(C)** Measured average FL (τ) of various cells over before and after EGF (turquoise lines). Mean ± SEM is shown in black. Scale bar represent 20 µm.

Taken together, CD95 and EGFR interact with each other in the un-stimulated state. EGF stimulation leads to translocation of both receptors to the plasma membrane and to a loss of the constitutive interaction over time, as the EGFR is internalization by vesicular transport, while CD95 remains bound to the PM.

3.1.2 RECYCLING AT STEADY STATE

Due to the observation that EGFR and CD95 co-localize and interact with each other in un-stimulated Huh7 and Cos-7 cells (Fig. 3.3 and 3.4), we asked whether both receptors are co-trafficked through the endocytic system. It was previously shown that EGFR is constitutively recycled via the Rab11a-positive recycling endosome (RE) in un-stimulated Cos-7 cells and that EGF binding redirects the receptor towards lysosomes, where ligand-bound receptors eventually get degraded (*143*). In the case of CD95, not much is known about its trafficking dynamics at steady state or the protein machinery involved.

To investigate whether also CD95 is constitutively recycled in un-stimulated Huh7 cells, we first investigated if CD95 recycles via Rab11a-positive RE, like EGFR. In a first experiment only CD95-mCitrine and BFP-Rab11a (Fig. 3.5 (A) left upper panel) or EGFR-mCherry and BFP-Rab11a (Fig. 3.5 (A) right upper panel) were co-expressed in Huh7 cells and in a second test both receptors, CD95-mCitrine and EGFR-mCherry were co-expressed together with BFP-Rab11a (Fig. 3.5 (A) bottom panel).

While CD95 clearly co-localized with Rab11a in all analysed cells, EGFR and Rab11a were found to co-localize only in some of the analysed cells (approximately 4%, Fig. 3.5 (B)). Co-expression of CD95-mCitrine with EGFR-mCherry slightly increased the proportion of cells that showed a co-localization of EGFR and Rab11a but overall the amount remained low. Conversely co-expression of EGFR-mCherry significantly decreased the proportion of CD95 in the Rab11a-positive compartment (Fig 3.5 (A)).

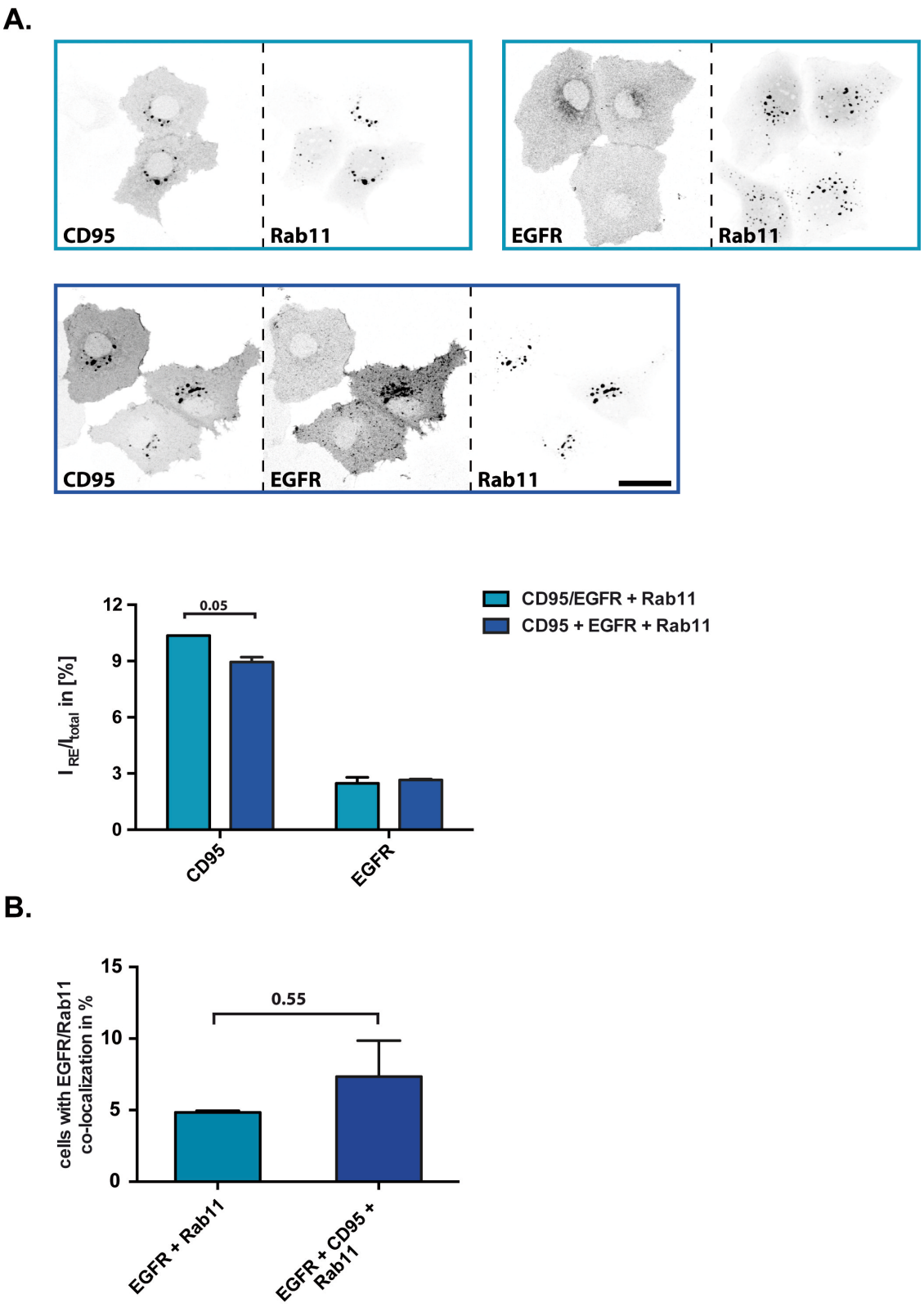

Figure 3.5: EGFR slows down recycling of CD95.
(A) Huh7 cells were either transfected with CD95-mCitrine and BFP-Rab11 (left upper panel, green frame) or EGFR-mCherry and BFP-Rab11 (right upper panel, green frame) or CD95-mCitrine, EGFR-mCherry and BFP-Rab11 (bottom panel, blue frame). Diagram shows the fluorescence intensity of CD95 or EGFR in the RE over the total fluorescence intensity of double (green bars) or triple (blue bars) transfected cells. Bars represent the fraction of both receptors within the RE in percent ± SEM (analyzed cells for CD95: CD95 + Rab11 n= 52; CD95 + EGFR + Rab11 n=63; analyzed cells for EGFR: EGFR + Rab11 n= 39; CD95 + EGFR + Rab11 n=63, of two independent experiments) (* $p < 0.05$, two-way ANOVA with Bonferroni's multiple comparison test) (B) Quantification of cells showing a co-localization of EGFR and Rab11 of two independent experiments. Scale bar represents 40 µm.

As EGFR is only co-localizing in some cells with Rab11a we repeated the experiment in Cos-7 cells, where a co-localization of EGFR and Rab11a has already described. Again cells were transfected with each receptor individually or with both receptors simultaneously along with Rab11a (Fig. 3.6). In Cos-7 cells, both CD95 and EGFR were found to co-localize with Rab11a in all observed cells (Fig. 3.6). Contrary to the Huh7 cells, receptor co-expression did not lead to a significant reduction of CD95 in the Rab11a compartment, but a significant increase in the amount of EGFR in the RE was observed upon CD95 co-expression.

Taken together, CD95 co-localizes with Rab11a suggesting an involvement of Rab11a in the recycling of CD95 at steady state. The ectopic expression of EGFR decreases the amount of CD95 in the RE, which might be due to a reduced recycling rate caused by the interaction between both proteins. EGFR is not co-localizing with Rab11a in Huh7 cells pointing towards a different recycling mechanism in those cells or changed recycling dynamics. In Cos-7 cells, however CD95 positively affects trafficking of EGFR.

3.1.3 CD95 RECYCLING AFTER EGF STIMULATION

At steady state, a fraction of EGFR is maintained at the PM by vesicular recycling from the RE to the PM. Once EGF binds, the receptor is redirected to lysosomes and thus the RE-bound receptor pool is temporarily depleted (*143*). As CD95 also co-localizes with Rab11a-positive recycling endosomes and since both receptors interact at steady state, we asked whether EGF stimulation also modulates the trafficking fate of CD95. To ascertain if EGF stimulation has an effect on CD95 trafficking, Huh7 cells were transfected with both receptors and BFP-Rab11a and imaged over time.

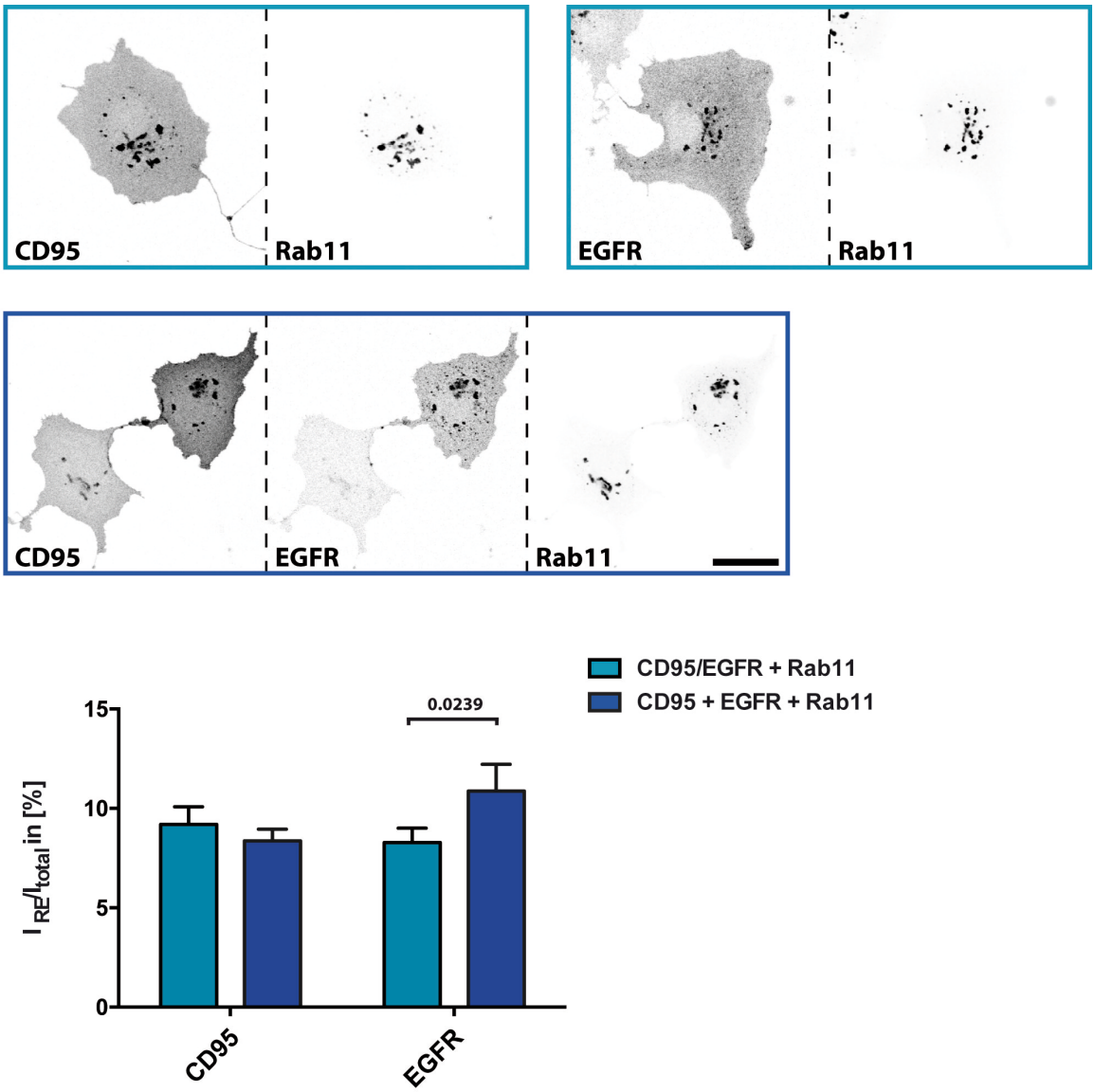

Figure 3.6: CD95 enhances the slow recycling of EGFR.
Cos-7 cells ectopically expressing either CD95-mCitrine and BFP-Rab11 (left upper panel, green frame) or EGFR-mCherry and BFP-Rab11 (right upper panel, green frame) or CD95-mCitrine, EGFR-mCherry and BFP-Rab11 (bottom panel, blue frame). Diagram displays the ratio of the fluorescence intensity of CD95 or EGFR measured in the RE over the total fluorescence intensity of double (green bars) or triple (blue bars) transfected cells. Bars represent the amount of both receptors within the RE in percent ± SEM (analyzed cells for CD95: CD95 + Rab11 n= 20; CD95 + EGFR + Rab11 n=33; analyzed cells for EGFR: EGFR + Rab11 n= 29; CD95 + EGFR + Rab11 n=33, of one experiment) (* p< 0.05, two-way ANOVA with Bonferroni's multiple comparison test). Scale bar represents 40 µm.

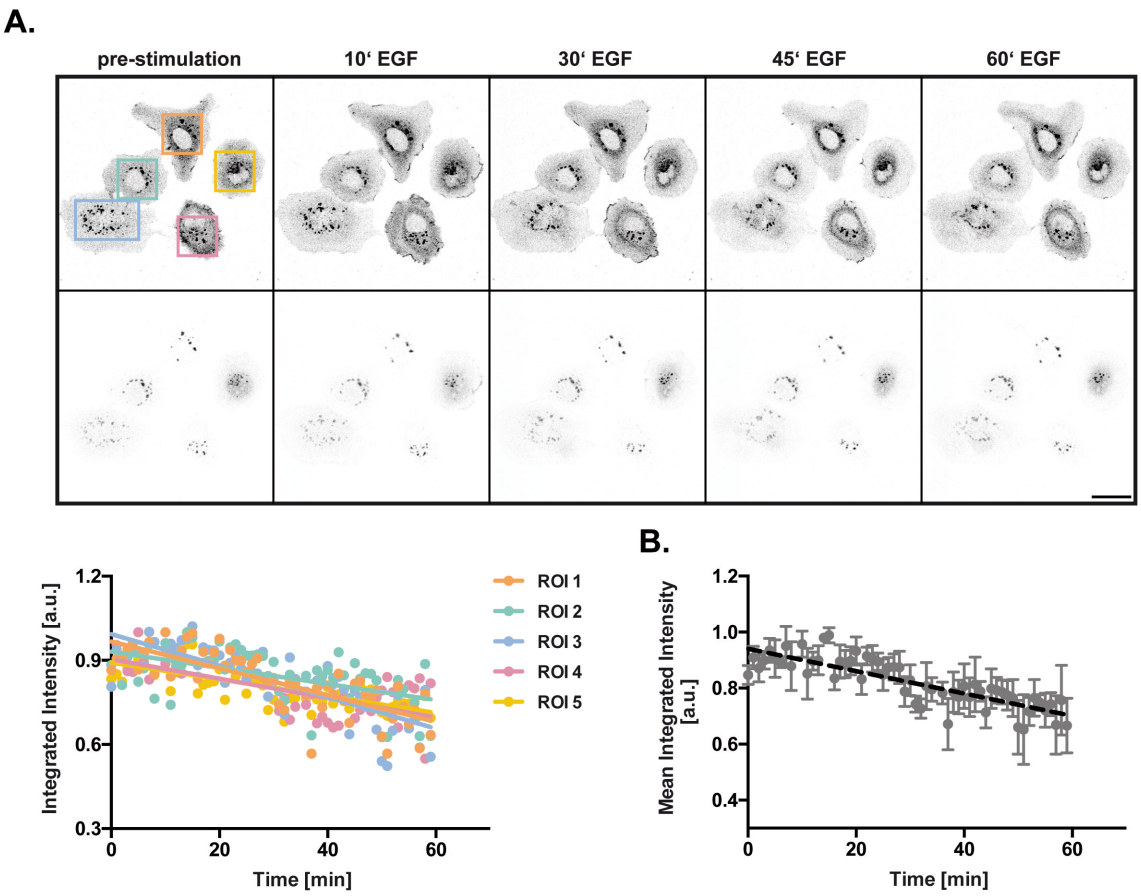

Figure 3.7: CD95 depletion from Rab11a-positive RE after EGF stimulation in Huh7 cells
(A) Huh7 cells ectopically expressing CD95-mCitrine, EGFR-mCherry and BFP-Rab11 were stimulated with 100 µg/ml EGF for 60 min and imaged over time with a confocal microscope. Changes of the fluorescence intensity of CD95-mCitrine were measured in the indicated regions and plotted over time. **(B)** Diagram shows the mean integrated intensity ± SEM of the in (A) measured cells. Scale bars represent 40 µm.

By using a mask of the RE, which was created by using the BFP-Rab11a fluorescence, the amount of CD95-mCitrine in that compartment was measured before and after EGF stimulation (Fig 3.7). The quantification revealed a more or less linear reduction of the CD95-mCitrine fluorescence intensity in the Rab11a-positive endosomes over time. This effect was even more rapid in the Cos-7 cells, where the reduction of the CD95-mCitrine fluorescence intensity in the RE was observable approximately after 10 min and stayed constantly low over time but rather followed an exponential reduction (Fig 3.8).

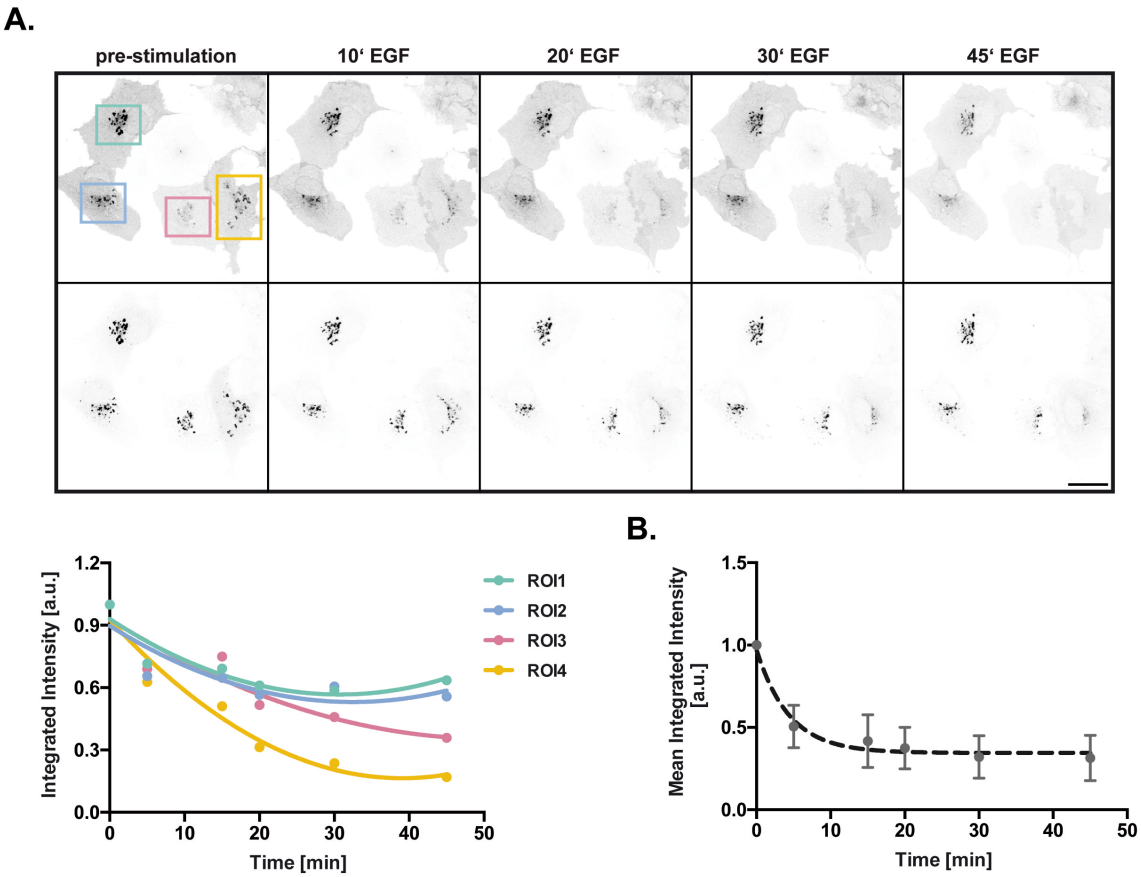

Figure 3.8: CD95 depletion from Rab11a-positive RE after EGF stimulation in Huh7 cells.
(A) Cos-7 cells transfected with CD95-mCitrine, EGFR-mCherry and BFP-Rab11 were stimulated with 100 µg/ml EGF and imaged at the indicated time points with a confocal microscope. Changes of the fluorescence intensity of CD95-mCitrine were measured in the indicated regions and plotted over time. **(B)** Diagram shows the mean integrated intensity ± SEM of n= 10 cells from three independent experiments. Scale bars represent 40 µm.

In summary it could be shown that the amount of CD95-mCitrine within the RE decreases after EGF stimulation in both tested cell lines, suggesting that EGF stimulation regulates CD95 trafficking, leading to changes in its spatial distribution.

3.1.4 EGFR-DEPENDENT PHOSPHORYLATION OF CD95

It was previously shown that CD95 exhibits two tyrosine residues, which are located within the DD at the positions 232 and 291 and are known to be phosphorylated in vivo (*50*). After finding that CD95 and EGFR show a constitutive interaction, we asked whether EGFR phosphorylates CD95. To assess if EGF stimulation and the resultant EGFR activation leads to CD95 phosphorylation, immunoprecipitation experiments were performed in Huh7 cells after ectopic expression of CD95-mCitrine and EGFR-mTFP. Transfected Huh7 cells were stimulated with EGF (100 ng/ml) or FasL (100 ng/ml), lysed and either EGFR or

CD95 was pulled-down with the respective antibody. Immunoblotting with antibodies against GFP to detect total CD95 and EGFR as well as pY72, a generic phospho-tyrosine antibody showed that upon EGF stimulation both receptors are phosphorylated (Fig 3.9). FasL stimulation, on the other hand, did not change the phosphorylation of CD95 (Fig 3.9 (A)). For EGFR, a basal phosphorylation was detectable in the un-stimulated case, which seems to slightly decrease after FasL addition (Fig 3.9 (B)).

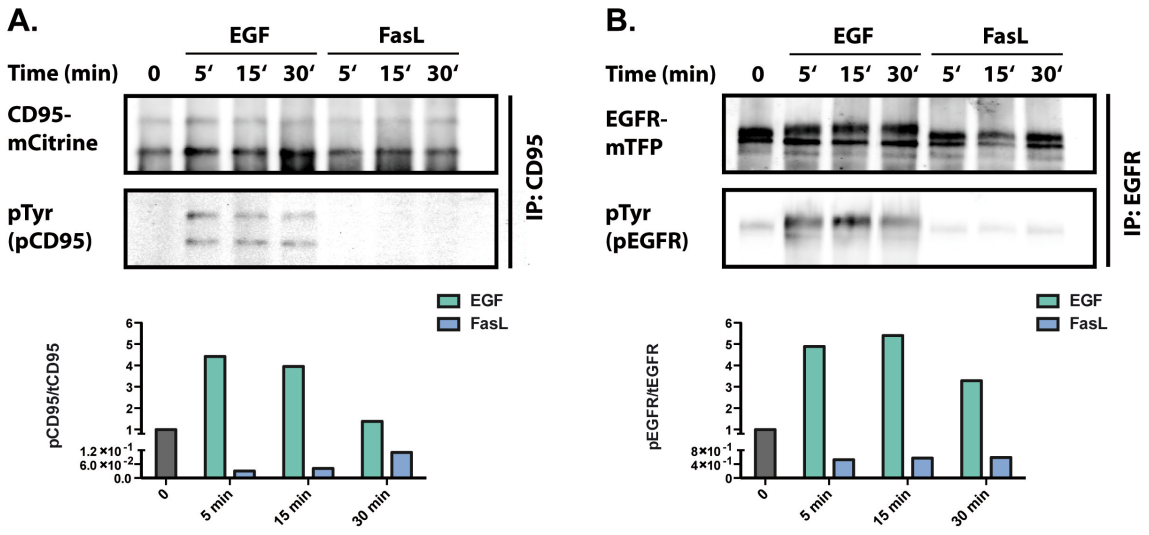

Figure 3.9: EGF-dependent phosphorylation of CD95.
Huh7 cells were transfected with CD95-mCitrine and EGFR-mTFP stimulated with EGF (100 ng/ml) or FasL (100ng/ml). After cell lysis immunoprecipitations of CD95-mCitrine or EGFR-mTFP were performed. Pull-down was probed with antibodies against anti-CD95 and anti-EGFR, respectively. Western Blots were probed with anti-EGFR (EGFR-mTFP), anti-GFP (CD95-mCitrine) and anti- pY72 (pEGFR and pCD95, respectively) antibodies. Diagrams show either the pCD95/tCd95 ratios or the pEGFR/tEGFR ratios after EGF stimulation.

As phosphorylation of CD95 appeared relatively low, we tested if its detection could be enhanced by inhibition of phosphatases with pervanadate. Again, Huh7 cells were transfected with CD95-mCitrine and EGFR-mTFP, stimulated with 100 ng/ml EGF or 1 mM pervanadate and immunoprecipitation experiments with subsequent Western Blots performed as described above. Both stimuli, EGF and pervanadate, induced phosphorylation of CD95 (Fig 3.10). However, the signal intensity of the pervanadate stimulation was almost 40-times higher then the EGF-induced phospho signal (Fig 3.10, see range of y-axis).

In summary, EGF stimulation but also phosphatase inhibition by pervanadate induced phosphorylation of CD95. FasL addition though did not induce any detectable phosphorylation of CD95.

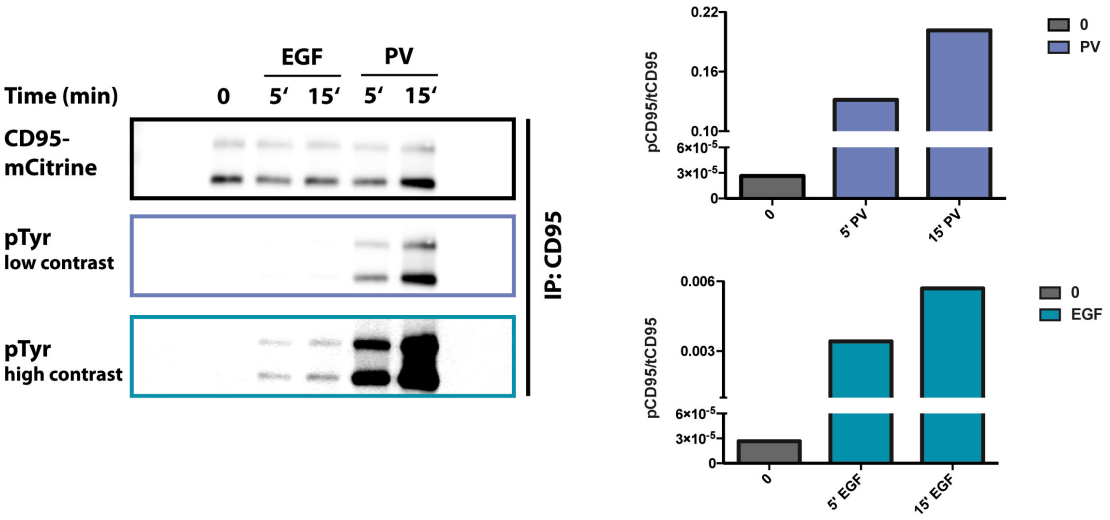

Figure 3.10: Inhibition of phosphates increases phosphorylation of CD95.
Huh7 cells ectopically expressing CD95-mCitrine and EGFR-mTFP were either stimulated with EGF (100 ng/ml) or treated with pervanadate (1 mM) for 5 and 15 minutes. After cell lysis CD95-mCitrine was immunoprecipitated with an anti-CD95 antibody and Western Blots were probed with antibodies against anti-GFP (CD95-mCitrine) and anti- pY72 (pCD95). The middle image shows a low-contrast-image of the detected CD95 phospho-signal while the bottom image shows the same image with increased contrast. Diagrams show the pCD95/tCd95 ratios after EGF stimulation and pervanadate treatment, respectively.

3.1.5 PHOSPHORYLATION SWITCHES THE FUNCTION OF CD95 TO SURVIVAL

After finding that EGF stimulation induced phosphorylation of CD95, we next questioned if EGF-promoted phosphorylation of CD95 influences its cellular function. For this, Huh7 cells ectopically expressing both receptors were first stimulated with EGF and subsequently treated with FasL for 2 hours. Measuring the number of apoptotic cells via flow cytometry showed that pre-stimulation with EGF had a protective effect on Huh7 cells, as FasL-induced apoptosis was reduced compared to cells only treated with FasL (Fig 3.11 (A)). To test if this effect is directly related to the kinase activity of EGFR we repeated the measurements using a kinase-dead mutant EGFR harboring a point mutation in its ATP-binding site (*171*). Huh7 cells transfected with the kinase-death mutant of the EGFR and stimulated with EGF showed, similar to cells only stimulated with FasL, an increased apoptosis rate compared to cells transfected with the wild type form of EGFR (Fig 3.11 (A)).

In order to investigate the protective, anti-apoptotic effect of EGF more precisely in space and time we performed time-lapse microscopy experiments. To further investigate the role of EGFR kinase activity in this effect, we used the tyrosine kinase inhibitor (TKI) Erlotinib, which completely reverses EGFR phosphorylation within 15' of treatment (Fig 3.11 (B)). For the microscopy experiments Huh7 cells

were transfected with CD95-mCitrine and EGFR-mTFP and either directly stimulated with EGF and FasL or pre-incubated with 1 µM Erlotinib for 2 hours. The addition of EGF for 10 minutes prior to the FasL addition protected Huh7 cell from undergoing apoptosis, whereas the pre-incubation with Erlotinib and the resulting kinase inhibition abolished the protective effect (Fig 3.11 (C) without Erlotinib and (D) with Erlotinib pre-incubation).

Figure 3.11: Phosphorylation of CD95 protects cells from FasL induced apoptosis
(A) Huh7 cells ectopically expressing CD95 and either EGFR wild type or the kinase death mutant of EGFR were pre-stimulated with 100 µg/ml EGF for 10 min and subsequently treated with FasL for 2 hours. The amount of apoptotic cells was measured via flow cytometry and the normalized apoptosis plotted for the individual conditions. EGF pre-treatment significantly reduces the amount of apoptosis compared to FasL stimulation without EGF pre-treatment. Diagram shows the mean fold-increase ± SEM of three individual experiments. (* $p < 0.05$, two-way ANOVA with Bonferroni's multiple comparison test). **(B)** Huh7 cells were transfected with EGFR-mTFP and pre-stimulated with 100 µg/ml EGF for 10 min and subsequently treated with 1 µM Erlotinib for different time points. After cell lysis Western Blots with antibodies against anti-EGFR and pY72 (pEGFR) were performed. Diagram shows the densitometric quantification of the pEGFR/tEGFR ratio. **(C)** Huh7 cells ectopically expressing CD95-mCitrine and EGFR-mTFP were first stimulated with 100 µg/ml EGF for 10 min and then treated with FasL for 2h. EGF pre-treatment is preventing apoptosis induction. **(D)** Huh7 cells transfected with CD95-mCitrine and EGFR-mTFP were first treated with 1 µM Erlotinib for 2h, then pre-stimulated with 100 µg/ml EGF for 10 min and finally treated with FasL for 2h. Inhibition of the EGFR abolishes the EGF-mediated protective effect. Scale bars represent 40 µm.

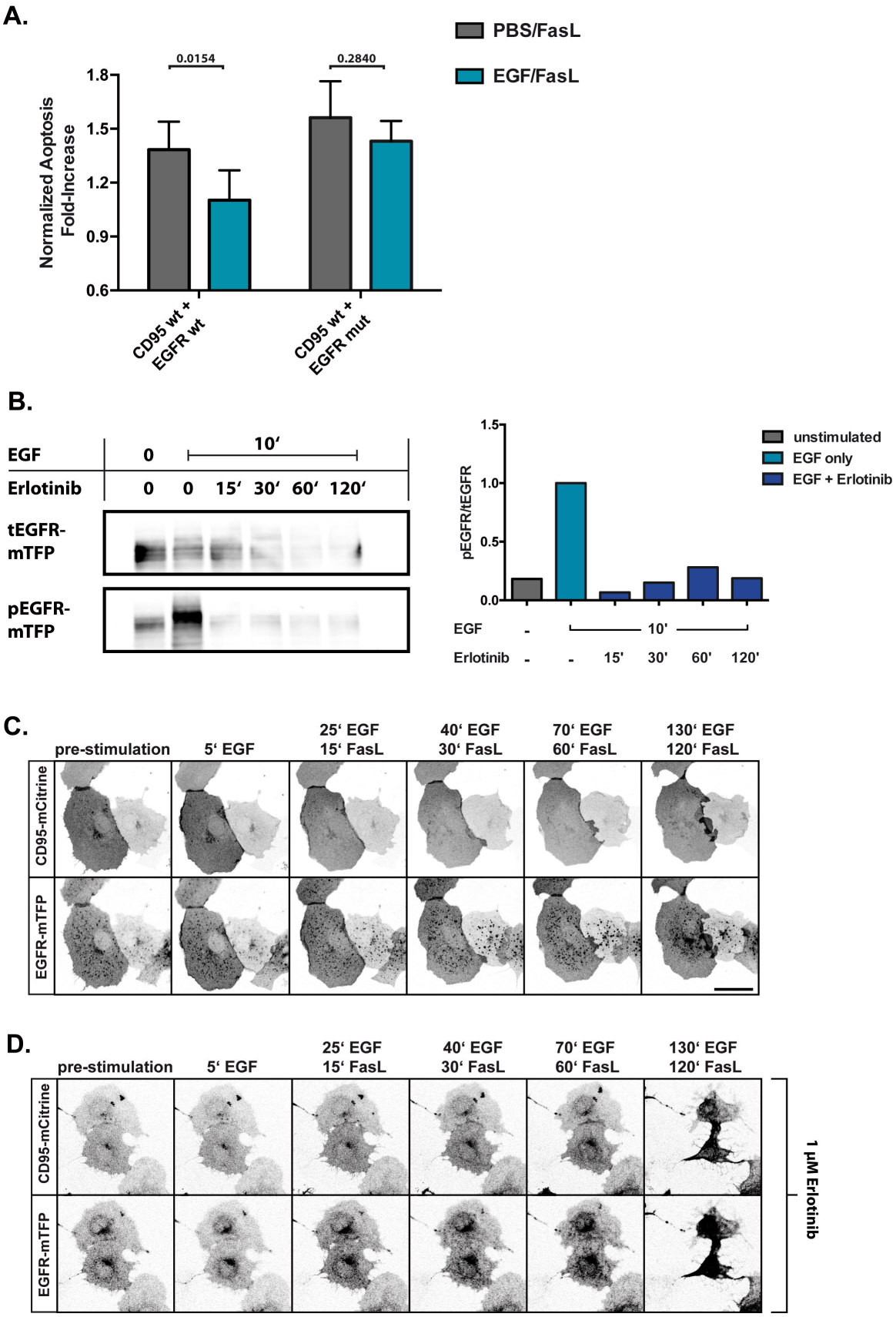
A.
PBS/FasL
EGF/FasL
0.0154
0.2840
Normalized Aoptosis Fold-Increase
1.8
1.5
1.2
0.9
0.6
CD95 wt + EGFR wt
CD95 wt + EGFR mut
B.
EGF
0
10'
Erlotinib
0 0 15' 30' 60' 120'
tEGFR-mTFP
pEGFR-mTFP
pEGFR/tEGFR
1.5
1.0
0.5
0.0
unstimulated
EGF only
EGF + Erlotinib
EGF - 10'
Erlotinib - - 15' 30' 60' 120'
C.
pre-stimulation
5' EGF
25' EGF 15' FasL
40' EGF 30' FasL
70' EGF 60' FasL
130' EGF 120' FasL
CD95-mCitrine
EGFR-mTFP
D.
pre-stimulation
5' EGF
25' EGF 15' FasL
40' EGF 30' FasL
70' EGF 60' FasL
130' EGF 120' FasL
CD95-mCitrine
EGFR-mTFP
1 µM Erlotinib

After showing that the kinase domain of EGFR is mandatory for the EGF-mediated protection against FasL-induced apoptosis, we wanted to confirm that the two-tyrosine residues in the DD of CD95 are the ones affected by the EGF pre-stimulation and responsible for the protective effect. For this, Huh7 cells were transfected with a construct in which these two tyrosine residues were exchanged by phenylalanine (CD95-Y232,291F-mCitrine)(*118*). Again, Huh7 cells were stimulated with FasL with and without EGF pre-treatment (Fig 3.12). Cells expressing the unphosphorylatable CD95 mutant remained highly sensitive for FasL induced apoptosis even after pre-stimulation with EGF.

Altogether, these results suggest that EGF-induced phosphorylation of Y232 and Y291 in the DD of CD95 has a protective effect against FasL-induced apoptosis. It was further shown that kinase activity of the EGFR is essential for the protective effect of the EGF pre-stimulation.

Figure 3.12: Tyrosine residues in the DD of CD95 are mandatory apoptosis protection
Huh7 cells were either transfected with CD95-mCitrine and EGFR-mCherry **(A)** or transfected with CD95-Y232,291F-mCitrine and EGFR-mCherry **(B)** In both cases cells were first stimulated with EGF for 10 min, then treated with FasL and imaged with a fluorescence microscope for in total 2 hours. Again, EGF pre-treatment significantly increases the amount of survival compared to FasL stimulation without EGF pre-treatment. Survival is strongly reduced though, if the two-tyrosine residues in the DD of CD95 are replaced by phenylalanine. Diagram shows the survival in percentage ± SEM of three individual experiments. (** $p < 0.01$, two-way ANOVA with Bonferroni's multiple comparison test). Scale bars represent 40 µm.

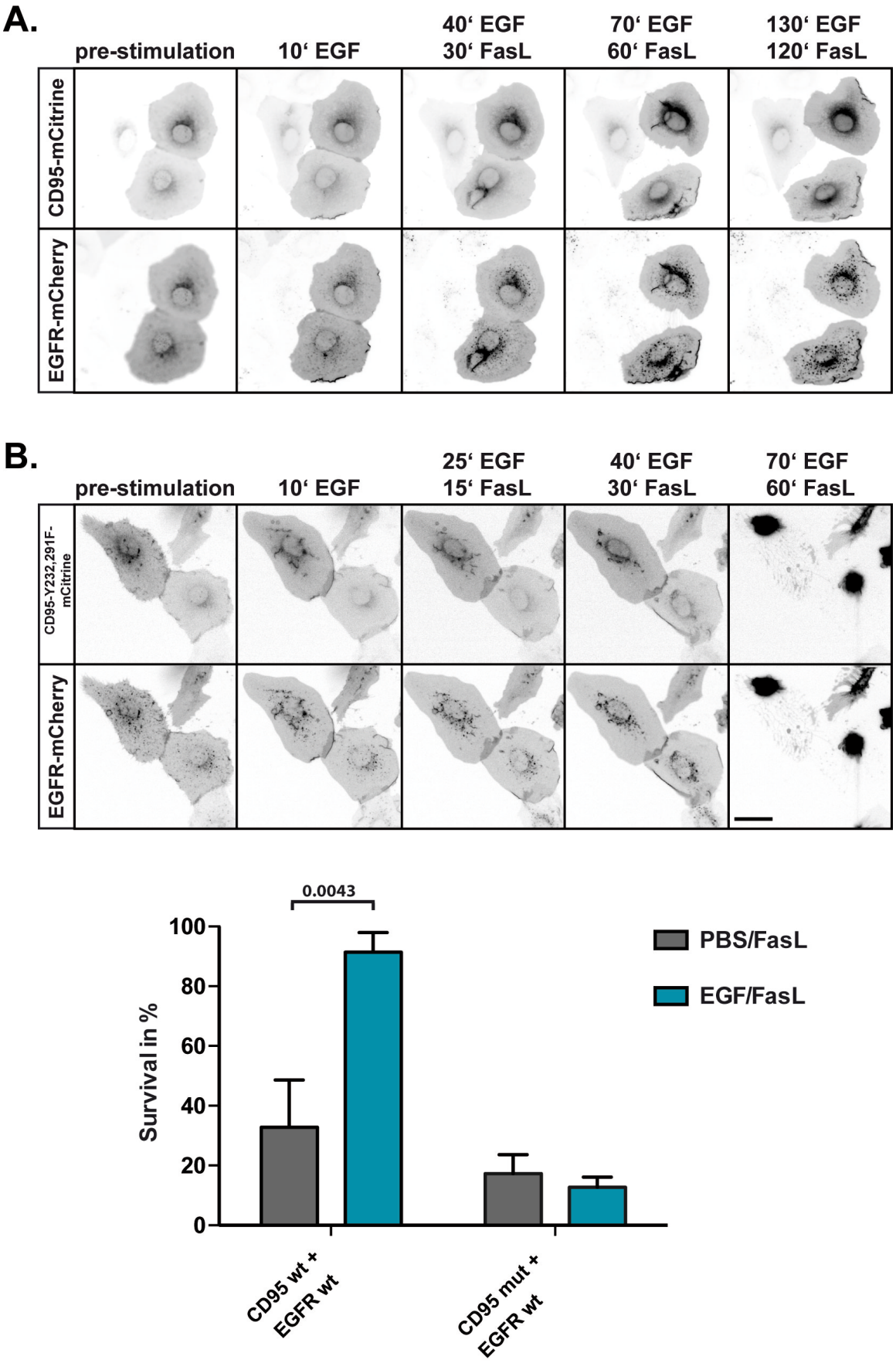
A.
pre-stimulation
10‘ EGF
40‘ EGF
30‘ FasL
70‘ EGF
60‘ FasL
130‘ EGF
120‘ FasL
CD95-mCitrine
EGFR-mCherry
B.
pre-stimulation
10‘ EGF
25‘ EGF
15‘ FasL
40‘ EGF
30‘ FasL
70‘ EGF
60‘ FasL
CD95-Y232,291F-mCitrine
EGFR-mCherry
0.0043
Survival in %
100
80
60
40
20
0
PBS/FasL
EGF/FasL
CD95 wt + EGFR wt
CD95 mut + EGFR wt

3.1.6 EGF-DRIVEN EFFECT ON CD95 CLUSTERING

CD95 is a pre-associated homo-trimer before ligand binding. It is commonly accepted that this conformation is mandatory for apoptosis induction and that mutations in regions required for the trimer formation cause apoptosis resistance. As EGF stimulation causes phosphorylation of CD95, we tested whether this posttranslational modification modulates the capacity of CD95 to self-associate. To do so, homo-FRET was measured with fluorescence anisotropy using widefield microscopy.

Homo-FRET is based on non-radiative transfer of energy between similar or identical fluorescent proteins. If the fluorescent proteins are close enough, like in a cluster of fluorescently labeled monomers, a decrease in the fluorophore's anisotropy can be measured (*167*).

First, anisotropy was measured in Huh7 cells stimulated with EGF that were transiently transfected with EGFR-mCherry and either CD95-mCitrine wt or CD95-Y232,291F-mCitrine. In the case of wt CD95, stimulation with a 100 ng/ml EGF led to a slight but significant increase of the anisotropy in nearly all binned intensity ranges (Fig. 3.13 (A)). Only the first intensity bin with a low fluorescent signal and the last two bins with high fluorescent signals gave no significant change. In the case of the CD95-Y232,291F mutant, EGF stimulation caused a slight decrease in the anisotropy, with a significant change only in the intensity range between 1000 and 1400 (Fig. 3.13 (B)). No change in the anisotropy was measured for cells stimulated with 100 ng/ml FasL for 15 min.

These anisotropy measurements, therefore, suggest that the anti-apoptotic effect of EGF-promoted CD95 phosphorylation might result from the dissociation of pre-associated homo-trimers necessary for apoptosis induction. This effect is lost with the unphosphorylatable mutant of CD95 and, in fact, an increase in cluster formation is observed after EGF stimulation, further implicating CD95 phosphorylation in regulating cluster formation.

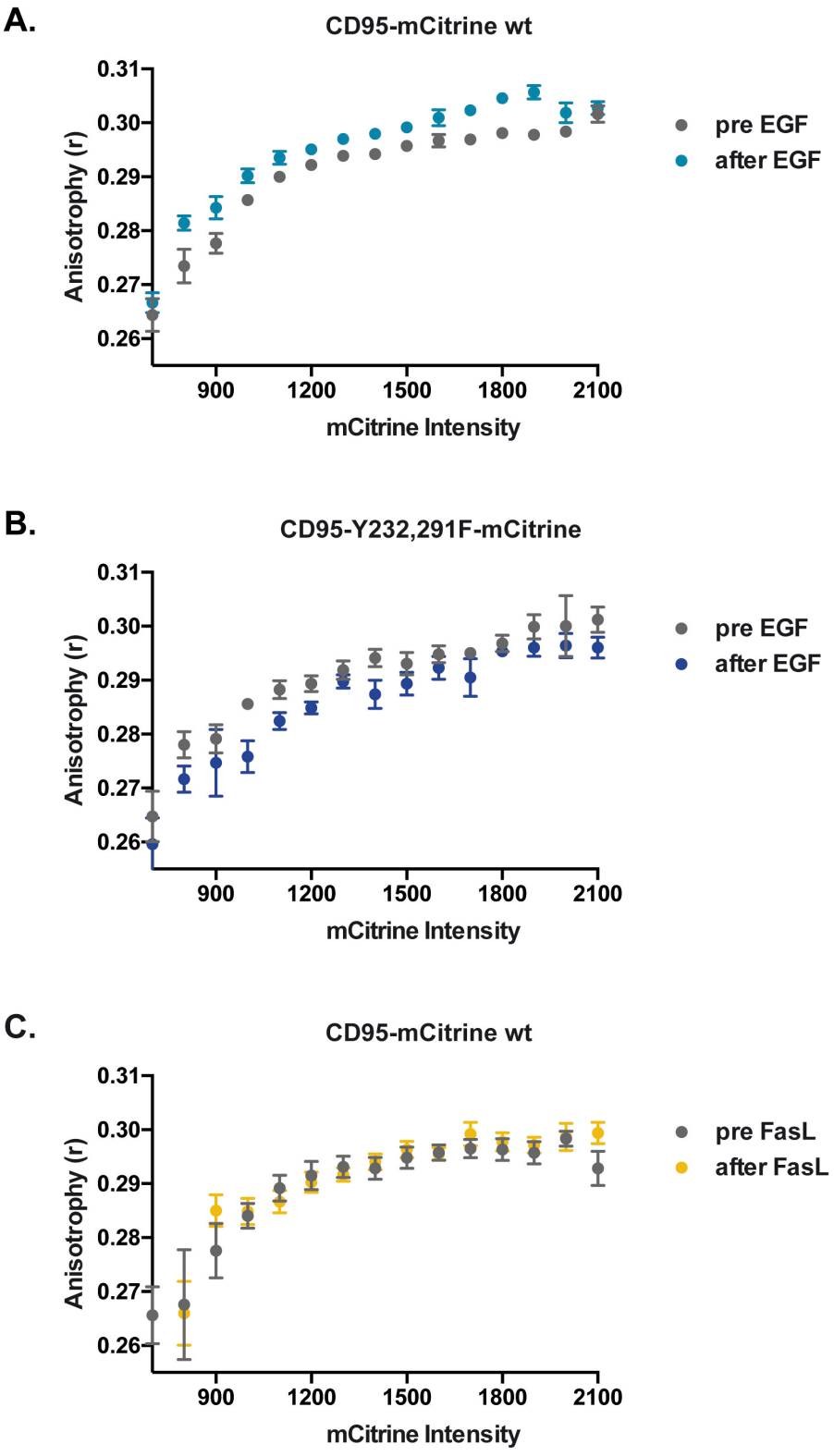

Figure 3.13: Measuring of CD95 clustering in Huh7 cells.
(A) Steady-state anisotropy was measured in Huh7 cells transiently expressing CD95-mCitrine wt and EGFR-mCherry before and 15 min after stimulation with 100 ng/ml EGF. Plot shows anisotropy ± SEM of n=33 cells of four individual experiments (B) Steady-state anisotropy was measured in Huh7 cells expressing CD95-Y232,291F-mCitrine and EGFR-mCherry again before and after stimulation with 100 ng/ml EGF. Plot shows anisotropy ± SEM of n=10 cells of two individual experiments (C) Steady-state anisotropy measured in Huh7 cells transiently expressing CD95-mCitrine wt and EGFR-mCherry before and after stimulation with FasL for 15 min. Plot shows anisotropy ± SEM of n=10 cells of two individual experiments.

3.1.7 DOWNSTREAM SIGNALING

An important survival-signaling pathway is the Akt/PI3K pathway. In previous reports, it could be shown that PI3K activation can modulate CD95 signaling (*38, 113, 172*). To ascertain whether the EGFR signaling contributes to the observed protection against FasL-induced apoptosis, we measured Akt- and/or Erk-pathway activation under different stimulation conditions. Huh7 and Cos-7 cells were co-transfected with either wt CD95-mCitrine or CD95-Y232,291F-mCitrine and EGFR-mTFP and the relative phosphorylation of Akt and Erk was determined via Western Blots.

Both cell lines were pre-stimulated with EGF (100 ng/ml) for 10 min and subsequently treated with 100 ng/ml FasL for at least 2 h. Akt activation in cells expressing wt CD95 was significantly higher compared to cells transfected with the phospho-deficient mutant of CD95 in both cell lines following treatment with EGF alone or in combination with FasL (Fig. 3.14 (A) & (B)). FasL alone had no effect on Akt activation.

The level of phosphorylated Erk was increased upon EGF stimulation but in contrast to Akt, showed no significant difference between the CD95 wild type and mutant. FasL stimulation also had no effect on the phosphorylation state of Erk.

These results suggest that the phosphorylation ability of the two-tyrosine residues of CD95 are positively influencing the amount of activated Akt.

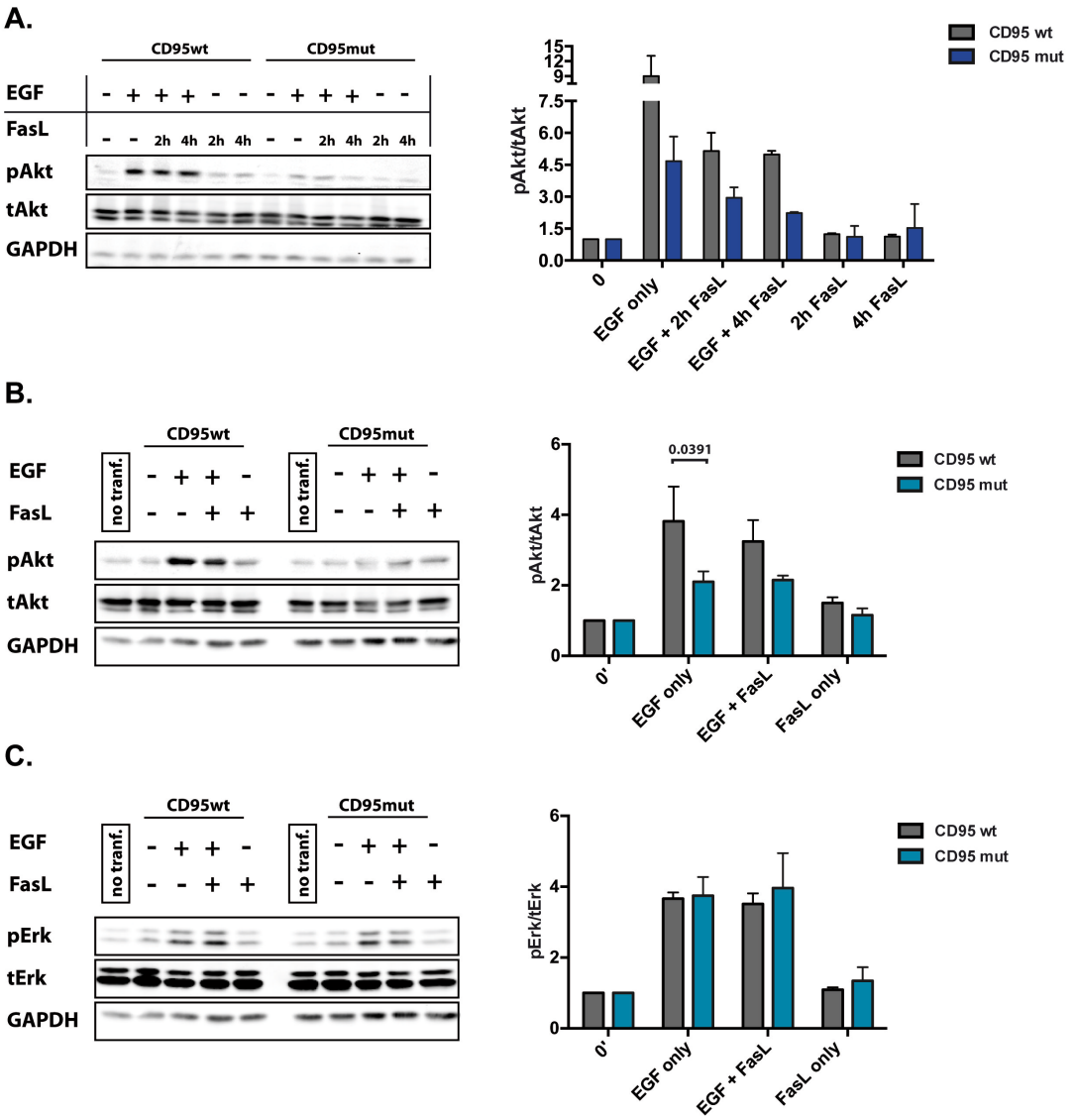

Figure 3.14: Ectopic expression of CD95 elevates pAkt level.
(A) Huh7 transfected with either CD95-mCitrine wt or mut and EGFR-mCherry were stimulated with 100 ng/ml EGF only (lane 2 and 8), pre-stimulated with EGF for 10 min (lanes 3-4 and 9-10) or PBS (lane 5-6 and 11-12) and subsequently stimulated with 100 ng/ml FasL for 2h (lanes 3 & 5; 9 & 11) or 4h (lanes 4 & 6; 10 & 12). Diagram shows the phospho-Akt level over total-Akt ratio and represents mean ± SEM of two independent experiments. **(B & C)** Cos-7 cells co-expressing CD95-mCitrine wt or mut and EGFR-mCherry were either pre-stimulated with 100 ng/ml EGF (lane 4 and 9) or PBS (lane 5 and 10) for 10 min and subsequently stimulated with 100 ng/ml FasL or treated with EGF alone as control (lane 3 and 8). For Western Blots either antibodies against p/tAkt **(B)** were used or against p/tErK **(C)**. Diagram in **(B)** shows the phospho-Akt level over total-Akt and diagram in **(C)** the phospho-Erk level over total-Erk. Both diagrams represent the mean ratio ± SEM of four independent experiments. (* $p < 0.05$, two-way ANOVA with Bonferroni's multiple comparison test). Individual repetitions were done by R. Ettelt.

3.2 CD95 IN NON-SMALL CELL LUNG CANCER CELLS

3.2.1 CD95-MEDIATED APOPTOSIS IN HCC827 CELLS

Based on our hypothesis that EGFR phosphorylates the two tyrosine residues in the DD of CD95 and thus prevents FasL-induced apoptosis, we used the non-small cell lung cancer (NSCLC) cell line HCC827, which is known for carrying an activating mutation in the EGFR gene, to reassess our hypothesis in a cellular background with constitutive EGFR activity and to examine the possible role of EGF-dependent CD95 phosphorylation on cell survival in an oncogenic context. The constitutive EGFR activity in HCC827 cells is a result of an in-frame exon19 deletion, which encodes part of the kinase domain.

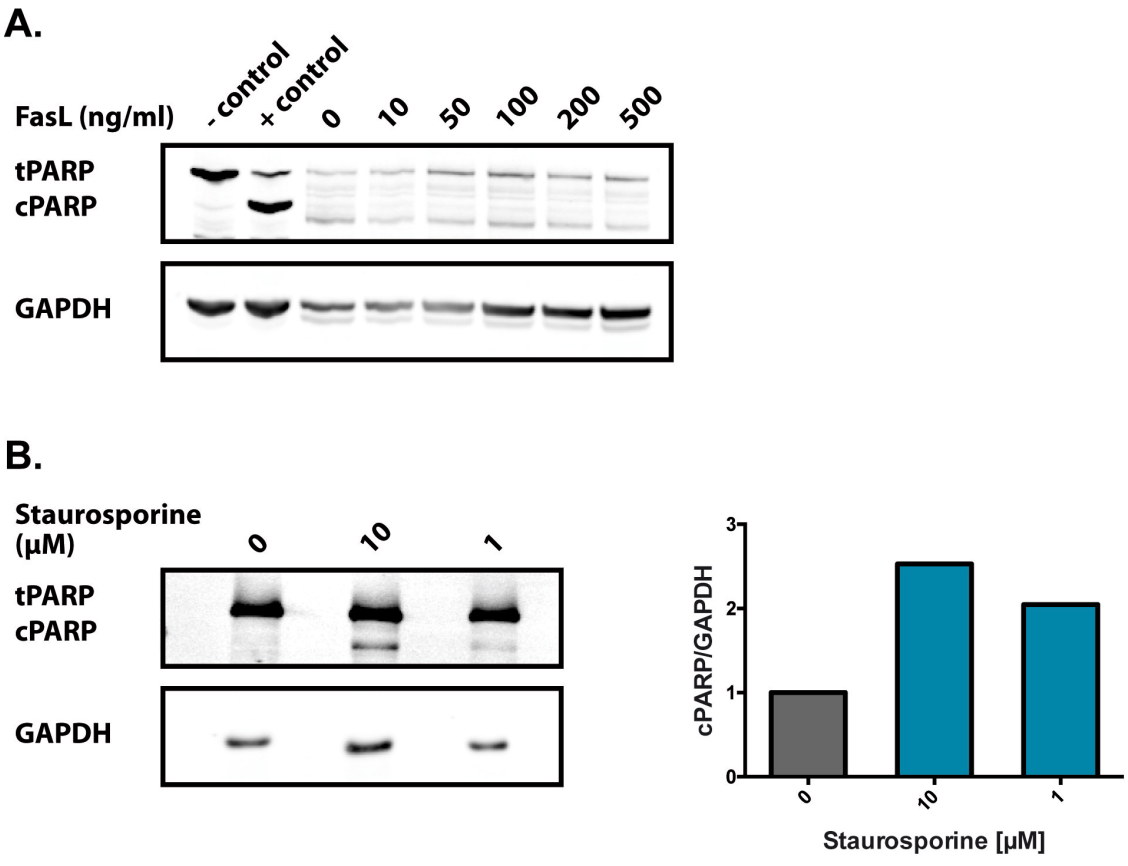

Figure 3.15: HCC827 cells are insensitive to FasL mediated apoptosis.
(A) Representative Western blot showing that FasL-stimulation does not increase apoptosis activity. HCC827 cells were stimulated for 6h with FasL in a dose-dependent manner. Immunoblots were probed with antibodies recognizing total and cleaved PARP and GAPDH. **(B)** Amount of cleaved PARP is increasing after stimulation with Staurosporine, as indicated by immunoblots. HCC827 cells were stimulated with 10 µM and 1µM Staurosporine for 5h. Immunoblots were probed with antibodies recognizing total and cleaved PARP and GAPDH. Diagram represents the normalized ratio of cPARP over GAPDH, n=1.

We first tested if HCC827 cells are able to undergo FasL-mediated apoptosis. Apoptosis induction was measured by the amount of cleaved PARP in a FasL dose dependent manner. Western blots showed that FasL-stimulation does not induce apoptosis (Fig. 3.15 (A)). To check if HCC827 cells are generally insensitive for apoptosis induction, cells were treated with two concentrations of the apoptosis inducer Staurosporine (10 µM and 1 µM) for 5h and cleaved PARP was measured. Immunoblots revealed that both concentrations of Staurosporine are sufficient to induce apoptosis as indicated by an increasing amount of cleaved PARP (Fig. 3.15 (B)).

Following the hypothesis that EGFR-mediated phosphorylation is blocking FasL-induced apoptosis, we asked whether the observed insensitivity towards FasL is due to an elevated basal phosphorylation of CD95 caused by the constitutive EGFR activity. In order to test if CD95 is basally phosphorylated in the presence of a constitutively active EGFR mutant immunoprecipitation experiments were performed, showing that CD95 is phosphorylated in both basal and EGF-treated HCC827 cells (Fig. 3.16). Densitometric analysis of the Western Blot revealed that the level of phosphorylation after EGF stimulation is only slightly higher compared to the basal phosphorylation level of CD95 (Fig. 3.16, see diagram).

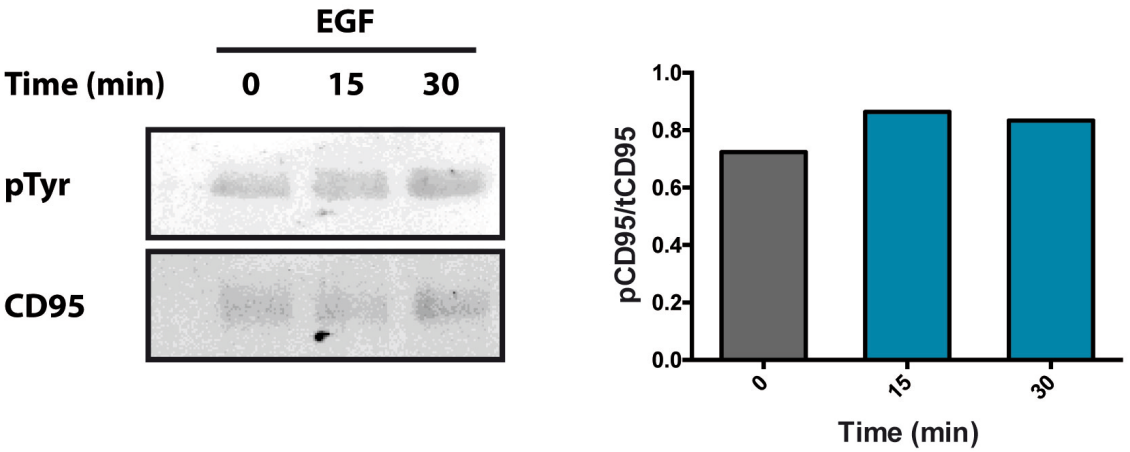

Figure 3.16: CD95 is phosphorylated in HCC827 cells.
Immunoprecipitation of CD95 in HCC827 cells after stimulation with EGF (100 ng/ml) for 15 and 30 minutes. Pull-down was achieved with antibodies against anti-CD95. Western Blots were probed with anti-CD95 and anti- pY72 (pCD95) antibodies. Diagram shows the ratio of pCD95 over total CD95, n=1.

These results demonstrate that HCC827 cells are in principle able to undergo apoptosis but seem to be insensitive for FasL-induced apoptosis, which might be due to the basal phosphorylation of CD95 detected.

3.2.2 EGFR ACTIVITY IN HCC827 CELLS

We next assessed how the phosphorylation status of EGFR in HCC827 cells relates to their sensitivity to FasL-mediated apoptosis. We first performed an EGF dose-response experiment in which HCC827 cells were treated with increasing EGF concentrations. Cells were stimulated with 0.25, 0.5, 1, 50 and 100 ng/ml EGF for 15 min, lysed and biochemically analyzed. While low doses of EGF were not sufficient to increase the EGFR phospho-signal in comparison to the high basal phospho-level, high EGF concentrations could still increase the EGFR activity (Fig. 3.17).

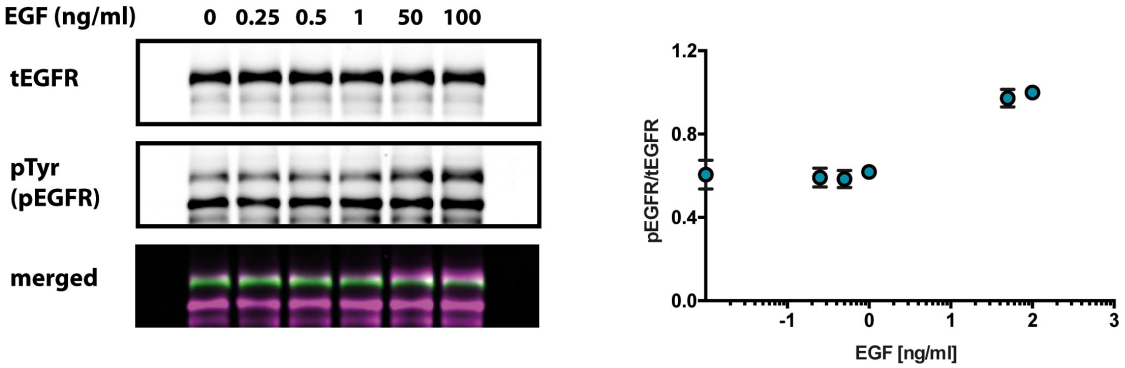

Figure 3.17: EGF dose-response in HCC827 cells.
HCC827 cells were stimulated with increasing EGF concentrations (0, 0.25, 0.5, 1, 50, 100 ng/ml). Immunoblots were probed with antibodies against EGFR and pY72 (pEGFR). Diagram represents the fold-change of the pEGFR/EGFR ratio ± SEM of n = 4. Individual repetitions were done by R. Ettelt.

Next, the ability to inhibit the constitutive EGFR activity was tested. An often-used inhibitor for NSCLC cell lines is the drug Erlotinib hydrochloride, which is a reversible tyrosine kinase inhibitor (TKI) (*152*). In a time-dose-response experiment different Erlotinib concentrations were tested for two different incubation times. The tested Erlotinib concentrations were ranging from 1 nM to 10 µM and the incubation time was either 1h or 24h. Western Blots revealed that the EGFR activity was similarly inhibited for both incubation times for all EGF concentrations (Fig. 3.18 (A) & (B)).

Taken together, HCC827 cells exhibit high constitutive EGFR activity, which can be further increased or decreased by EGF or Erlotinib, respectively.

3.2.3 RECONSTITUTION OF CD95-MEDIATED APOPTOSIS IN HCC827 CELLS

As already mentioned, HCC827 cells are insensitive to FasL-induced apoptosis and have a high basal phosphorylation level of both EGFR and CD95. We next assessed if sensitivity to FasL-induced apoptosis can be restored in these cells by inhibition of EGFR. To test if inhibition of the constitutive EGFR activity influences FasL-induced apoptosis, real-time cell analyzer (RTCA) assays and flow cytometric measurements were performed following FasL treatment with and without pre-treatment with Erlotinib.

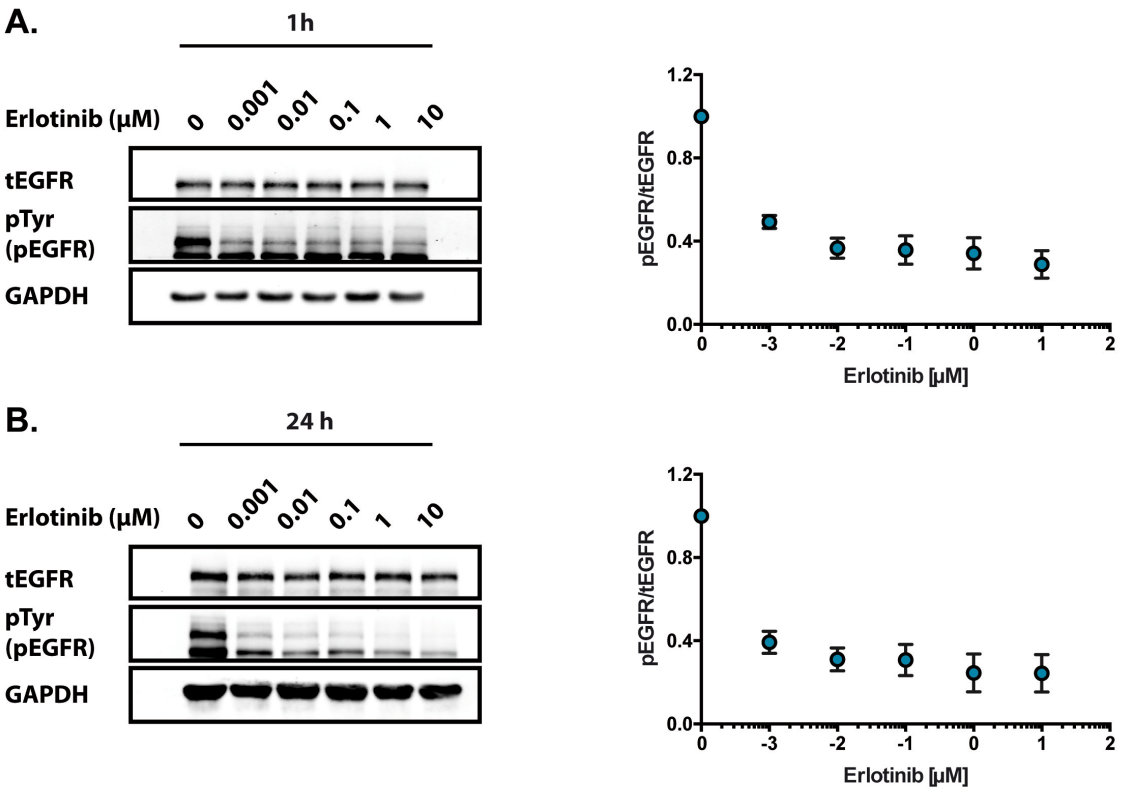

Figure 3.18: EGF time-dose-response in HCC827 cells.
HCC827 cells were stimulated with increasing EGF concentrations (0, 0.25, 0.5, 1, 50, 100 ng/ml) for either 1h **(A)** or 24h **(B)**. Immunoblots were probed with antibodies against EGFR and pY72 (pEGFR). Diagrams represent the fold-change of the pEGFR/EGFR ratio normalized to the basal phosphorylation level. Plotted are means ± SEM of n = 4. Individual repetitions were done by R. Ettelt.

For both assays HCC827 cells were either stimulated with FasL only (500 ng/ml), Erlotinib only (1 μM) or first with Erlotinib and subsequently with FasL. The pre-stimulation with Erlotinib was carried out either for 1h or for 24h. RTCA assays revealed that treatment with FasL alone induced a growth arrest of the HCC827 cells, while pre-treatment with Erlotinib led to a reduced cell number after about 48h (Figure 3.19, 1h (A) and 24h (B)). To test whether the reduction in cell growth is due to apoptosis induction, flow cytometric measurements were performed under the same conditions. As shown before, stimulation with FasL only was not sufficient to induce apoptosis. The treatment with Erlotinib only increased the amount of dead cells after 1h slightly and after 24h incubation nearly 1.5 –fold. Pre-treatment with Erlotinib enhanced FasL-induced apoptosis induction by over 1.5-fold compared to FasL alone.

To summarize, it could be shown that the inhibition of constitutive EGFR activity in NSCLC leads to the re-sensitization of HCC827 cells towards FasL-induced apoptosis.

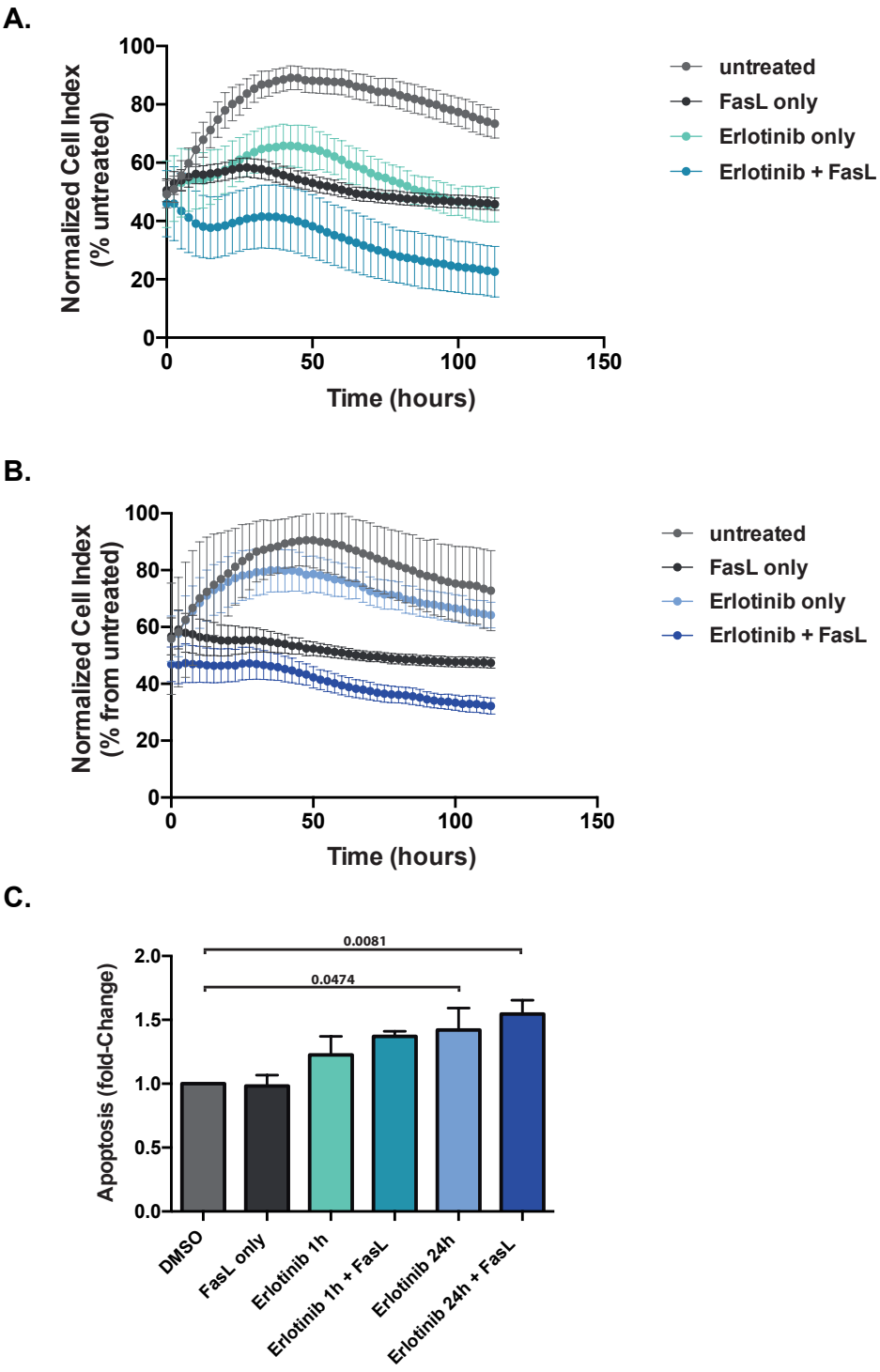

Figure 3.19: Inhibition of constitutively active EGFR re-sensitizes HCC827 cells towards apoptosis
(A & B) Growth curves of HCC827 cells recorded by RTCA measurements. HCC827 cells were either treated with FasL only (500 ng/ml), Erlotinib only (1 µM) or both together. In the latter case the Erlotinib pre-treatment took place either for 1h (A) or for 24h (B). The RTCA measurements were carried out for approximately 5 days. Curves show the normalized cell index as percentage from the untreated condition. The intersection with the y-axis represents the time of FasL addition. Shown is the mean ± SEM of n=3 **(C)** Inhibition of EGFR increases apoptosis induction. Diagram shows the apoptosis rate of HCC827 cells after different stimuli flow cytometrically analyzed. Shown is the apoptosis fold-change in percent normalized to the DMSO control. Bars represent means ± SEM of three independent experiments. (* $p < 0.05$ and ** $p < 0.01$, two-way ANOVA with Bonferroni's multiple comparison test)

4. DISCUSSION

CD95 clearly represents a protein that exhibits contrary functional roles in the cell. Although initially identified as a cytokine receptor mainly known for its function as an apoptosis inducing protein, it is becoming increasingly recognised for its apoptosis-independent functions. Already in the late 1990, reports describing functions of CD95 distinct from apoptosis induction accumulated and even became the focus for a whole decade. One reason for the growing interest in the non-apoptotic function of CD95 is increasing evidence for a growth-promoting role in tumours. The first reported indications of the non-apoptotic functions of CD95 were the observations that CD95 and/or FasL are often overexpressed in certain tumours and that stimulation with FasL-induced activation of CD95 in some contexts actually promoted events like proliferation, migration and angiogenesis (*88, 113, 114*). However, the mechanisms underlying this switch in the function of CD95 still remain unclear, as is the reason why FasL ligation causes in one cell type apoptosis and in another cell type survival.

In this work we show that posttranslational modifications of CD95 are sufficient to shift CD95's function from apoptosis to survival. We show for the first time that the EGF receptor, once activated, phosphorylates CD95 and that cells harbouring the phosphorylated form of CD95 are protected against apoptosis induction. On the other hand, we show that the phospho-deficient form of CD95 (CD95-Y232,291F) is hypersensitive towards FasL induced apoptosis. We also present indications for a CD95-mediated elevation of Akt activation, which might be important the survival signalling initiated by CD95. Finally, we show the importance of understanding the underlying mechanism for the opposing tendencies of CD95 in a cancer model. We could show that inhibition of the EGFR activity in combination with FasL stimulation increases the apoptosis rate of NSCLC cells, which provides an interesting possibility for a therapeutic implementation.

4.1 INTERACTION OF CD95 AND EGFR IS STIMULATION INDEPENDENT

The literature that describes a connection between EGFR and CD95, like an interaction between both receptors, is contradictory. As some reports observe a death-promoting role of the EGFR, other reports describe a rather protective role of the EGFR in the context of CD95-mediated cell death (*118, 119, 155, 172-174*). To untangle these ambiguous observations, we started our own experiments and first asked if both receptors share similar spatial and temporal dynamics after stimulation with FasL or EGF. As a model cell line we chose the liver carcinoma cell line Huh7, as previous reports observed an interaction between CD95 and EGFR in those cells (*118, 175*). Another advantage of Huh7 cells is that they are negative for CD95 and endogenous CD95 would not mask effects of, for example, further experiments with mutated versions of CD95 (*168*). Surprisingly, in unstimulated Huh7 cells a strong spatial correlation of both receptors was detectable in all experiments (Fig. 3.1, 3.2 A, 3.3 B, 3.11 C & D, 3.12 A & B). Stimulation with FasL did not induce any change of the localization pattern for both receptors (Fig 3.1), while EGF stimulation lead to increased translocation of both receptors from the RE to the PM (Fig 3.2 A, 3.3).

As seen in previous reports, addition of FasL to Huh7 cells that co-express fluorescently tagged CD95 and EGFR successfully induced apoptosis (*118, 175*). Eberle and colleges observed an interaction between the receptors after FasL exposure and translocation of both proteins to the PM after approximately 120 min FasL stimulation (*118*), while the effect of EGF-stimulation was not tested. We observe instead that after 120 min FasL exposure most cells underwent apoptosis. Furthermore, our results indicate that the strong initial co-localization between both receptors is due to a direct interaction and does not require stimulation with FasL or EGF (Fig 3.2 B and 3.4).

The inconsistencies between our observations and the findings of Eberle and colleges concerning the interaction between both receptors in unstimulated Huh7 cells might be explained by different activation states of the receptors. It is known, for example, that a high EGFR concentration at the PM is directly affecting its activity state, as it is leading to spontaneous receptor activation (*143*). As most experiments in both studies are performed with cells overexpressing both receptors, different expression levels caused by variation in transfection efficiently

might affect especially the initial receptor states. Whether especially the activity state of EGFR is changing the response properties of CD95 will be discussed below (see chapter 4.3).

The reason that CD95 does not translocate towards the PM upon FasL stimulation, as previously shown, remains unclear. As FasL engagement is neither causing aggregation of CD95 nor induces receptor trafficking, it is possible that Huh7 cells rather act like type II cells which have less DISC formation and a caspase-9-mediated apoptosis execution (*67, 122*). But, whether Huh7 cells belong to type I or type II cells was not tested here or elsewhere.

4.2 RECEPTOR TRAFFICKING

Besides of the initial interaction of CD95 and EGFR, an equally interesting observation is that the EGF stimulation induces an initial translocation of both CD95 and EGFR to the PM followed by a loss of interaction after some time as EGFR is endocytosed and CD95 remains at the periphery (Fig 3.4). In un-stimulated cells ectopically expressing both receptors, a high fraction of both proteins appears to be localized in the perinuclear area and only a small fraction is visible at the PM. In the case of the EGFR, the membrane fraction of the receptor is under dynamic flow, continuously internalizing via vesicular transport and recycling back to the PM as part of a mechanism to safeguard against autonomous receptor activation (*141, 143*). EGF binding promotes EGFR enrichment on the PM due to dimer stabilization and leads to fully active receptors. Ligand-induced internalization negatively regulates receptor activity and culminates in the degradation of the receptor. For CD95, however, no reports exist that describe steady state trafficking and whether recycling of CD95 is important for apoptosis induction or other functions of the receptor. All reports that address internalization and subcellular compartmentalization of CD95 only focus on ligand-induced effects and about the differences in type I vs. type II cells (*122, 176-178*).

Due to the interaction of CD95 and EGFR as well as the accumulation of both receptors in the perinuclear area, co-expression experiments were performed to investigate whether a similar trafficking route is observable also for CD95. Recycling of the EGFR was previously described for different cell types, for

example, Cos-7 cells, but unknown in Huh7 cells. We found that in Huh7 cells the amount of EGFR in Rab11a-positive RE is for unknown reasons quite low and that co-localization of both receptors was barely found (Fig 3.5). One possibility is that in those cells EGFR recycles through an alternative, Rab11-independent route. CD95, however, was found in the Rab11a-positive RE in Huh7 cells and stays more or less stable even if EGFR is ectopically co-expressed. In fact, the amount of CD95 in the RE is only slightly reduced if EGFR is co-expressed. This might be because CD95 is kept more efficiently on the PM due to the interaction of both proteins. However, as the actual idea was to test whether EGFR is influencing trafficking of CD95 or *vice versa*, we also investigated trafficking of both receptors in Cos-7 cells, because for those cells trafficking of the EGFR is well described and EGFR is associating with Rab11a-positive RE (*143*). Similar to Huh7 cells, CD95 is highly expressed in Rab11a-positive RE and also EGFR is accumulated in the RE of all investigated cells. Interestingly, our data indicate that in un-stimulated Cos-7 cells CD95 co-expression increases the amount of EGFR that co-localizes with Rab11a-positive RE. Ectopic expression of all three proteins seems to either enhance the internalization rate of EGFR from the PM to the RE or to decreases the recycling rate from the RE to the PM in comparison to cells that only over-express the EGFR and Rab11a. However, as the performed co-expression experiments only indirectly offer information about the recycling rate, other experiments, like photoactivation-microscopy experiments or similar would be more suitable.

Next, we wanted to examine how stimulation with EGF is affecting the subcellular distribution of both receptors. As mentioned above, EGF binding leads to an initial enrichment of EGFR on the PM, which promotes receptor activation due to the autocatalytic nature of EGFR, followed by receptor internalization and degradation. CD95 was also observed to accumulate on the PM after EGF treatment (Fig 3.2 A, 3.3), but unlike EGFR the amount of vesicular CD95 that is internalized upon EGF stimulation is smaller and a higher fraction seems to stay on the PM (Fig. 3.3 B and 3.4 A). Furthermore, the proportion of CD95 residing in the RE after EGF stimulation decreases with time. Interestingly, while in Huh7 cells the depletion of CD95 in the RE was more linear and appeared slower, in Cos-7 cells the depletion occurred in an exponential relatively rapid progression (Fig 3.7 and 3.8), pointing to additional differences in the trafficking dynamics between Huh-7 and Cos-7 cells.

It is conceivable that, in un-stimulated cells, CD95 and EGFR are co-trafficked and that high expression level of either receptor increases the vesicular fraction to avoid self-activation of both systems. Upon EGF stimulation both receptors translocate from the RE and accumulate at the PM, and while ligand-bound EGFR is progressively internalized and degraded, CD95 remains at the PM. It is possible that, for example, the EGFR-mediated phosphorylation is trapping CD95 at the PM. Nevertheless, more experiments are required to proof these hypotheses as most data are exclusively based on co-localisation experiments.

4.3 THE EFFECT OF EGF STIMULATION ON CD95

Undoubtedly, EGF stimulation leads to activation of the protein-tyrosine kinase domain of the EGFR and recruitment of several proteins to the regulatory domain, such as adaptor protein and many others. After observing co-localisation between CD95 and EGFR in unstimulated cells, translocation of both proteins towards the PM upon EGF stimulation and a strong indication for a physical interaction, the next obvious step was to test whether CD95 is phosphorylated in an EGFR-mediated fashion. Pull-down experiments, indeed, confirmed a weak but detectable phosphorylation of CD95 upon EGF addition but not upon FasL exposure (Fig 3.9 A and 3.10). We believe that the weak detected signal in Western Blots is because EGFR only phosphorylates the membranal fraction of CD95, as inhibition of phosphatases by the addition of pervanadate, which should lead to the phosphorylation of CD95 throughout the cell, promoted a substantial increase in CD95 phosphorylation (Fig. 3.10).

Posttranslational modifications such as tyrosine phosphorylation represent a suitable mechanism for a switch of CD95's function in a more general way and yet the purpose of tyrosine-phosphorylated CD95 remains puzzling. CD95 is serine, threonine and also tyrosine phosphorylated, as indicated by one of the very early studies, but it was also shown that tyrosine phosphorylation is not obligatory for CD95-mediated apoptosis, which raised the question of the role of such posttranslational modifications in regulating CD95 activity (*31, 50*).

If kinase activity and consequently phosphorylated CD95 are not required for apoptosis induction, what is then the function of EGFR-mediated phosphorylation of CD95? Pre-stimulation of EGFR decreased the sensitivity of Huh7 cells to FasL-

induced apoptosis (Fig 3.11, 3.12). This effect required the kinase activity of EGFR, strengthening the idea of a direct phosphorylation of CD95 via EGFR. On the other hand, experiments with a mutated version of CD95, in which the tyrosine residues 232 and 291 are exchanged by phenylalanine residues, revealed that phosphorylation of those two tyrosine residues is essential for the EGF-mediated inhibition of apoptosis. Those effects point towards a regulatory role of the EGFR activity in the framework of CD95-mediated cell fate. So far, nearly all studies that investigated the role of phosphorylated CD95 focus on FasL-induced phosphorylation (*113-117, 119, 175*). In those reports, however, phosphorylation of CD95 seems to be important for both apoptosis induction but also survival. While early reports show that tyrosine phosphorylation is dispensable for apoptosis induction, later studies claim that CD95 phosphorylation is necessary for apoptosis induction. It was, for example, shown that in hepatocytes and liver carcinoma cells CD95 is phosphorylated, that phosphorylation of CD95 is EGFR-mediated and that by regulating CD95 receptor oligomerization, this phosphorylation is required for apoptosis induction (*118, 119, 123, 175*). Other reports suggest rather an anti-apoptotic function of FasL-induced CD95 tyrosine phosphorylation (*113-117*). In this context, a recent study shows the importance of the tyrosine residues Y232 and Y291 in an evolution-guided analysis (*117*). They show that a FasL-induced phosphorylation-based pro-survival mechanism that favours apoptosis resistance. It is mentioned that dephosphorylation of both tyrosine residues provokes cell death. Consistent to other studies, Chakrabandhu *et al.* indicated that phosphorylation of the death domain is SFK-mediated.

Another hypothesis implies that the tyrosine residue at position 291 in the C-terminal DD of the CD95 is important for internalization of the receptor after FasL binding. In this context Lee *et al.* showed that internalization of CD95 is impaired if this particular tyrosine is mutated and replaced by a phenylalanine(*122*). Interestingly, in the same report it was described that A20 cells, a murine B cell lymphoma line, transfected with CD95 Y291F are unable to undergo apoptosis as a result of the impaired internalization, thereby speculating about the importance of internalization for CD95-mediated apoptosis (*122*). However, Chakrabandhu and colleges repeated those experiments and could not observe impaired internalization of CD95 (*117*). On the contrary, mutation of the tyrosine residue at

position 291 resulted in a more efficient FasL uptake, indicating that the added negative charge favoured receptor trafficking.

4.4 CD95 PHOSPHORYLATION? WHAT IS IT IMPORTANT FOR?

How is EGFR-mediated phosphorylation of CD95 changing its responsiveness towards FasL and why does survival signaling becomes dominant once CD95 is phosphorylated? CD95 exists as a pre-associated homotrimer and this configuration is required for FasL binding and DISC formation (*43*). Therefore, one potential way to switch the functionality of CD95 would be to influence its ability to self-aggregate. To investigate this hypothesis, we performed anisotropy measurements of cells ectopically expressing EGFR and either wild type CD95 or mutated CD95 (Fig 3.13). Interestingly, EGF stimulation in cells expressing wild type CD95 caused a slight increase of the anisotropy, which corresponds to a decrease in CD95 self-association. On the other hand, if the tyrosine residues 232 and 291 in death domain are exchanged by phenylalanine, the EGF stimulation promotes a decrease in anisotropy, indicating an increase in cluster formation. FasL addition had no effect on the measured anisotropy. Wang *et al.* pursued a similar idea, but they targeted in their studies the relationship between the HGF receptor c-Met and CD95 (*179*). They showed that CD95 and c-Met pre-exist as a complex and physically interact with each other. This interaction inhibits self-aggregation of CD95, thereby preventing FasL binding and leading to apoptosis resistance with a consequently increased survival rate. In contrast to our observation that EGF prevents FasL-induced apoptosis, Wang *et al.* tried to explain why high concentrations of HGF lead to apoptosis induction in some cells, such as liver cells. As HGF stimulation abrogates the association between both receptors, Wang *et al.* concluded that this sensitizes cells again to FasL-induced apoptosis. In spite of the different intentions of Wang and colleges, this study clearly supports the idea that RTK-CD95 interactions can affect the self-aggregation of CD95 and might regulate the function of CD95.

Apart from effects on self-aggregation as a potential switching mode, an often-observed 'phenomenon' of the non-apoptotic function of CD95 is activation of the PI3K/Akt signaling pathway (reviewed in (*38*)). To also consider downstream signaling as potential source for the dominating survival signaling, we determined

the activation state of Akt but also of Erk in cells that ectopically express EGFR and either wild type or a phospho-deficient mutant of CD95 (Fig 3.14). The level of phosphorylated Erk is increased upon EGF addition, but no differences were observed between cells expressing the wild type CD95 and the mutant CD95. In contrast, in cells expressing the phospho-deficient CD95 the level of phosphorylated Akt was significantly reduced upon EGF stimulation compared to cells expressing the wild type protein. Kleber *et al.* showed similar results in glioblastoma cells upon the addition of a specific FasL, which obtains a stable trimer-building capacity (*113*). They showed that CD95 directly contributes to the aggressively invasive phenotype of glioblastoma multiforme via activation of the PI3K/Akt signaling pathway. The authors provide evidence that the p85 subunit of PI3K directly binds to CD95, leading to elevated Akt phosphorylation and activation. In their proposed model, activated Akt phosphorylates and inactivates GSK3β, which allows for β-catenin translocation into the nucleus, where it induces transcription of MMPs. Activation of MMPs then triggers invasion of glioma cells.

The constancy of an Akt participation in the non-apoptotic signaling of CD95 might point towards a more general survival pathway of CD95 that might include Akt activation. Also our data provides some evidence of a positive correlation between phosphorylation of CD95 and elevated level of phospho-Akt.

4.5 THE MECHANISTIC POINT OF VIEW

By gathering all observations together we suggest the following model for the EGF-mediated effect on CD95 signaling. In the un-ligated state both receptors weakly interact with each other and are localized at the PM but also in the perinuclear area (Fig. 4.1 I). From the PM both receptors get constantly internalized to the endosomal compartment and recycle back to the PM. Upon EGF-binding both receptors accumulate at the PM and activated EGFR phosphorylates the membrane fraction of CD95 (Fig. 4.1 II). The weak initial interaction of both receptors is depleted after some time, as ligand-bound EGFR follows a different internalization route compared to un-ligated receptor, which is culminating in degradation (Fig. 4.1 III).

In the phosphorylated state induction of apoptosis is inhibited by three mechanisms.

- First phosphorylation of CD95 prevents internalization of CD95 and thus leads to accumulation of phosphorylated CD95 at the PM.
- Second the EGF-promoted phosphorylation of CD95 effects pre-association and thereby leads to hindrance of cluster formation, which is required for DISC formation (Fig. 4.1 IV).
- Third phosphorylated CD95 serves as docking site for SH2 domain containing proteins like PI3K, which is resulting in increased pAkt levels and enhanced survival signaling (Fig. 4.1 IV).

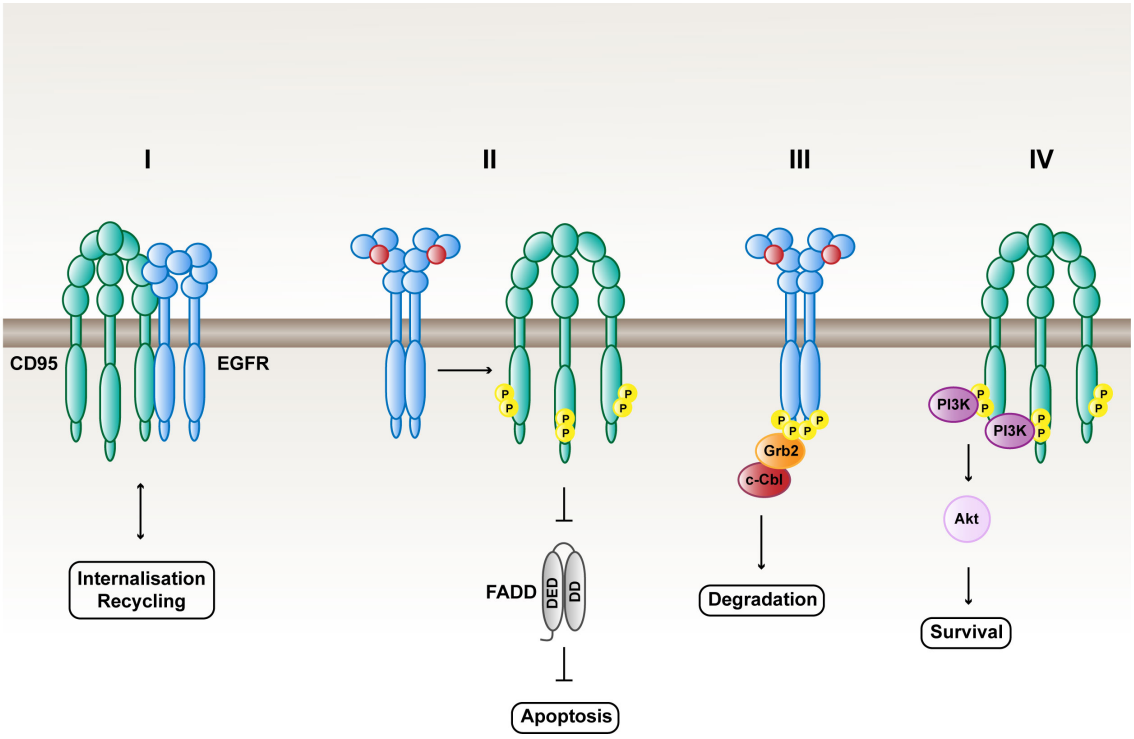

Figure 4.1: Model of the EGF-mediated switch in CD95 signaling

4.6 NSCLC CELLS AS MODEL

To validate parts of our model in a physiologically and therapeutically relevant context we chose the non-small cell lung cancer (NSCLC) cell line, HCC827, which expresses constitutively active EGFR due to an exon 19 deletion. Furthermore, CD95 has previously been demonstrated to play an anti-apoptotic role in lung cancer cells was already published in 2003 by Lee and colleges. They showed that overexpression of CD95 in Lewis lung carcinoma (3LL) cells causes enhanced tumour progression in vivo (*180*). Another remarkable role of CD95 specifically in

NSCLC cells was shown by Bivona *et al.*, as they showed that knockdown of CD95 and individual components of the NF-κB pathway specifically enhanced cell death in lung cancer cells (*181*). Those findings together with the fact that NSCLC cell lines often have a constitutive EGFR activation made the HCC827 cells to an attractive model cell line to examine the cellular consequences of our model.

We first assessed the cellular response to FasL stimulation in the constitutively active EGFR background provided by HCC827 cells. According to our model, persistent EGFR activity should promote basal CD95 phosphorylation and provide protection against FasL-induced apoptosis. We could indeed demonstrate both; first that stimulation with FasL does not induce apoptosis (Fig 3.15) and second that CD95 is phosphorylated in those cells and that the basal phosphorylation is relatively high compared to the EGF-stimulated state (Fig 3.16). The next question we wanted to address was whether inhibition of EGFR, and a resultant decrease in CD95 phosphorylation could restore sensitivity to FasL-induced apoptosis. To inhibit EGFR we used the TKI Erlotinib, which rapidly and efficiently suppressed constitutive EGFR activity (Fig 3.18). Moreover, we observed that Erlotinib treatment also restored sensitivity of HCC827 cells towards FasL induced apoptosis (Fig 3.19). However, we also observed that Erlotinib alone exhibited negative effect on survival and although subsequent FasL stimulation further decreased survival compared to Erlotinib alone, we cannot exclude the possibility that this effect is purely additive. A further point that needs to be confirmed is whether inhibition of EGFR indeed leads to a reduction in CD95 phosphorylation.

Several lines of evidence point towards the validation of our model in HCC827 cells. As activating mutations are often found in tumours, the presented model provides a potential mechanism for tumour cells to become insensitive towards apoptosis induction. The fact that the activation status of EGFR tremendously influences the cellular response to CD95 activation represents a fascinating regulatory mechanism that acts in a context dependent manner.

4.7 FUTURE DIRECTIONS

CD95 is a multifunctional protein, with several regulating mechanisms that precisely act in space and time to ensure a robust and appropriate response in a given cellular context. Its importance is therefore not only manifested by its role as

a classical ‘death receptor’, but also, and maybe to some extent, by its non-apoptotic functions. The results presented here demonstrate the importance of context in the CD95-mediated signaling output and may even provide a model of how CD95s function is switching in a more general manner. A better understanding of how such an important protein functions and how the historical and environmental context influences its signaling outcome might reveal promising new therapeutic avenues in dysregulated systems like cancer.

It would, for example, be interesting to investigate whether phosphorylation of CD95 is preventing DISC formation. The tyrosine residues that are important for the non-apoptotic function of CD95 are located in the DD. So it is likely that due to the recruitment and binding of proteins that rather signal survival, such as PI3K, the induction of apoptosis is literally blocked. Alternatively it is possible that the negative charge that is added to CD95 by the two phospho-groups is affecting its conformation, and therefore FADD binding and ultimately DISC formation.

Further experiments would be required to precisely explain the elevated pAkt level. The current idea sees CD95 as an additional ‘signaling hub’ that provides two phosphorylated tyrosine residues as docking site for different proteins. We proposed that the elevated pAkt level is, for example, caused by PI3K recruitment to CD95, which was indeed shown before, but is not experimentally confirmed here.

Furthermore, a role for Src and other members has previously been described in the phosphorylation of CD95 and some SFK members are activated upon EGF stimulation. It would be interesting to address whether the EGF-mediated effect on CD95 requires the activity of SFK members.

Not much is known about how vesicular trafficking of CD95 regulates its function, as is the case for other transmembrane signaling proteins like EGFR. We provide first insights into a potential recycling mechanism via the Rab11a-positive endosome. A more quantitative investigation describing, for example, trafficking rates, but also studying the involved proteins and cell-type specific regulation might elucidate important features about the role of CD95 trafficking in its regulation.

5. REFERENCES

1. M. A. Lemmon, J. Schlessinger, Cell signaling by receptor tyrosine kinases. *Cell* **141**, 1117-1134 (2010).
2. B. B. Aggarwal, Signalling pathways of the TNF superfamily: a double-edged sword. *Nature reviews. Immunology* **3**, 745-756 (2003).
3. D. A. Flusberg, P. K. Sorger, Surviving apoptosis: life-death signaling in single cells. *Trends Cell Biol* **25**, 446-458 (2015).
4. T. Suda, H. Hashimoto, M. Tanaka, T. Ochi, S. Nagata, Membrane Fas ligand kills human peripheral blood T lymphocytes, and soluble Fas ligand blocks the killing. *J Exp Med* **186**, 2045-2050 (1997).
5. A. Murthy *et al.*, Ectodomain shedding of EGFR ligands and TNFR1 dictates hepatocyte apoptosis during fulminant hepatitis in mice. *The Journal of clinical investigation* **120**, 2731-2744 (2010).
6. O. R. LA *et al.*, Membrane-bound Fas ligand only is essential for Fas-induced apoptosis. *Nature* **461**, 659-663 (2009).
7. N. Itoh, S. Nagata, A novel protein domain required for apoptosis. Mutational analysis of human Fas antigen. *The Journal of biological chemistry* **268**, 10932-10937 (1993).
8. L. A. Tartaglia, T. M. Ayres, G. H. Wong, D. V. Goeddel, A novel domain within the 55 kd TNF receptor signals cell death. *Cell* **74**, 845-853 (1993).
9. J. Li, Q. Yin, H. Wu, Structural basis of signal transduction in the TNF receptor superfamily. *Adv Immunol* **119**, 135-153 (2013).
10. P. Xie, TRAF molecules in cell signaling and in human diseases. *J Mol Signal* **8**, 7 (2013).
11. H. Ha, D. Han, Y. Choi, TRAF-mediated TNFR-family signaling. *Curr Protoc Immunol* **Chapter 11**, Unit11 19D (2009).
12. B. C. Trauth *et al.*, Monoclonal antibody-mediated tumor regression by induction of apoptosis. *Science* **245**, 301-305 (1989).
13. S. Yonehara, A. Ishii, M. Yonehara, A cell-killing monoclonal antibody (anti-Fas) to a cell surface antigen co-downregulated with the receptor of tumor necrosis factor. *J Exp Med* **169**, 1747-1756 (1989).
14. N. Itoh *et al.*, The polypeptide encoded by the cDNA for human cell surface antigen Fas can mediate apoptosis. *Cell* **66**, 233-243 (1991).
15. T. Suda, T. Takahashi, P. Golstein, S. Nagata, Molecular cloning and expression of the Fas ligand, a novel member of the tumor necrosis factor family. *Cell* **75**, 1169-1178 (1993).
16. I. Behrmann, H. Walczak, P. H. Krammer, Structure of the human APO-1 gene. *European journal of immunology* **24**, 3057-3062 (1994).
17. B. Huang, M. Eberstadt, E. T. Olejniczak, R. P. Meadows, S. W. Fesik, NMR structure and mutagenesis of the Fas (APO-1/CD95) death domain. *Nature* **384**, 638-641 (1996).
18. J. Bajorath, A. Aruffo, Prediction of the three-dimensional structure of the human Fas receptor by comparative molecular modeling. *J Comput Aided Mol Des* **11**, 3-8 (1997).
19. F. C. Kischkel *et al.*, Cytotoxicity-dependent APO-1 (Fas/CD95)-associated proteins form a death-inducing signaling complex (DISC) with the receptor. *The EMBO journal* **14**, 5579-5588 (1995).

20. M. P. Boldin *et al.*, A novel protein that interacts with the death domain of Fas/APO1 contains a sequence motif related to the death domain. *The Journal of biological chemistry* **270**, 7795-7798 (1995).
21. A. M. Chinnaiyan, K. O'Rourke, M. Tewari, V. M. Dixit, FADD, a novel death domain-containing protein, interacts with the death domain of Fas and initiates apoptosis. *Cell* **81**, 505-512 (1995).
22. A. M. Chinnaiyan *et al.*, FADD/MORT1 is a common mediator of CD95 (Fas/APO-1) and tumor necrosis factor receptor-induced apoptosis. *The Journal of biological chemistry* **271**, 4961-4965 (1996).
23. S. Grimm, B. Z. Stanger, P. Leder, RIP and FADD: two "death domain"-containing proteins can induce apoptosis by convergent, but dissociable, pathways. *Proceedings of the National Academy of Sciences of the United States of America* **93**, 10923-10927 (1996).
24. M. P. Boldin, T. M. Goncharov, Y. V. Goltsev, D. Wallach, Involvement of MACH, a novel MORT1/FADD-interacting protease, in Fas/APO-1- and TNF receptor-induced cell death. *Cell* **85**, 803-815 (1996).
25. M. Muzio *et al.*, FLICE, a novel FADD-homologous ICE/CED-3-like protease, is recruited to the CD95 (Fas/APO-1) death--inducing signaling complex. *Cell* **85**, 817-827 (1996).
26. J. P. Medema *et al.*, FLICE is activated by association with the CD95 death-inducing signaling complex (DISC). *The EMBO journal* **16**, 2794-2804 (1997).
27. P. Juo, C. J. Kuo, J. Yuan, J. Blenis, Essential requirement for caspase-8/FLICE in the initiation of the Fas-induced apoptotic cascade. *Curr Biol* **8**, 1001-1008 (1998).
28. A. M. Chinnaiyan, V. M. Dixit, Portrait of an executioner: the molecular mechanism of FAS/APO-1-induced apoptosis. *Seminars in immunology* **9**, 69-76 (1997).
29. C. M. Eischen, C. J. Dick, P. J. Leibson, Tyrosine kinase activation provides an early and requisite signal for Fas-induced apoptosis. *Journal of immunology* **153**, 1947-1954 (1994).
30. B. Schraven, M. E. Peter, APO-1(CD95)-mediated apoptosis in Jurkat cells does not involve src kinases or CD45. *FEBS letters* **368**, 491-494 (1995).
31. O. Janssen, B. Lengl-Janssen, H. H. Oberg, M. J. Robertson, D. Kabelitz, Induction of cell death via Fas (CD95, Apo-1) may be associated with but is not dependent on Fas-induced tyrosine phosphorylation. *Immunology letters* **49**, 63-69 (1996).
32. K. E. Schlottmann, E. Gulbins, S. M. Lau, K. M. Coggeshall, Activation of Src-family tyrosine kinases during Fas-induced apoptosis. *Journal of leukocyte biology* **60**, 546-554 (1996).
33. E. Gulbins *et al.*, Cellular stimulation via CD95 involves activation of phospho-inositide-3-kinase. *Pflugers Arch* **435**, 546-554 (1998).
34. B. B. Aggarwal, S. Singh, R. LaPushin, K. Totpal, Fas antigen signals proliferation of normal human diploid fibroblast and its mechanism is different from tumor necrosis factor receptor. *FEBS letters* **364**, 5-8 (1995).
35. R. A. Freiberg *et al.*, Fas signal transduction triggers either proliferation or apoptosis in human fibroblasts. *The Journal of investigative dermatology* **108**, 215-219 (1997).
36. J. Desbarats, T. Wade, W. F. Wade, M. K. Newell, Dichotomy between naive and memory CD4(+) T cell responses to Fas engagement. *Proceedings of the*

National Academy of Sciences of the United States of America **96**, 8104-8109 (1999).
37. M. R. Alderson *et al.*, Fas transduces activation signals in normal human T lymphocytes. *J Exp Med* **178**, 2231-2235 (1993).
38. I. Sancho-Martinez, A. Martin-Villalba, Tyrosine phosphorylation and CD95: a FAScinating switch. *Cell Cycle* **8**, 838-842 (2009).
39. E. Brint, G. O'Callaghan, A. Houston, Life in the Fas lane: differential outcomes of Fas signaling. *Cellular and molecular life sciences : CMLS*, (2013).
40. M. E. Peter *et al.*, The CD95 receptor: apoptosis revisited. *Cell* **129**, 447-450 (2007).
41. B. L. Aken *et al.*, The Ensembl gene annotation system. *Database (Oxford)* **2016**, (2016).
42. J. L. Huret *et al.*, Atlas of genetics and cytogenetics in oncology and haematology in 2013. *Nucleic Acids Res* **41**, D920-924 (2013).
43. H. Wajant, Principles and mechanisms of CD95 activation. *Biological chemistry*, (2014).
44. G. Papoff *et al.*, Identification and characterization of a ligand-independent oligomerization domain in the extracellular region of the CD95 death receptor. *The Journal of biological chemistry* **274**, 38241-38250 (1999).
45. R. M. Siegel *et al.*, Fas preassociation required for apoptosis signaling and dominant inhibition by pathogenic mutations. *Science* **288**, 2354-2357 (2000).
46. V. Edmond *et al.*, Precise mapping of the CD95 pre-ligand assembly domain. *PloS one* **7**, e46236 (2012).
47. P. Schneider *et al.*, Characterization of Fas (Apo-1, CD95)-Fas ligand interaction. *The Journal of biological chemistry* **272**, 18827-18833 (1997).
48. S. Tauzin, L. Debure, J. F. Moreau, P. Legembre, CD95-mediated cell signaling in cancer: mutations and post-translational modulations. *Cellular and molecular life sciences : CMLS* **69**, 1261-1277 (2012).
49. F. L. Scott *et al.*, The Fas-FADD death domain complex structure unravels signalling by receptor clustering. *Nature* **457**, 1019-1022 (2009).
50. G. Gradl *et al.*, The CD95 (Fas/APO-1) receptor is phosphorylatedin vitro andin vivo and constitutively associates with several cellular proteins. *Apoptosis* **1**, 131-140 (1996).
51. I. Daigle, S. Yousefi, M. Colonna, D. R. Green, H. U. Simon, Death receptors bind SHP-1 and block cytokine-induced anti-apoptotic signaling in neutrophils. *Nature medicine* **8**, 61-67 (2002).
52. T. Sato, S. Irie, S. Kitada, J. C. Reed, FAP-1: a protein tyrosine phosphatase that associates with Fas. *Science* **268**, 411-415 (1995).
53. Y. Li *et al.*, Negative regulation of Fas-mediated apoptosis by FAP-1 in human cancer cells. *Int J Cancer* **87**, 473-479 (2000).
54. D. R. Green, C. F. Ware, Fas-ligand: privilege and peril. *Proceedings of the National Academy of Sciences of the United States of America* **94**, 5986-5990 (1997).
55. Y. Oshimi, S. Oda, Y. Honda, S. Nagata, S. Miyazaki, Involvement of Fas ligand and Fas-mediated pathway in the cytotoxicity of human natural killer cells. *Journal of immunology* **157**, 2909-2915 (1996).
56. D. Bellgrau *et al.*, A role for CD95 ligand in preventing graft rejection. *Nature* **377**, 630-632 (1995).

57. D. Berg *et al.*, Enforced covalent trimerization increases the activity of the TNF ligand family members TRAIL and CD95L. *Cell Death Differ* **14**, 2021-2034 (2007).
58. F. K. Chan, Three is better than one: pre-ligand receptor assembly in the regulation of TNF receptor signaling. *Cytokine* **37**, 101-107 (2007).
59. B. J. Ferguson *et al.*, Biophysical and cell-based evidence for differential interactions between the death domains of CD95/Fas and FADD. *Cell Death Differ* **14**, 1717-1719 (2007).
60. R. M. Siegel *et al.*, SPOTS: signaling protein oligomeric transduction structures are early mediators of death receptor-induced apoptosis at the plasma membrane. *The Journal of cell biology* **167**, 735-744 (2004).
61. C. Feig, V. Tchikov, S. Schutze, M. E. Peter, Palmitoylation of CD95 facilitates formation of SDS-stable receptor aggregates that initiate apoptosis signaling. *The EMBO journal* **26**, 221-231 (2007).
62. J. R. Muppidi *et al.*, Homotypic FADD interactions through a conserved RXDLL motif are required for death receptor-induced apoptosis. *Cell Death Differ* **13**, 1641-1650 (2006).
63. K. Schleich *et al.*, Stoichiometry of the CD95 death-inducing signaling complex: experimental and modeling evidence for a death effector domain chain model. *Mol Cell* **47**, 306-319 (2012).
64. L. S. Dickens *et al.*, A death effector domain chain DISC model reveals a crucial role for caspase-8 chain assembly in mediating apoptotic cell death. *Mol Cell* **47**, 291-305 (2012).
65. S. Ozturk, K. Schleich, I. N. Lavrik, Cellular FLICE-like inhibitory proteins (c-FLIPs): fine-tuners of life and death decisions. *Experimental cell research* **318**, 1324-1331 (2012).
66. M. Irmler *et al.*, Inhibition of death receptor signals by cellular FLIP. *Nature* **388**, 190-195 (1997).
67. B. C. Barnhart, E. C. Alappat, M. E. Peter, The CD95 type I/type II model. *Seminars in immunology* **15**, 185-193 (2003).
68. C. Scaffidi *et al.*, Two CD95 (APO-1/Fas) signaling pathways. *The EMBO journal* **17**, 1675-1687 (1998).
69. P. J. Jost *et al.*, XIAP discriminates between type I and type II FAS-induced apoptosis. *Nature* **460**, 1035-1039 (2009).
70. N. Roy, Q. L. Deveraux, R. Takahashi, G. S. Salvesen, J. C. Reed, The c-IAP-1 and c-IAP-2 proteins are direct inhibitors of specific caspases. *The EMBO journal* **16**, 6914-6925 (1997).
71. Q. L. Deveraux *et al.*, IAPs block apoptotic events induced by caspase-8 and cytochrome c by direct inhibition of distinct caspases. *The EMBO journal* **17**, 2215-2223 (1998).
72. Q. L. Deveraux, R. Takahashi, G. S. Salvesen, J. C. Reed, X-linked IAP is a direct inhibitor of cell-death proteases. *Nature* **388**, 300-304 (1997).
73. C. Du, M. Fang, Y. Li, L. Li, X. Wang, Smac, a mitochondrial protein that promotes cytochrome c-dependent caspase activation by eliminating IAP inhibition. *Cell* **102**, 33-42 (2000).
74. R. Watanabe-Fukunaga, C. I. Brannan, N. G. Copeland, N. A. Jenkins, S. Nagata, Lymphoproliferation disorder in mice explained by defects in Fas antigen that mediates apoptosis. *Nature* **356**, 314-317 (1992).

75. J. L. Chu, J. Drappa, A. Parnassa, K. B. Elkon, The defect in Fas mRNA expression in MRL/lpr mice is associated with insertion of the retrotransposon, ETn. *J Exp Med* **178**, 723-730 (1993).
76. M. Kimura, A. Matsuzawa, Autoimmunity in mice bearing lprcg: a novel mutant gene. *Int Rev Immunol* **11**, 193-210 (1994).
77. A. Matsuzawa *et al.*, A new allele of the lpr locus, lprcg, that complements the gld gene in induction of lymphadenopathy in the mouse. *J Exp Med* **171**, 519-531 (1990).
78. T. Takahashi *et al.*, Generalized lymphoproliferative disease in mice, caused by a point mutation in the Fas ligand. *Cell* **76**, 969-976 (1994).
79. G. H. Fisher *et al.*, Dominant interfering Fas gene mutations impair apoptosis in a human autoimmune lymphoproliferative syndrome. *Cell* **81**, 935-946 (1995).
80. F. Rieux-Laucat *et al.*, Mutations in Fas associated with human lymphoproliferative syndrome and autoimmunity. *Science* **268**, 1347-1349 (1995).
81. S. E. Straus *et al.*, The development of lymphomas in families with autoimmune lymphoproliferative syndrome with germline Fas mutations and defective lymphocyte apoptosis. *Blood* **98**, 194-200 (2001).
82. V. K. Rao, S. E. Straus, Causes and consequences of the autoimmune lymphoproliferative syndrome. *Hematology* **11**, 15-23 (2006).
83. A. Strasser, P. J. Jost, S. Nagata, The many roles of FAS receptor signaling in the immune system. *Immunity* **30**, 180-192 (2009).
84. K. Miwa *et al.*, Caspase 1-independent IL-1beta release and inflammation induced by the apoptosis inducer Fas ligand. *Nature medicine* **4**, 1287-1292 (1998).
85. F. Benigni, S. Sacco, L. Aloe, P. Ghezzi, Intracerebroventricular injection of anti-Fas activates the hypothalamus-pituitary-adrenal axis and induces peripheral interleukin-6 and serum amyloid A in mice: comparison with other ligands of the tumor necrosis factor/nerve growth factor receptor superfamily. *The American journal of pathology* **153**, 1377-1381 (1998).
86. N. L. Malinin, M. P. Boldin, A. V. Kovalenko, D. Wallach, MAP3K-related kinase involved in NF-kappaB induction by TNF, CD95 and IL-1. *Nature* **385**, 540-544 (1997).
87. C. Sekine *et al.*, Fas-mediated stimulation induces IL-8 secretion by rheumatoid arthritis synoviocytes independently of CPP32-mediated apoptosis. *Biochem Biophys Res Commun* **228**, 14-20 (1996).
88. L. Biancone *et al.*, Development of inflammatory angiogenesis by local stimulation of Fas in vivo. *J Exp Med* **186**, 147-152 (1997).
89. G. Jarad *et al.*, Fas activation induces renal tubular epithelial cell beta 8 integrin expression and function in the absence of apoptosis. *The Journal of biological chemistry* **277**, 47826-47833 (2002).
90. J. Desbarats, M. K. Newell, Fas engagement accelerates liver regeneration after partial hepatectomy. *Nature medicine* **6**, 920-923 (2000).
91. J. Desbarats *et al.*, Fas engagement induces neurite growth through ERK activation and p35 upregulation. *Nature cell biology* **5**, 118-125 (2003).
92. C. Lambert, A. M. Landau, J. Desbarats, Fas-beyond death: a regenerative role for Fas in the nervous system. *Apoptosis* **8**, 551-562 (2003).
93. M. E. Peter, P. Legembre, B. C. Barnhart, Does CD95 have tumor promoting activities? *Biochimica et biophysica acta* **1755**, 25-36 (2005).

94. M. E. Peter *et al.*, The role of CD95 and CD95 ligand in cancer. *Cell Death Differ* **22**, 549-559 (2015).
95. A. Martin-Villalba, E. Llorens-Bobadilla, D. Wollny, CD95 in cancer: tool or target? *Trends in molecular medicine*, (2013).
96. L. Chen *et al.*, CD95 promotes tumour growth. *Nature* **465**, 492-496 (2010).
97. A. Hadji *et al.*, Death induced by CD95 or CD95 ligand elimination. *Cell reports* **7**, 208-222 (2014).
98. M. E. Peter, DICE: A novel tumor surveillance mechanism-a new therapy for cancer? *Cell Cycle* **13**, 1373-1378 (2014).
99. C. Scaffidi, I. Schmitz, P. H. Krammer, M. E. Peter, The role of c-FLIP in modulation of CD95-induced apoptosis. *The Journal of biological chemistry* **274**, 1541-1548 (1999).
100. D. W. Chang *et al.*, c-FLIP(L) is a dual function regulator for caspase-8 activation and CD95-mediated apoptosis. *The EMBO journal* **21**, 3704-3714 (2002).
101. A. Golks, D. Brenner, P. H. Krammer, I. N. Lavrik, The c-FLIP-NH2 terminus (p22-FLIP) induces NF-kappaB activation. *J Exp Med* **203**, 1295-1305 (2006).
102. I. N. Lavrik, P. H. Krammer, Regulation of CD95/Fas signaling at the DISC. *Cell Death Differ* **19**, 36-41 (2012).
103. I. N. Lavrik, Systems biology of death receptor networks: live and let die. *Cell death & disease* **5**, e1259 (2014).
104. H. Wajant, K. Pfizenmaier, P. Scheurich, Non-apoptotic Fas signaling. *Cytokine Growth Factor Rev* **14**, 53-66 (2003).
105. A. Ponton, M. V. Clement, I. Stamenkovic, The CD95 (APO-1/Fas) receptor activates NF-kappaB independently of its cytotoxic function. *The Journal of biological chemistry* **271**, 8991-8995 (1996).
106. B. C. Barnhart *et al.*, CD95 ligand induces motility and invasiveness of apoptosis-resistant tumor cells. *The EMBO journal* **23**, 3175-3185 (2004).
107. B. Z. Stanger, P. Leder, T. H. Lee, E. Kim, B. Seed, RIP: a novel protein containing a death domain that interacts with Fas/APO-1 (CD95) in yeast and causes cell death. *Cell* **81**, 513-523 (1995).
108. S. Kreuz *et al.*, NFkappaB activation by Fas is mediated through FADD, caspase-8, and RIP and is inhibited by FLIP. *The Journal of cell biology* **166**, 369-380 (2004).
109. P. Legembre, B. C. Barnhart, M. E. Peter, The relevance of NF-kappaB for CD95 signaling in tumor cells. *Cell Cycle* **3**, 1235-1239 (2004).
110. H. Shinohara, H. Yagita, Y. Ikawa, N. Oyaizu, Fas drives cell cycle progression in glioma cells via extracellular signal-regulated kinase activation. *Cancer Res* **60**, 1766-1772 (2000).
111. C. Tamm *et al.*, Differential regulation of the mitochondrial and death receptor pathways in neural stem cells. *Eur J Neurosci* **19**, 2613-2621 (2004).
112. L. C. Cantley, The phosphoinositide 3-kinase pathway. *Science* **296**, 1655-1657 (2002).
113. S. Kleber *et al.*, Yes and PI3K bind CD95 to signal invasion of glioblastoma. *Cancer cell* **13**, 235-248 (2008).
114. M. Teodorczyk *et al.*, CD95 promotes metastatic spread via Sck in pancreatic ductal adenocarcinoma. *Cell Death Differ* **22**, 1192-1202 (2015).

115. E. J. Steller *et al.*, The death receptor CD95 activates the cofilin pathway to stimulate tumour cell invasion. *EMBO reports* **12**, 931-937 (2011).
116. E. Letellier *et al.*, CD95-ligand on peripheral myeloid cells activates Syk kinase to trigger their recruitment to the inflammatory site. *Immunity* **32**, 240-252 (2010).
117. K. Chakrabandhu *et al.*, An Evolution-Guided Analysis Reveals a Multi-Signaling Regulation of Fas by Tyrosine Phosphorylation and its Implication in Human Cancers. *PLoS Biol* **14**, e1002401 (2016).
118. A. Eberle, R. Reinehr, S. Becker, D. Haussinger, Fluorescence resonance energy transfer analysis of proapoptotic CD95-EGF receptor interactions in Huh7 cells. *Hepatology* **41**, 315-326 (2005).
119. R. Reinehr, F. Schliess, D. Haussinger, Hyperosmolarity and CD95L trigger CD95/EGF receptor association and tyrosine phosphorylation of CD95 as prerequisites for CD95 membrane trafficking and DISC formation. *Faseb J* **17**, 731-733 (2003).
120. C. Gajate, F. Mollinedo, Lipid rafts and raft-mediated supramolecular entities in the regulation of CD95 death receptor apoptotic signaling. *Apoptosis* **20**, 584-606 (2015).
121. J. H. Song *et al.*, Lipid rafts and nonrafts mediate tumor necrosis factor related apoptosis-inducing ligand induced apoptotic and nonapoptotic signals in non small cell lung carcinoma cells. *Cancer Res* **67**, 6946-6955 (2007).
122. K. H. Lee *et al.*, The role of receptor internalization in CD95 signaling. *The EMBO journal* **25**, 1009-1023 (2006).
123. R. Reinehr, A. Sommerfeld, D. Haussinger, CD95 ligand is a proliferative and antiapoptotic signal in quiescent hepatic stellate cells. *Gastroenterology* **134**, 1494-1506 (2008).
124. T. Vargo-Gogola, H. C. Crawford, B. Fingleton, L. M. Matrisian, Identification of novel matrix metalloproteinase-7 (matrilysin) cleavage sites in murine and human Fas ligand. *Archives of biochemistry and biophysics* **408**, 155-161 (2002).
125. A. Fouque, L. Debure, P. Legembre, The CD95/CD95L signaling pathway: A role in carcinogenesis. *Biochimica et biophysica acta* **1846**, 130-141 (2014).
126. K. M. Ferguson, Structure-based view of epidermal growth factor receptor regulation. *Annu Rev Biophys* **37**, 353-373 (2008).
127. N. Jura *et al.*, Mechanism for activation of the EGF receptor catalytic domain by the juxtamembrane segment. *Cell* **137**, 1293-1307 (2009).
128. K. M. Ferguson *et al.*, EGF activates its receptor by removing interactions that autoinhibit ectodomain dimerization. *Mol Cell* **11**, 507-517 (2003).
129. Y. Yarden, J. Schlessinger, Epidermal growth factor induces rapid, reversible aggregation of the purified epidermal growth factor receptor. *Biochemistry* **26**, 1443-1451 (1987).
130. C. Cochet *et al.*, Demonstration of epidermal growth factor-induced receptor dimerization in living cells using a chemical covalent cross-linking agent. *The Journal of biological chemistry* **263**, 3290-3295 (1988).
131. J. T. Jones, R. W. Akita, M. X. Sliwkowski, Binding specificities and affinities of egf domains for ErbB receptors. *FEBS letters* **447**, 227-231 (1999).
132. J. Schlessinger, Ligand-induced, receptor-mediated dimerization and activation of EGF receptor. *Cell* **110**, 669-672 (2002).

133. X. Yu, K. D. Sharma, T. Takahashi, R. Iwamoto, E. Mekada, Ligand-independent dimer formation of epidermal growth factor receptor (EGFR) is a step separable from ligand-induced EGFR signaling. *Molecular biology of the cell* **13**, 2547-2557 (2002).
134. M. A. Lemmon *et al.*, Two EGF molecules contribute additively to stabilization of the EGFR dimer. *The EMBO journal* **16**, 281-294 (1997).
135. X. Zhang, J. Gureasko, K. Shen, P. A. Cole, J. Kuriyan, An allosteric mechanism for activation of the kinase domain of epidermal growth factor receptor. *Cell* **125**, 1137-1149 (2006).
136. S. E. Egan *et al.*, Association of Sos Ras exchange protein with Grb2 is implicated in tyrosine kinase signal transduction and transformation. *Nature* **363**, 45-51 (1993).
137. N. Li *et al.*, Guanine-nucleotide-releasing factor hSos1 binds to Grb2 and links receptor tyrosine kinases to Ras signalling. *Nature* **363**, 85-88 (1993).
138. M. Rozakis-Adcock, R. Fernley, J. Wade, T. Pawson, D. Bowtell, The SH2 and SH3 domains of mammalian Grb2 couple the EGF receptor to the Ras activator mSos1. *Nature* **363**, 83-85 (1993).
139. A. Sorkin, L. K. Goh, Endocytosis and intracellular trafficking of ErbBs. *Experimental cell research* **314**, 3093-3106 (2008).
140. G. Carpenter, S. Cohen, 125I-labeled human epidermal growth factor. Binding, internalization, and degradation in human fibroblasts. *The Journal of cell biology* **71**, 159-171 (1976).
141. A. Sorkin, L. K. Goh, Endocytosis and intracellular trafficking of ErbBs. *Experimental cell research* **315**, 683-696 (2009).
142. A. Sorkin, M. von Zastrow, Endocytosis and signalling: intertwining molecular networks. *Nat Rev Mol Cell Biol* **10**, 609-622 (2009).
143. M. Baumdick *et al.*, EGF-dependent re-routing of vesicular recycling switches spontaneous phosphorylation suppression to EGFR signaling. *Elife* **4**, (2015).
144. X. Jiang, F. Huang, A. Marusyk, A. Sorkin, Grb2 regulates internalization of EGF receptors through clathrin-coated pits. *Molecular biology of the cell* **14**, 858-870 (2003).
145. A. A. de Melker, G. van der Horst, J. Borst, Ubiquitin ligase activity of c-Cbl guides the epidermal growth factor receptor into clathrin-coated pits by two distinct modes of Eps15 recruitment. *The Journal of biological chemistry* **279**, 55465-55473 (2004).
146. N. Normanno *et al.*, The ErbB receptors and their ligands in cancer: an overview. *Curr Drug Targets* **6**, 243-257 (2005).
147. C. L. Arteaga, Epidermal growth factor receptor dependence in human tumors: more than just expression? *Oncologist* **7 Suppl 4**, 31-39 (2002).
148. N. Normanno *et al.*, Epidermal growth factor receptor (EGFR) signaling in cancer. *Gene* **366**, 2-16 (2006).
149. S. K. Chan, W. J. Gullick, M. E. Hill, Mutations of the epidermal growth factor receptor in non-small cell lung cancer -- search and destroy. *Eur J Cancer* **42**, 17-23 (2006).
150. A. E. Wakeling *et al.*, ZD1839 (Iressa): an orally active inhibitor of epidermal growth factor signaling with potential for cancer therapy. *Cancer Res* **62**, 5749-5754 (2002).

151. M. Hidalgo *et al.*, Phase I and pharmacologic study of OSI-774, an epidermal growth factor receptor tyrosine kinase inhibitor, in patients with advanced solid malignancies. *J Clin Oncol* **19**, 3267-3279 (2001).
152. P. Norman, OSI-774 OSI Pharmaceuticals. *Curr Opin Investig Drugs* **2**, 298-304 (2001).
153. C. H. Yun *et al.*, Structures of lung cancer-derived EGFR mutants and inhibitor complexes: mechanism of activation and insights into differential inhibitor sensitivity. *Cancer cell* **11**, 217-227 (2007).
154. M. Santarpia *et al.*, Tyrosine kinase inhibitors for non-small-cell lung cancer: finding patients who will be responsive. *Expert Rev Respir Med* **5**, 413-424 (2011).
155. S. Gibson, S. Tu, R. Oyer, S. M. Anderson, G. L. Johnson, Epidermal growth factor protects epithelial cells against Fas-induced apoptosis. Requirement for Akt activation. *The Journal of biological chemistry* **274**, 17612-17618 (1999).
156. T. Tanaka *et al.*, Enhanced Fas/CD95-mediated apoptosis by epidermal growth factor in human endometrial epithelial cells. *European journal of obstetrics, gynecology, and reproductive biology* **86**, 189-194 (1999).
157. L. Musallam, C. Ethier, P. S. Haddad, M. Bilodeau, Role of EGF receptor tyrosine kinase activity in antiapoptotic effect of EGF on mouse hepatocytes. *American journal of physiology. Gastrointestinal and liver physiology* **280**, G1360-1369 (2001).
158. J. P. Steinbach, P. Supra, H. J. Huang, W. K. Cavenee, M. Weller, CD95-mediated apoptosis of human glioma cells: modulation by epidermal growth factor receptor activity. *Brain pathology* **12**, 12-20 (2002).
159. S. Cursi *et al.*, Src kinase phosphorylates Caspase-8 on Tyr380: a novel mechanism of apoptosis suppression. *The EMBO journal* **25**, 1895-1905 (2006).
160. J. Senft, B. Helfer, S. M. Frisch, Caspase-8 interacts with the p85 subunit of phosphatidylinositol 3-kinase to regulate cell adhesion and motility. *Cancer Res* **67**, 11505-11509 (2007).
161. M. Malleter *et al.*, CD95L cell surface cleavage triggers a prometastatic signaling pathway in triple-negative breast cancer. *Cancer Res* **73**, 6711-6721 (2013).
162. P. I. Bastiaens, A. Squire, Fluorescence lifetime imaging microscopy: spatial resolution of biochemical processes in the cell. *Trends Cell Biol* **9**, 48-52 (1999).
163. J. R. Lakowicz, *Principles of Fluorescence Spectroscopy.*, (Kluwer Academic/Plenum Publishers, 1999).
164. F. Festy, S. M. Ameer-Beg, T. Ng, K. Suhling, Imaging proteins in vivo using fluorescence lifetime microscopy. *Mol Biosyst* **3**, 381-391 (2007).
165. P. J. Verveer, A. Squire, P. I. Bastiaens, Global analysis of fluorescence lifetime imaging microscopy data. *Biophys J* **78**, 2127-2137 (2000).
166. H. E. Grecco, P. Roda-Navarro, P. J. Verveer, Global analysis of time correlated single photon counting FRET-FLIM data. *Opt Express* **17**, 6493-6508 (2009).
167. F. T. Chan, C. F. Kaminski, G. S. Kaminski Schierle, HomoFRET fluorescence anisotropy imaging as a tool to study molecular self-assembly in live cells. *Chemphyschem* **12**, 500-509 (2011).

168. S. Seki *et al.*, Expression of Fas and Bcl-2 proteins and induction of apoptosis in human hepatocellular carcinoma cell lines. *Medical electron microscopy : official journal of the Clinical Electron Microscopy Society of Japan* **32**, 199-203 (1999).
169. Q. Li *et al.*, A syntaxin 1, Galpha(o), and N-type calcium channel complex at a presynaptic nerve terminal: analysis by quantitative immunocolocalization. *J Neurosci* **24**, 4070-4081 (2004).
170. S. Bolte, F. P. Cordelieres, A guided tour into subcellular colocalization analysis in light microscopy. *J Microsc* **224**, 213-232 (2006).
171. A. M. Honegger *et al.*, A mutant epidermal growth factor receptor with defective protein tyrosine kinase is unable to stimulate proto-oncogene expression and DNA synthesis. *Molecular and cellular biology* **7**, 4568-4571 (1987).
172. N. S. Corsini *et al.*, The death receptor CD95 activates adult neural stem cells for working memory formation and brain repair. *Cell Stem Cell* **5**, 178-190 (2009).
173. R. Reinehr, D. Haussinger, CD95 death receptor and epidermal growth factor receptor (EGFR) in liver cell apoptosis and regeneration. *Archives of biochemistry and biophysics* **518**, 2-7 (2012).
174. M. Rodrigues, H. Blair, L. Stockdale, L. Griffith, A. Wells, Surface tethered epidermal growth factor protects proliferating and differentiating multipotential stromal cells from FasL-induced apoptosis. *Stem cells* **31**, 104-116 (2013).
175. A. Eberle, R. Reinehr, S. Becker, V. Keitel, D. Haussinger, CD95 tyrosine phosphorylation is required for CD95 oligomerization. *Apoptosis* **12**, 719-729 (2007).
176. A. Eramo *et al.*, CD95 death-inducing signaling complex formation and internalization occur in lipid rafts of type I and type II cells. *European journal of immunology* **34**, 1930-1940 (2004).
177. N. Foger, S. Bulfone-Paus, A. C. Chan, K. H. Lee, Subcellular compartmentalization of FADD as a new level of regulation in death receptor signaling. *FEBS J* **276**, 4256-4265 (2009).
178. P. Matarrese *et al.*, Endosomal compartment contributes to the propagation of CD95/Fas-mediated signals in type II cells. *The Biochemical journal* **413**, 467-478 (2008).
179. X. Wang *et al.*, A mechanism of cell survival: sequestration of Fas by the HGF receptor Met. *Mol Cell* **9**, 411-421 (2002).
180. J. K. Lee, T. J. Sayers, T. C. Back, J. M. Wigginton, R. H. Wiltrout, Lack of FasL-mediated killing leads to in vivo tumor promotion in mouse Lewis lung cancer. *Apoptosis* **8**, 151-160 (2003).
181. T. G. Bivona *et al.*, FAS and NF-kappaB signalling modulate dependence of lung cancers on mutant EGFR. *Nature* **471**, 523-526 (2011).

6. ACKNOWLEDGEMENT

My special thanks goes to Prof. Dr. Philippe Bastiaens for his guidance and supervision through an exciting project and pleasant PhD time. The project evolved quite a lot over the past years and this evolution sometimes reminded me of a ride on a crazy rollercoaster – pretty hilly, sometimes scary but mostly funny and enjoyable.

I would like to thank Prof. Dr. Christian Kaltschmidt for taking over the representative supervision and for his expertise and advice during some interesting progress meetings in Bielefeld.

In the following I would like to thank all the other beautiful people that have helped me through the years of surviving my PhD ☺
Instead of naming the individual people, friends and family members, I'd rather like to be a bit more general, which also helps me not to forget someone.

There were sooo many people in the last past years that have somehow made my way of getting my PhD possible, easier or more enjoyable and thus influenced me in a positive way so that I'm now able to write this acknowledgements.

Still I would like to say that I'm extremely grateful for having such a fantastic hugggge family that has supported me so much, has always pushed me to go my way and never lost faith in me.

I'm grateful to have my close friends that kept me happy with lots of laughter, G&T's and always an open ear and some comforting words if required.

I'm also thankful for the support and help of my former colleges, but also for all the fun we shared at work or after work.

I'm thankful for all the assistance form the administrative people at the institute and all facility services that have made working pretty smooth.

Finally, I would like to at least try to express how grateful and blessed I'm for having my little cute family at home. It'll be hard to find the right words to emphasize how much my two men at home supported me in every single situation

I can think of, but especially during the phase of writing my thesis. It was really not easy to write my PhD thesis first pregnant and then with a little baby, but thanks to you it worked and I cannot mention the two words ‘THANK YOU’ often enough. I also want to say ‘thank you’ to my little adorable Baby for being the biggest motivation, for proving me with lots of positive energy and just for being my little son. I love you both!